

Electronic Thesis and Dissertation Repository

---

3-15-2016 12:00 AM

## Application of Natural Convection for Photovoltaic Cooling and Photocatalytic Disinfection

Usman J. Rajput  
*The University of Western Ontario*

Supervisor  
JUN YANG  
*The University of Western Ontario*

Graduate Program in Mechanical and Materials Engineering  
A thesis submitted in partial fulfillment of the requirements for the degree in Master of Engineering Science  
© Usman J. Rajput 2016

Follow this and additional works at: <https://ir.lib.uwo.ca/etd>



Part of the [Heat Transfer, Combustion Commons](#), and the [Other Mechanical Engineering Commons](#)

---

### Recommended Citation

Rajput, Usman J., "Application of Natural Convection for Photovoltaic Cooling and Photocatalytic Disinfection" (2016). *Electronic Thesis and Dissertation Repository*. 3671.  
<https://ir.lib.uwo.ca/etd/3671>

This Dissertation/Thesis is brought to you for free and open access by Scholarship@Western. It has been accepted for inclusion in Electronic Thesis and Dissertation Repository by an authorized administrator of Scholarship@Western. For more information, please contact [wlsadmin@uwo.ca](mailto:wlsadmin@uwo.ca).

## Abstract

Two investigations for improving renewable technologies are engaged. First is the examination of the enhancement of heat transfer at the rear of a hot photovoltaic panel by natural convection using various configurations and the other is analyzing a new photocatalytic collector for water heating and cleaning. A 20 Watt polycrystalline panel is exposed to indoor simulated solar light, under constant ambient temperature and stagnant wind conditions. Three configurations are considered: a partial heat sink, a water cavity and a water channel. The experimentally obtained convective heat transfer coefficients are  $4.4 \text{ W}\cdot\text{m}^{-2}\cdot\text{K}^{-1}$  at the rear of the bare panel,  $1.1 \text{ W}\cdot\text{m}^{-2}\cdot\text{K}^{-1}$  with the heat sink,  $26.6 \text{ W}\cdot\text{m}^{-2}\cdot\text{K}^{-1}$  with the water cavity and  $177 \text{ W}\cdot\text{m}^{-2}\cdot\text{K}^{-1}$  with the water channel. The channel is attached to a cold reservoir and thermosyphoning is forcing flow through it. This is an efficient method for cooling. In the second part of this study, an integrated solar photocatalytic collector is fabricated and tested. Methylene blue dye and photo-activated catalyst were mixed with the testing fluid. The results show that the system was able to disinfect 1.2 ppm of the dye in water by 80% in the presence of  $127 \text{ mg}\cdot\text{L}^{-1}$  of AEROXIDE<sup>®</sup> TiO<sub>2</sub> P90 with the thermal efficiency of  $\eta_{\text{th}} = 0.67$  under the laboratory conditions. It was analyzed under stagnant wind conditions and the heat losses were assessed.

**Keywords:** Photovoltaic cooling; heat sink; PV/T collector; solar photocatalytic collector; waste water treatment.

## **Co-authorship Statement**

I hereby declare the co-authorship for the following chapters:

Chapter 2 is a Journal Article to be submitted to the International Journal of Solar Energy (2016) titled: “Experimental investigation of natural cooling of Polycrystalline modules using three configurations”.

Chapter 3 is a Journal Article submitted to Applied Energy (2016) titled “A two-chamber integrated photocatalytic & solar-thermal system for water cleaning and heating”.

## **Acknowledgements**

I would like to give special thanks to Allah. I would like to give due thanks to my Mother, Shahida Jamil, my sister Ayesha Asad Ali. I am very thankful for my supervisor Dr. Jun Yang`s support in this research work.

I am grateful for the financial support offered by Federal Economic Development Agency for South Ontario and Research Endowment Fund (WAQF), at King Abdulaziz University, Jeddah, Kingdom of Saudi Arabia.

# Table of Contents

Abstract .....	i
Co-authorship Statement.....	ii
Acknowledgements.....	iii
Table of Contents .....	iv
List of Tables .....	vii
List of Figures .....	viii
Nomenclature .....	ix
CHAPTER 1	
Introduction.....	1
1.1 Topic Overview .....	1
1.2 Literature review .....	3
1.2.1 Photovoltaic heating .....	3
1.2.2 Cooling with heat sinks and cavities .....	7
1.2.3 Cooling with PV/T collectors .....	10
1.2.4 Issues in PV-photocatalytic devices .....	12
1.2.5 Solar water heaters-cleaners .....	14
1.3 Problem statement .....	17
1.4 Research hypothesis .....	18
1.5 Objectives.....	19
1.6 Methodology .....	19
1.7 Thesis layout.....	20
1.8 References.....	20

## CHAPTER 2

Experimental investigation of natural cooling of polycrystalline modules using three different configurations.....	27
2.1 Abstract .....	27
2.2 Introduction .....	28
2.3 Experimental methods.....	32
2.3.1 The setup.....	33
2.3.2 The solar simulator .....	36
2.3.3 Temperature and power measurement .....	41
2.3.4 Calibration of sensors and data acquisition system .....	46
2.4 Experimental results.....	47
2.5 Data analysis .....	54
2.5.1 Uncertainty calculation .....	54
2.5.2 Comparative heat transfer coefficient .....	55
2.5.3 Evaluation of heat sink performance .....	63
2.5.4 Evaluation of channel performance .....	64
2.6 Discussion .....	67
2.7 Conclusion.....	72
2.8 References .....	73

## CHAPTER 3

A two-chamber integrated photocatalytic and solar-thermal system for water heating and cleaning.....	78
3.1 Abstract .....	78
3.2 Introduction .....	79

3.3	Experimental setup.....	83
3.3.1	The solar photocatalytic collector.....	86
3.3.2	The solar simulator.....	88
3.3.3	Dye concentration and temperature measurement.....	90
3.3.4	Calibration of equipment and data acquisition system.....	94
3.4	Experimental results.....	94
3.5	Data analysis.....	99
3.6	Discussion.....	105
3.7	Conclusion.....	107
3.8	References.....	108
CHAPTER 4		
	Conclusion.....	113
4.1	Research summary.....	113
4.2	Significance of the findings.....	118
4.3	Future recommendations.....	119
	Curriculum Vitae.....	120

## List of Tables

Table 2-1: Percentage reference spectrums normalized for the 300 - 1100 nm compared to Halogen light .....	40
Table 3-1: Front glass and inside chamber temperatures of the collector under $G = 1004.7$ $\text{W}\cdot\text{m}^{-2}$ of halogen light at steady state .....	96



## List of Figures

Figure 2-1: The four devices under investigation; the Kyocera 20 Watt pc-Si solar panel and the three configurations with cooling devices at the rear of this panel .....	35
Figure 2-2: The Halogen light spectral distribution (above) and irradiance distribution (below) on the devices.....	39
Figure 2-3: Experimental setup of the bare pc-Si panel and the pc-Si panel with heat sink .....	42
Figure 2-4: Experimental setup of the cavity and channel at rear of pc-Si panel .....	44
Figure 2-5: Front surface/glass temperatures over 36 cells of Kyocera Pc-si panel under $G = 1378.2 \text{ W}\cdot\text{m}^{-2}$ with different configurations at the rear .....	48
Figure 2-6: Rear temperatures of the pc-Si panel in bare state, with heat sink, water cavity and channel and its rear and its corresponding power output .....	51
Figure 2-7: Illustration of various heat transfer modes present in the configurations considered in the present study .....	59
Figure 2-8: Convective heat transfer coefficients at the rear of the panel .....	68
Figure 2-9: Local Nusselt numbers along the channel in the present study compared to previous work and hypothetical scenarios .....	71
Figure 3-1: The solar collector and the flow setup .....	84
Figure 3-2: Halogen light spectral distribution and spatial irradiance distribution on the collector.....	89
Figure 3-3: Experimental setup layout and placement of temperature sensors inside the collector and the system.....	93
Figure 3-4: Decomposition of Methylene blue dye ( $\text{C}_{18}\text{H}_{18}\text{C}_1\text{N}_3\text{S}$ ) under $G = 1004.7 \text{ W}\cdot\text{m}^{-2}$ of Halogen light ( $7.0 \text{ W}\cdot\text{m}^{-2}$ of UV light in $\lambda = 300\text{-}400 \text{ nm}$ ) without hydrogen peroxide and oxygen using ( $\square$ ), $12.7 \text{ mg}\cdot\text{L}^{-1}$ ; ( $\blacksquare$ ), $25.7 \text{ mg}\cdot\text{L}^{-1}$ , ( $\blacktriangle$ ) $50.9 \text{ mg}\cdot\text{L}^{-1}$ , ( $\bullet$ ) $76.9 \text{ mg}\cdot\text{L}^{-1}$ and ( $\blacklozenge$ ) $127.4 \text{ mg}\cdot\text{L}^{-1}$ of $\text{TiO}_2 \text{ P90}$ .....	97
Figure 3-5: The heat transfer model of the collector .....	100

## Nomenclature

Symbol	Description
$A$	Area (m <sup>2</sup> )
$A_{base}$	Area of heat sink base (m <sup>2</sup> )
$A_{fin}$	Area of heat sink fins (m <sup>2</sup> )
$C$	Concentration of MB dye (ppm)
$c$	Specific heat capacity (kJ•kg <sup>-1</sup> •K <sup>-1</sup> )
$d$	Diameter of fin (m)
$e$	Experimental error
$E$	Effectiveness of heat sink
$G$	Irradiance/ incident radiation on a surface (W•m <sup>-2</sup> )
$g$	Acceleration due to gravity (m•s <sup>-2</sup> )
$h$	Heat transfer coefficient (W•m <sup>-2</sup> •K <sup>-1</sup> )
$H$	Height of PV panel(m)
$h_{conv,r}$	Convective heat transfer coefficient from the rear of the panel(W•m <sup>-2</sup> •K <sup>-1</sup> )
$h_f$	Total heat transfer coefficient from the front (W•m <sup>-2</sup> •K <sup>-1</sup> )
$k$	thermal conductivity (W•m <sup>-1</sup> •K <sup>-1</sup> )
$l$	Length of one pin fin (m)
$L$	Characteristic length of heat transfer (m)
$M$	Mass (kg)
$\dot{m}$	Mass flow rate of water/mixture (kg•s <sup>-1</sup> )
$n$	Data sample number
$\eta$	efficiency
$\eta_{el}$	Electrical efficiency of PV panel
$\eta_{th}$	thermal efficiency/thermal conversion efficiency
$N$	Population of fins
$Nu$	Nusselt number
$Pr$	Pradtl Number
$P$	Power output of the panel (W)
$q$	Heat transfer rate (W)
$q''$	Heat flux (W•m <sup>-2</sup> )
$q''_{abs}$	Heat flux transferred from the absorber to the water (W•m <sup>-2</sup> )
$q''_b$	Heat flux from the back of the cavity and channel (W•m <sup>-2</sup> )
$q''_{conv}$	Convective heat flux (W•m <sup>-2</sup> )

$q''_{conv,f}$	Convective heat flux from the front ( $W \cdot m^{-2}$ )
$q_{conv,fin}$	Convective heat transfer rate from the fins of heat sink ( $W \cdot m^{-2}$ )
$q''_{conv,base}$	Convective heat transfer by the base of heat sink ( $W \cdot m^{-2}$ )
$q''_f$	Total convective and radiation heat flux from the front ( $W \cdot m^{-2}$ )
$q''_{fin}$	Total convective and radiation heat flux from the fins of heat sink ( $W \cdot m^{-2}$ )
$q''_{rad}$	Radiation heat flux ( $W \cdot m^{-2}$ )
$q''_{rad,f}$	Radiation heat flux at the front ( $W \cdot m^{-2}$ )
$q_{rad,fin}$	Radiation heat transfer rate from the fins of heat sink ( $W \cdot m^{-2}$ )
$q''_{out}$	Heat flux out of solar collector ( $W \cdot m^{-2}$ )
$q''_{in}$	Heat flux into the water of solar collector ( $W \cdot m^{-2}$ )
$Ra$	Rayleigh's Number
$Ra_{cr}$	Critical Rayleigh number
$Ra^*$	Rayleigh number based on fin spacing of heat sink
$S$	Spacing between the fins (m)
$t$	time (s)
$T$	Temperature ( $^{\circ}C$ )
$t_{95}$	Sample-t distribution value at confidence level 95 %
$T_{(x)}$	Local temperature on surface ( $^{\circ}C$ )
$T_a$	Ambient temperature ( $^{\circ}C$ )
$T_b$	Temperature of cavity/channel back cover ( $^{\circ}C$ )
$T_{base}$	Temperature of the base plate of heat sink ( $^{\circ}C$ )
$T_{cell}$	PV panel cell temperature ( $^{\circ}C$ )
$T_{fin}$	Average temperature of the fins of heat sink ( $^{\circ}C$ )
$T_g$	Inner glass temperatures of photocatalytic collector ( $^{\circ}C$ )
$T_{in}$	Inlet temperature of solar collector ( $^{\circ}C$ )
$T_{out}$	outlet temperature of solar collector ( $^{\circ}C$ )
$T_r$	Rear temperature of the PV panel ( $^{\circ}C$ )
$T_w$	Water temperature ( $^{\circ}C$ )
$W$	Width of the PV panel (m)
$x$	Longitudinal distance (m)
$x^*$	Longitudinal non-dimensional distance from the edge of the channel
$y$	Transverse distance (m)

<b>Greek Symbols</b>	<b>Description</b>
$\eta$	Efficiency
$\alpha^*$	Horizontal aspect ratio of channel
$\beta$	Volumetric expansion coefficient ( $K^{-1}$ )
$\beta^*$	Longitudinal aspect ratio of cavity
$\Delta$	Change in quantity
$\varepsilon$	Emissivity
$\theta$	Inclination from the ground ( $^\circ$ )
$\lambda$	Wavelength (nm)
$\nu$	Fluid Kinematic viscosity ( $m^2 \cdot s$ )
$\phi$	Dependent variable (for uncertainty calculation)
$\gamma$	Independent variable (for uncertainty calculation)
$\rho$	Fluid Density ( $kg \cdot m^{-3}$ )
$\sigma$	Stefan-Boltzmann constant ( $W \cdot m^{-2} \cdot K^{-1}$ )
$\delta$	Thickness of pc-Si cell of PV panel (m)

<b>Subscripts</b>	<b>Description</b>
<i>a</i>	ambient
<i>b</i>	back cover
<i>base</i>	Base of fin array
<i>c</i>	Cross section of channel
<i>conv</i>	convection
<i>cr</i>	critical
<i>el</i>	electrical
<i>f</i>	Front
<i>fin</i>	Fin
<i>pv</i>	photovoltaic
<i>r</i>	Rear of panel
<i>rad</i>	Radiation
<i>th</i>	thermal
<i>w</i>	Water

<b>Abbreviations</b>	<b>Description</b>
a.u	Arbitrary Units
ARC	Anti-reflective coating

CPC	Compound Parabolic Collector
DI	De-ionized
DSSR	Double skin sheet reactor
EVA	Ethylene Vinyl Acetate
IEA	International Energy Agency
NIR	Near Infra-Red
MB	Methylene blue
NI	National Instruments
P25	Grade 25 catalyst
P90	Grade 90 catalyst
pc-Si	Polycrystalline silicon
PTC	Parabolic Trough Collector
PV	Photovoltaic
ppm	Parts per million ( concentration)
PV/T	Photovoltaic/ thermal
Std	Standard deviation
TFFBR	Thin film falling film reactor
TiO <sub>2</sub>	Titanium (IV) Oxide
UV	Ultraviolet
VIS	Visible

# CHAPTER 1

## Introduction

### 1.1 Topic Overview

Global climate destabilization as a result of the anthropogenic emission of greenhouse gases is today's most urgent issue because more than half of anthropogenic greenhouse gas emissions are comprised of carbon dioxide from fossil fuel combustion [1]. The alleviation of these harmful emissions from the atmosphere is being performed using PV technology as a sustainable energy generation method.

Polycrystalline silicon (pc-Si) cells in photovoltaic (PV) panels are the preferred cell type for solar energy harvesting. The best-performing pc-Si panels offer individual cell efficiency of  $\eta_{el} = 0.21$  and a collective of  $\eta_{el} = 0.117$  when connected in the panel body [2]. This translates to a conversion of 11.7% of the energy from the sun equivalent to an intensity of  $G = 1000 \text{ W}\cdot\text{m}^{-2}$  normal to the panel surface. This efficiency is attained when cell temperatures are low. One problem with pc-Si PV panels is their inevitable decrease in electrical efficiency/power output due to overheating of cells under the combined effect of intense solar light, low/lack of wind and moderate to high ambient temperatures. Excess heat from the panel is dissipated to the ambient air via convection and radiation heat transfer only in this scenario. Convection (both forced and free) and radiation heat transfer are two mechanisms of heat dissipation, which are insufficient to lower the panel's cell temperature to ideal operating conditions.

Work on enhancing heat transfer at the rear of this panel using passive cooling methods is more economical compared to the artificial forced convection enhancement using non-conservative electrical power dependent methods. One configuration to enhance natural convection heat transfer is attaching extended surfaces at the rear of the PV panel [3]. The present author is not aware of any previous study that deploys highly populated cylindrical pin fin heat sinks at the rear of a PV panel to naturally cool it. There is a need to investigate

this configuration along with adopting other stand-alone configurations that can provide natural cooling. Stand-alone configurations are the least investigated methods to cool PV panels. Currently, conventional water type PV/T collectors are the most effective technique. A PV panel is configured in a heat collecting device that converts a portion of incident solar light to thermal energy which is transported to a cold reservoir. The collector is present in a closed loop system [4]. The water is either forced through the collector or naturally circulating in the loop via thermosyphon effect. This thermosyphon effect is induced by the buoyancy difference between the hot lighter water in the collector and the cold denser water in the reservoir. Thermosyphoning has been recommended to be induced in these systems to circulate the water, as a replacement for water pumps. Thermosyphoning is present in newer photovoltaic-thermal collectors (PV/T collectors) [5]. Current collectors deploy multiple channels below the PV panel as the heat exchanger configurations, but the heat transfer from the rear of the panel to the water is limited by the channels' large aspect ratios. Previous work in heat transfer studies has investigated that a single channel with a small aspect ratio, near to zero, that has thermally developing flow can provide higher heat transfer rates than that from thermally developed flow [6]. There is work missing on comparing the cooling effects achieved between channel with thermally developing flow and heat sinks, and or other stand-alone configurations, as compared to a hot PV panel.

Currently, the combination of improving PV technology, or any form of generation of useful energy from solar light with solar based waste water treatment is a need for society. Extensive wastewater treatment costs and lack of fresh water are burdens on the economy and environment [7]. Over the past few years, the excessive use of pharmaceuticals, personal care products and major textile dyes have introduced toxins into drinking water. One way to remove the dye in water and generate electrical power simultaneously is by solar photocatalytic-PV devices [8]. This combines some designs of PV/T collectors and photo-induced dye reduction via photo-activated Titanium (IV) Oxide ( $\text{TiO}_2$ ) nano-particle catalysts. Much work has been done using light weight  $\text{TiO}_2$  P25 type catalysts to decompose Methylene blue (MB) dye in water with solar light with this combined technology. Current combined technology consists of a channel containing the mixture of this catalyst and dye water flowing above the pc-Si panel. The device is installed in a closed

loop system just like collector setups. This mixture of dye and catalysts absorbs Ultra-violet (UV) and Visible (VIS) light which are also needed by the pc-Si cells to generate electricity [9]. PV panel output suffers and the pumping power is used to circulate the mixture. Traditional solar photocatalytic collectors that clean and heat water only are the leading technology to clean water via solar light and generate hot water for households and should rather be utilized [10]. These solar photocatalytic collectors whose sole purpose is to provide clean water without using PV panels, are a better option.

Solar photocatalytic collectors are present as concentrating and non-concentrating designs and are not concerned with providing efficient water heating. The present author is not aware of any study that addresses the combination of photocatalytic water cleaning with water heating in one collection device that utilize thermosyphoning as the water circulation mechanism, which is a common flow type and cost-free. The present study designed such a device along with addressing its limitations.

## **1.2 Literature review**

### **1.2.1 Photovoltaic heating**

During PV panel testing, the standard test condition (STC) is present where a panel is illuminated under solar light normal to its surface. Normal solar light is termed irradiance with an intensity  $G = 1000 \text{ W}\cdot\text{m}^{-2}$  as shown in Figure 1-1 during STC [2]. This irradiance is the sum of the diffuse, direct and ground reflection of solar radiation when the zenith angle from the sun is at  $48.2^\circ$ . Cell temperature remains constant in the test at  $T_{\text{cell}} = 25^\circ\text{C}$  and the pc-Si PV panel outputs an efficiency of  $\eta_{\text{el}} = 0.117$  [11]. Their efficiency is the ratio of the power output (in Watts) by the product of the front area of the panel and the intensity of light normal to its surface. These are opaque PV panels comprising of a layer of Pyrex-ARC-pc-Si cells-electrical back contact-EVA-Tedlar (layers shown in Figure 1-1). Their efficiency is attained under indoor solar simulators and at constant low cell temperatures. Solar harvesting/when the PV panel is outdoors, is performed by placing it on an open rack mount support frame/using a holding device (on posts) ensuring that its front and rear surfaces are exposed to the ambient air.



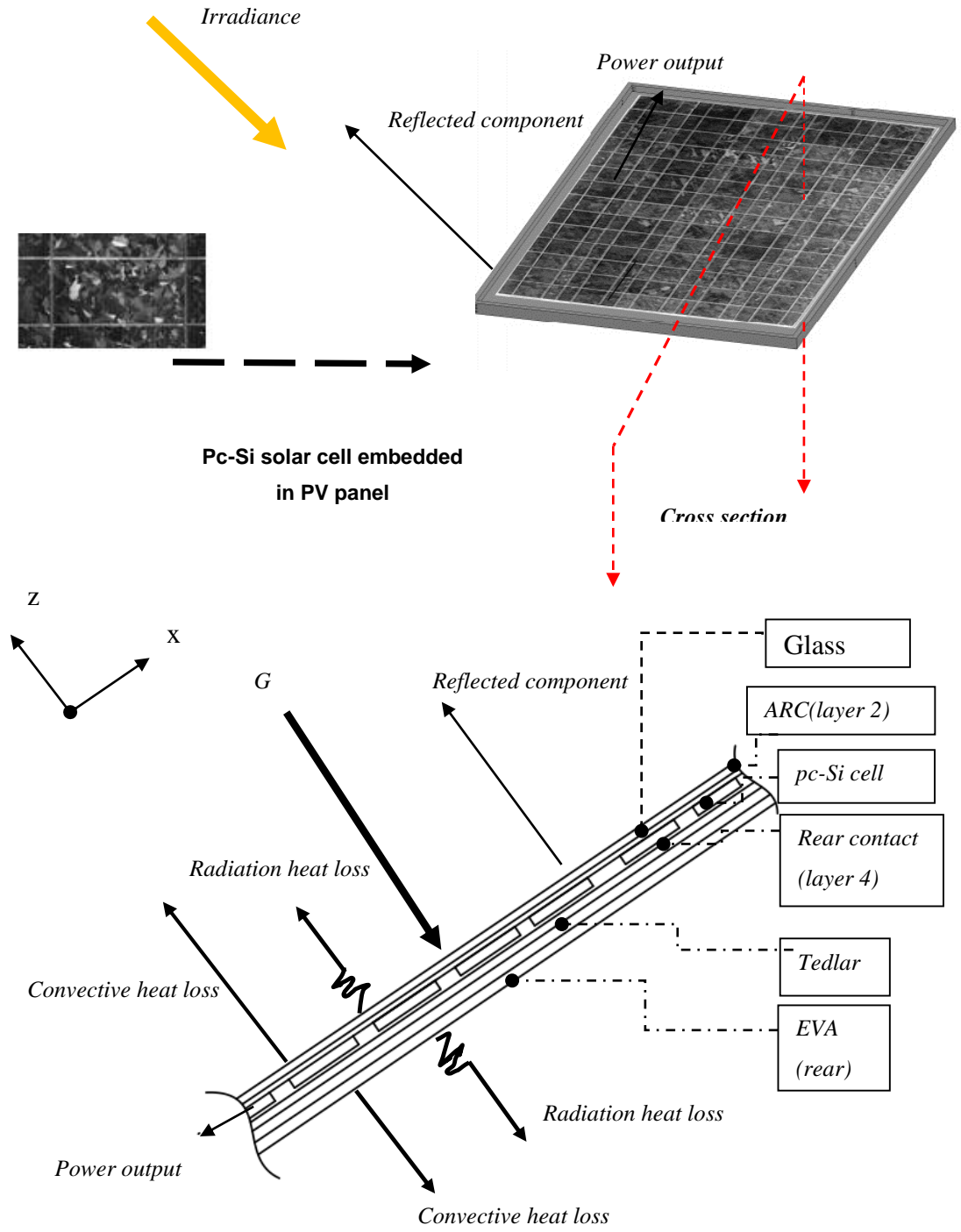


**Figure 1-1: The commercial pc-Si panel (above) and the modes of heat transfer and the outline of its material layers (below) adapted from [12]**

Indoor solar simulators provide the solar radiation which has an AM 1.5 spectrum type on the panel, which is of irradiance  $G = 1000 \text{ W}\cdot\text{m}^{-2}$ . However, the intensity of outdoor solar radiation on the panel varies according to the longitude and latitude of a location, the month of the year and time of day, hence; it does not provide the factory rated output. The PV panel on an open rack mount is inclined at an angle from the ground. The angle's value is based on attaining the maximum power output from the panel. It has been recommended that it should be  $\theta = 30^\circ$ , and the panels orientation is to be; facing south, for solar harvesting in North America [13]. For instance, a PV panel in an open rack mount inclined between  $32^\circ < \theta < 38.1^\circ$  from the ground facing south (in Ottawa and Toronto) still yields an annual production of 272.97 - 283.53 kWh (maximum values) of energy when fluctuating irradiance is present [14], a production value of less than  $500 \text{ W}\cdot\text{m}^{-2}$ . Even with low irradiance, promising power outputs from open rack PV panels have been demonstrated.

This is because the pc-Si cells selectively avail advantage from the different wavelengths of solar light. AM 1.5 spectrum of solar light has UV light ( $\lambda < 400 \text{ nm}$ ) of  $< 5\%$ , a large amount of VIS light ( $\lambda = 400 - 700 \text{ nm}$ ), which is  $57.1\%$  and some NIR (near-infrared) radiation (between  $\lambda = 700 - 1100 \text{ nm}$ ) which is  $42.6\%$  [15]. Over all the conversion is  $\eta_{el} = 0.117$  from the panel when solar light irradiance is  $G = 1000 \text{ W}\cdot\text{m}^{-2}$  of this specific spectrum. Variation in the light source type, such as higher VIS light or drastically low UV light, as those from halogen light simulators still provides power output depending on the light sources, closeness to solar light. The closer the irradiance is to solar light the more chances the panel provides the factory rated output [16]. High intensity of solar irradiance and lack of winds provide a non-idealistic condition of cell heating, which deteriorates electrical efficiency, which the author is aware of.

Literature suggests that cell temperatures in such scenarios increase beyond  $25^\circ\text{C}$  which impacts the pc-Si PV panel efficiency negatively ( $\eta_{el} < 0.117$ ). It is concluded by Evans' [17] that  $\eta_{el}$  is explicitly an indirect function of  $T_{cell}$  and it was assured by King *et al.* [18] that high values of  $G$  and  $0 \text{ m}\cdot\text{s}^{-1}$  wind speeds provide the highest rear panel temperature. A simple data reduction from these previous works [17] & [18], that have been significantly utilized in the past to attain cell temperature for a measured irradiance and wind speed.

They provide some knowledge of the associated panel temperatures. This is a common method of cell temperature determination for given weather conditions without experimental work. For instance, when the solar light is in a range of  $945.8 \text{ W}\cdot\text{m}^{-2} < G < 2449.2 \text{ W}\cdot\text{m}^{-2}$ , cell temperature would be in the range of  $60^\circ\text{C} < T_{\text{cell}} < 125^\circ\text{C}$  when wind speeds are  $0 \text{ m}\cdot\text{s}^{-1}$ . These cell temperatures should be avoided since they deteriorate their efficiency significantly.

An irradiance of  $G > 2449.2 \text{ W}\cdot\text{m}^{-2}$  is not realistic but  $G \geq 945.8 \text{ W}\cdot\text{m}^{-2}$  can occur in hotter climates which yield  $T > 60^\circ\text{C}$ . Along with these cell temperatures, there can be localized hot regions which randomly appear. Localized hot spots can have temperatures up to  $125^\circ\text{C}$ . At this temperature the cell is permanently damaged. These hot spots are random, localized sites where situations of  $T_{\text{cell}} > 125^\circ\text{C}$  are present even if the rest of the panel is at low temperature (i.e.  $T_{\text{cell}} = 40^\circ\text{C}$  in a previous study) and the irradiance is moderately low [19]. They must be avoided. Hot spots arise from impurities in the cell and non-uniform irradiance. Thus solar light should be uniform on the panel and its cooling is essential, if otherwise. However, hot spot temperatures cannot be predicted beforehand. It is thus concluded that a certain bad scenario is  $G \geq 945.8 \text{ W}\cdot\text{m}^{-2}$  and  $T_{\text{cell}} > 60^\circ$  in the present study.

The panel has two modes of heat transfer in such a scenario; natural convection (when no winds are present) and radiation heat transfer as shown in Figure 1-1. The irradiance is absorbed by the panel and after a period of time, the cell temperatures are high and steady. The heat is dissipated by the cells to the front and rear of the panel across the material layers. This heat is then dissipated to the environment by the front glass surface of the panel and the EVA rear surface by natural convection and radiation heat transfer. The total irradiance on the panel is the sum of these heat transfers and the power output of the panel, when steady state is present.

The natural convection heat transfer and radiation heat transfer values can be attained from a hot panel from thermal models in previous work [20, 21]. The Nusselt number (Nu) is a non-dimensional number and is equal to the ratio of convective to conduction heat transfer at the surfaces. Nu is the function of the Rayleigh number, Ra, and the Prandtl number, Pr, of the surface air layers. Rayleigh number is the ratio of buoyancy to the viscous force and

it must be greater than a value of  $1708/\cos\theta$  to ensure natural convection heat transfer is occurring from the surfaces.  $Nu > 1$  means that heat transfer from natural convection is present [22]. Increasing the natural convective heat transfer at the rear, ensuring that  $Nu > 1$  at the rear, is an economical method to attain panel cooling without using electrical powered wind inducement. Such is the case when using standalone methods to cool the panel from its rear, increasing the heat transfer at the rear of the panel (in Figure 1-1), when no winds are present.

### **1.2.2 Cooling with heat sinks and cavities**

One method to cool a hot PV panel is by attaching extended surfaces at the rear [23]. Cylinders, bars, and plates are used to increase the flow of heat from these extended surfaces to the quiescent medium (air). When a hot surface is extended by appendages intimately connected with it, the heat transfer rate from it increases several fold due to the increased surface area. But natural convection from the heat sink,  $Nu > 1$ , at the heat sink, can only be achieved if the geometry of its appendages and their spacing from one another are optimized [24]. In previous work optimized plate fin heat sinks have been used to cool concentrating PV panels [25]. These concentrating devices are different from flat non-concentrating pc-Si PV panels. They contain exterior reflectors. 1 mm thick and 140 mm in height, 1.28 m longitudinal plates with 10 mm spacing from each other are attached to large concentrating PV panels under irradiance of  $G = 814.6 \text{ W}\cdot\text{m}^{-2}$ . Results using no concentration of solar light on the panel are; an increase in the PV panel efficiency. The electrical efficiency  $\eta_{el} = 0.14$  at  $T_{cell} = 58.14^\circ\text{C}$  is present with low natural convection, quantified in this work by the natural convection heat transfer coefficient at the rear of the panel,  $h_{conv,r}$ . The panel is cooling by increasing this coefficient from  $7.46 \text{ W}\cdot\text{m}^{-2}\cdot\text{K}^{-1}$  to  $17.86 \text{ W}\cdot\text{m}^{-2}\cdot\text{K}^{-1}$ . This convective heat transfer coefficient is the proportionality constant of the convective heat transfer flux and the thermodynamic driving force for the flow of heat. The driving force is the temperature difference between the source (heat sink in this scenario) and the quiescent fluid (ambient air in this scenario).

These plate fin heat sinks at the rear of the panel have also been investigated for their optimum length and spacing to cool another concentrating PV panel cell [26]. A  $20 \times 60$  mm cell under solar light of intensity  $G = 1000 \text{ W}\cdot\text{m}^{-2}$  was cooled by 3 plates at its rear of

1 mm thicknesses and heights of 5 mm. Cell temperatures dropped from 68.3°C to 51.3°C when  $1 \text{ m}\cdot\text{s}^{-1}$  wind speeds were present. The heat transfer coefficient utilized in this simulation work was assumed and kept as a constant at  $h_{\text{conv,r}} = 5.8 \text{ W}\cdot\text{m}^{-2}\cdot\text{K}^{-1}$ . This is never the case in realistic scenarios. The heat transfer coefficient is highly dependent on the Nusselt number, Nu, which in-turn is a function of Rayleigh number and the fluid property, Prandtl number. To acquire natural convection,  $\text{Nu} > 1$  and  $\text{Ra} > 1708/\cos\theta$  ( $\theta$  is the inclination of the hot plate/panel) must be present [22]. The present author is not aware of any work that characterizes the cooling from various heat sinks. Hence, there might be a potential for cylindrical pin fin heat sink cooling. These heat sinks have provided the possibility of much larger natural convection heat transfer for a specific range of Rayleigh numbers in previous work. They also provide the added benefit of an increased surface area of heat transfer. It has to be ensured that a heat sink's overall effectiveness is greater than 2 ( $E > 2$ ) [27], while its efficiency should be close to idealistic conditions of  $\eta = 1$ . This guarantees that the heat transfer at the rear of the panel, in Figure 1-1, would be increased by two folds, and also ensures that the thermodynamic driving force of heat transfer from the sink to the ambient air is maximized. The latter is an ideal condition which is used as a comparison tool for heat sink performance. Previous plate fin heat sinks mentioned are down facing heat sinks.

One issue in using down-facing heat sinks with cylindrical fins is that this orientation decreases the heat transfer as compared to when they are up-facing or horizontal facing. However, Sparrow & Vemuri [28] compared a set of five staggered, widely spaced cylindrical pins, diameter  $d = 0.625 \text{ cm}$ , length  $l = 2.54 \text{ cm}$  and investigated the viability of downward facing heat sinks. They utilized 18 - 68 pins on a square base of height 7.62 cm and fin densities of  $0.31 - 1.17 \text{ fins}\cdot\text{cm}^{-2}$ . The Rayleigh number range of experimentation was  $\text{Ra} = 0.8 \times 10^5 - 15 \times 10^5$  which demonstrates laminar natural convection. They attained  $\text{Nu} > 80$  for down-facing heat sinks compared to  $\text{Nu} > 100$  for up facing heat sink when the fin density is  $1.17 \text{ fins}\cdot\text{cm}^{-2}$  and  $\text{Ra} > 15 \times 10^5$ . There is a 15% reduction in the overall heat transfer when using down-facing heat sinks but it is still a viable solution for cooling a hot surface. Both natural convection and radiation heat transfer contribute to the heat losses from this heat sink. They also compared the heat transfer coefficients achieved from longitudinal plate fin heat sinks with these cylindrical

pin fin heat sinks, and have directly mentioned that they encourage the use of the latter in these conditions.

The following criteria are given to attain natural convection for horizontal fin heat sink:  $\eta$   $Ra^* = 0.3 - 600$ ,  $S/d = 1.7-3.5$ , and  $l/L = 0.16-1.37$  as per the investigations of Aihari *et al.* [29] for fin densities between  $1.86 - 9.90$  fins $\cdot$ cm $^{-2}$ .  $Ra^*$  is the modified Rayleigh number, and it is stated that if the product of  $Ra^*$  and  $\eta$  is close to 600, and the geometry of the heat sink is within the ranges above, then surely  $Nu > 1$  can be achieved [30]. They have recommended that  $Ra > 1 \times 10^5$  should be achieved on the base of the heat sink for these criteria to be applicable. It is not known from previous work, that the present author is aware of, that strong natural convection cooling can occur using these heat sinks at the rear of the panel, while meeting these criteria.

Another viable solution can be a differentially heated water cavity at the rear of the panel. Inclined differentially heated cavities have sufficient natural convection strength to provide  $Nu > 1$ , where  $\theta$  is the inclination of the cavity. The longitudinal aspect ratio of the cavity must be greater than unity, ( $\beta^* > 1$ ) and  $Ra > 1708/\cos\theta$  must be surpassed in the water to attain natural convection [31]. Experimental work in the past demonstrates that for Rayleigh numbers in the range of  $1708 < Ra < 5 \times 10^4$ , fluid motion consist of regularly spaced roll cells that are aiding in natural convection [31] and when this cavity is tilted from the ground, the strength of natural convection increases. Larger aspect ratio cavities, such as  $\beta^* = 12$  have a critical tilt angle of  $67^\circ$  after which the natural convection heat transfer in this cavity increases drastically but when an inclination of  $90^\circ$  is surpassed, the heat transfer decreases. This leaves a problem of the hot wall above and cold wall below.

Catton *et al.* [32] has stated that in such a cavity, for low aspect ratios,  $\beta^* = 1, 0.5, 0.2$  inclined at  $\theta = 30^\circ$ , no natural convection is present. For  $\beta^* = 3, 5-7$  and  $10$ , natural convection is present experimentally determined in this previous work to be signified from the Nusselt number range of  $Nu = 1-7$  when  $Ra > 1708/\cos\theta$ . No previous study is present that addresses the usage of such a cavity at the rear of the panel, where the panel is acting as the hot plate placed above the cavity. This seems like a promising cooling method since Arnold *et al.* [33] have demonstrated that  $Nu = 1-10$  are possible for  $Ra = 6 \times 10^4 - 4 \times 10^7$  for inclinations between  $\theta = 15-60^\circ$  in high aspect ratio cavities. The present author is

not aware of any work that has accomplished these numbers from a water cavity at the rear of a hot panel.

### 1.2.3 Cooling with PV/T collectors

Ultimately, the most superior method to enhance the heat transfer at the rear of the panel is the water type PV/T collectors. These collectors are heat exchangers with direct attachment to a hot PV panel. The water passing through the heat exchanger removes the heat from the hot panel and transports it out of this collector to be stored in a reservoir. The reservoir and collector are attached in a closed looped water circuit. The reservoir is placed directly above the collector's top/trailing edge [34]. Insulated tubing is used to connect the apparatus and to avoid heat losses to the environment from the moving water. The collector contains substantial amount of insulation to sustain the heat extracted by the panel and ensures maximum heat transport to the reservoir.

In these collector systems, cooling PV panels and attaining a high thermal efficiency/ a high conversion of solar light to thermal output, are both compulsory. The heat exchanger is either transparent, placed above the panel in Figure 1-1, or below it [34]. The most popular devices are tube and sheet PV/T collector, multiple channels below the panel and a single channel below the panel. The channel types are installed in systems that use thermosyphoning/natural circulation as the water transport mechanism.

A traditional tube with sheet PV/T/collector was recently designed and tested for delivering PV cooling and thermal efficiency by Dubey & Tiwari [35]. At steady state, they demonstrated  $\eta_{el} = 0.11$ ,  $T_{cell} = 45^{\circ}\text{C}$  at reduced temperature of  $0^{\circ}\text{C}\cdot\text{m}^2\cdot\text{W}^{-1}$  and a reasonable thermal efficiency range from varying weather conditions of  $\eta_{th} = 0.5-0.6$ . This reduced temperature is the difference of the inlet and the ambient air by the total irradiance on the panel and the thermal efficiency,  $\eta_{th}$ . The thermal efficiency is the ratio of the thermal output (in flux) by the irradiance on the collector. The maximum thermal efficiency is always attained at  $0^{\circ}\text{C}\cdot\text{m}^2\cdot\text{W}^{-1}$  reduced temperature. A maximum of 60% of the irradiance was transferred from the panel to water in the tubes in this collector. The electrical output of the panel remained near of that when it is expedited under STC value of  $\eta_{el} = 0.117$  of the panel. Thus cooling was significant.

However, channel type PV/T collectors, as per the numerical work of Zondag *et al.* [36] are a better option of cooling since they provide  $\eta_{th} = 0.65$  when a channel is placed above the panel and  $\eta_{th} = 0.63$  when a channel is placed at the rear of the panel. The single channel below a PV panel was the best option from the efficiency point of view and had the higher electrical efficiency of  $\eta_{el} = 0.09$  at  $T_{cell} = 41^\circ\text{C}$ .

Sandnes & Rekstad [37] used PV panel with 26 square-shape box-type channels at its rear (at the rear of the panel in Figure 1-1). This drastically decreased panel temperature from  $T_{cell} = 54^\circ\text{C}$  to  $T_{cell} = 18^\circ\text{C}$  and irradiance of  $G = 748 \text{ W}\cdot\text{m}^{-2}$  on the panel. They included conductive ceramic granules to enhance heat transfer in the channels. It reported the highest ever thermal efficiency,  $\eta_{th} = 0.7$  at zero reduced temperature in cold climates.

One of the most comprehensive works using thermosyphoning in PV/T collectors is by Chow *et al.* [38] (also termed natural circulation), who first proposed a multiple channel below the panel made of aluminum. The electrical efficiency of the panel dropped from  $\eta_{el} = 0.105$  to  $0.085$  and no cell temperature was reported. They created a numerical model of this collector under variable irradiance and concluded that  $\eta_{th} = 0.58$  at  $0 \text{ }^\circ\text{C}\cdot\text{m}^2\cdot\text{W}^{-1}$  reduced temperature and  $\eta_{el} = 0.124$ , which is almost full PV panel output of this collector.

He *et al.* [39] used a collector of the same design as Chow *et al.* [38] with water circulating naturally. They place some solar light absorber sheet around the front of the panel to increase heat gain from the sun. Graphical depiction of  $\eta_{th}$  versus reduced temperatures is given in this work. It is deciphered that  $\eta_{th} = 0.51$  at reduced temperature of  $-0.00814 \text{ }^\circ\text{C}\cdot\text{m}^2\cdot\text{W}^{-1}$  has been attained. Thus, not much effect has been achieved from this modification. Ji *et al.*[40], further optimized (a claim) the same multiple channel at the rear of the PV panel by increasing its collector area to gain more heat from the sun. They also added more channels to increase the mass of water. In the previous two collectors [38, 39],  $65.4 \text{ kg}\cdot\text{m}^{-2}$  of water ( $65.4 \text{ kg}$  of water per  $\text{m}^2$  of the front of the collector) was used while Ji *et al.* increased the mass of water to  $80 \text{ kg}\cdot\text{m}^{-2}$ . This had little or no benefit to thermal efficiencies and cooling of the PV panel. Literature states that more heat can be extracted from the rear of the panel and cool it by using a single channel of a zero aspect ratio.



The profound effect of the aspect ratio of the channel,  $\alpha^*$ , has not been addressed in these collectors. The Nusselt number in this channel increases with decreasing  $\alpha^*$ , which means a higher extraction of heat from the panel will occur. The multiple channel collectors mentioned have aspect ratios  $\alpha^* = 1$  [37] and  $\alpha^* = 0.2$  [39] and  $\alpha^* = 0.5$  [38, 40]. The Nusselt numbers in these channels can be attained from literature [6]. For  $\alpha^* = 1$ ;  $Nu = 3.61$ , for  $\alpha^* = 0.5$   $Nu = 4.11$  and for  $\alpha^* = 0.2$ ;  $Nu = 5.35$  and for  $\alpha^* = 0$ ,  $Nu = 5.385$ . Thus it is sensible to utilize a single channel below the PV panel as the collector heat exchanger configuration to attain the most amount of cell cooling. Furthermore, these previous designs assume developed flow in the channels that designate constant  $Nu$  values along the channel height.

Previous work has indicated that using thermally developing flow in the channel provides higher heat transfer. This is because the Nusselt number is high at the entrance with value  $Nu = 8.44$  which decays to  $Nu = 5.35$  (for  $\alpha^* = 0.25$ ). If this is integrated along the channel,  $Nu > 5.35$  can occur [41]. Thus thermally developing flow is stronger than developed flow. Such a channel, a single channel with thermally developed flow, has not been utilized to cool the panel. There is no work that has addressed its cooling strength as compared to the heat sinks or water cavities at the rear of the panel. Such work is needed since it is not known otherwise and an ease of selection between these cooling methods can be performed in calm wind conditions and high panel temperatures if

From the above review, it is evident that maintaining high electrical efficiency of PV panels is absolutely essential. Deliberate decrease in PV panel efficiency from a collector design is unwise, since pc-Si panels are an expensive technology. Such is an issue is made aware by the present author in recent multifunctional devices that provide electrical power and water cleaning. Such a device combine the generation of electrical power using PV panels and deliver clean water using photocatalysis. Particularly, their power has been realized to be below optimum.

#### **1.2.4 Issues in PV-photocatalytic devices**

Pc-Si panels power output has been sacrificed in combined photocatalytic–PV devices that the present author is addressing. In this device a mixture of MB dye solution (in water) and

TiO<sub>2</sub> catalyst suspension flows over the panel (in Figure 1-1). The MB dye decomposes via UV activated TiO<sub>2</sub> photocatalysis. The type of catalyst used is TiO<sub>2</sub> grade P25. This mixture flows over a commercial pc-Si panel which is generating power output and the mixture under solar light is being cleaned by the phenomena of photocatalysis and photosensitization.

The mixture of VIS light absorbing dye in water, such as MB dye, with TiO<sub>2</sub> P25, responds well to solar light. TiO<sub>2</sub> responds to UV light in a region  $0 < \lambda < 400$  nm to provide photocatalysis and MB dye responds to higher wavelengths of UV light,  $340 < \lambda < 400$  nm to provide photolysis. MB dye undergoes photocatalysis with the catalyst and photolysis under higher wavelengths of UV light without catalyst. No catalyst is needed to achieve the results from photolysis. However, photolysis is a weak cleaning mechanism. As per the investigations of previous work [42, 43], MB dye does not respond to UV light but has an exceptional response to VIS light. This concept is called photosensitization. This phenomenon is present in outdoor solar devices that are experimenting with MB dye and TiO<sub>2</sub>. Experiments without catalyst, to demonstrate photosensitization suggest 20% degradation of 10 mg•L<sup>-1</sup> of MB dye under solar light [44]. However, photocatalysis using TiO<sub>2</sub> is the strongest reaction mechanism that provides the cleanest water.

However, TiO<sub>2</sub> harnesses only a small fraction (~5%) of the entire solar spectrum (in the range  $\lambda = 300-400$  nm). Only 20-30 W•m<sup>-2</sup> of UV light is available from the sun for this reaction to take place [45]. Along with this setback, the catalyst has a smaller surface area and is capable of 10-13.5% surface adsorption of the MB dye. Large adsorption of MB dye on the catalyst signifies the possibility of strong photocatalysis. The present author has made it aware that solar photocatalysis is not a strong method of cleaning MB dye, as compared to artificial indoor UV lamps. It is suggested that combined photocatalytic-PV devices, that utilize solar light, are inadequate of attaining high PV panel power outputs along with these water cleaning setbacks.

Indoor experiments have demonstrated the best results to achieve MB dye cleaning, i.e the testing by Houas *et al.* [46] who utilized a 125 W mercury lamp in a Pyrex glass reactor to decompose this dye with the catalyst. They report an indoor method for the decomposition of MB dye within 110 minutes of initial concentration of  $\approx 22$  ppm using 2.5 g•L<sup>-1</sup> of TiO<sub>2</sub>

P25. These results cannot be attained in outdoor devices such as the combined device mentioned or any other outdoor method.

In combined devices, the pc-Si panel is outputting a diminished 4 Watts as compared to its factory rated 14.5 Watts. 10 Watts are lost by the panel from the design of this particular technology. Furthermore, the mixture of MB dye and catalyst is pushed over the panel using an electrical motor which is rated at 6 Watts, which are being extracted by the panel [8]. This is not an energy efficient method, and involves a design redundancy. The mixture flowing over the panel, responds to 20-30% of the incident solar light between wavelengths of  $700 < \lambda < 1100$  nm. This range is also the response of the pc-Si cells in the panel that are needed to generate electrical power. Thus no material should be placed over the panel for high power output.

Similarly, other studies demonstrate that VIS light absorbing dye, termed Acid Red 26, which has an absorption peak at  $\lambda = 505$  nm, when used against  $0.2 \text{ g}\cdot\text{L}^{-1}$  of  $\text{TiO}_2$  P25 catalyst, a 10 W power output is achieved from the PV panel rated at 30 W [47]. Secondly a similar combined PV-photocatalytic device in previous work was tested using different glass coverings of the channel, to trails for the possibilities of attaining higher power outputs [9]. Results concluded that 14% power loss from a PV panel occurred when the channel had a UV transmittable Pyrex glass and 22% power loss occur using commercial borosilicate glass. Henceforth, no matter what the glass covering would be, a panel will provide lower than factory rated power output with combined devices.

It is more reasonable to utilized parabolic trough collectors (PTCs) and compounds parabolic collectors (CPCs) and non-concentrating collectors that are designed for photocatalytic water cleaning only. However, these devices are not reputed for collecting hot water efficiently, as the PV/T collectors discussed in section 1.2.3.

### **1.2.5 Solar water heaters-cleaners**

These solar photocatalytic collectors are utilized for solar photocatalytic water cleaning only. PTCs concentrate light tremendously, CPCs are low concentrating collectors and non-concentrating collectors do not have light concentration. Concentrating collectors concentrate solar light on the mixture of waste water and catalyst. PTCs utilize direct solar

light while the others utilize direct and diffuse solar light. There is an exhaustive review on these devices in previous publications, but no work addresses their thermal efficiencies when being used for water cleaning [48]. Reviews state that each collector type has its specific use according to their size and deliverance of clean water for various model pollutants and thus they cannot be thoroughly compared.

However, specifically for MB dye water cleaning, CPCs and non-concentrating collectors are the only two devices used for this purpose, of which the present author is aware of. Arias *et al.* [49] report that cleaning of 10 ppm (concentration term) of MB dye was carried out in a CPC and tubular collector (TC) within 315 minutes. This tubular collector was a CPC without the concentrating design and characterized as a non-concentrating collector. The best results were attained using hydrogen peroxide as the reducing agent and oxygen bubbles as the oxidizing agent in the mixture. Results show a 70.8% decrease of 5 ppm of initial concentration of MB dye using the CPC (0.44 g•L<sup>-1</sup> of TiO<sub>2</sub> P25 and a mixture pH of 8.41), and the TC provides 63.4% (using 0.38 g•L<sup>-1</sup> of TiO<sub>2</sub> P25 and mixture pH of 6.34). This work utilized UV lamps as the light source and no thermal efficiency evaluation was performed. There can be no studies reviewed to provide the reader with an evaluated thermal efficiency using solar photocatalytic collectors. However, their water cleaning abilities are by far, the most efficient.

This is because PTCs and CPCs for water cleaning are protégés of their water heating versions [50]. These water heating versions have thoroughly addressed their thermal efficiencies but are incapable of water cleaning. The water heaters are modified so that they may be utilized for water cleaning. The modifications from the heating to cleaning versions are; extraction of the insulation to contain the heat gained by the mixture, removal of the solar absorber materials and the non existence of thermosyphoning (to transport the water). The copper absorber tubes used in water heaters are replaced by borosilicate glass tubes in which the mixture of dye water and catalyst flow [51].

One of the largest collectors for water cleaning is the PTC. It concentrates the direct component of the photo-active ultra-violet part of the solar spectrum by a factor of 30–50 times the incident solar light on the transparent tubes. This provides high intensity UV light for photocatalysis [52]. The catalyst used is TiO<sub>2</sub>, suspended in the tubes with waste water

that has flow rates between 250 and 3500 L•h<sup>-1</sup> [53]. A CPC is comprised of transparent tubing placed in the axis of compound reflectors. Each reflector has one tube and multiples of this pair is placed on a flat bed. CPCs for water cleaning were first developed by Ajona *et al.* [54]. These reflectors have a concentrating factor of 1-1.5 times the irradiance. They utilize the direct component and diffuse component of solar light while their mass flow rates, from the author's knowledge of the present study is not addressed in previous studies. Thermosyphoning is an unused phenomenon in these devices, which can potentially conserve electrical power cost that is used by a water pump.

It is known that these devices are characterized based on their fluid temperatures, i.e TCs and CPCs are low temperature systems that contain mixtures up to 150°C [55] while most PTCs are for above 150°C mixture temperatures. Hence, it is certain that their thermal efficiency evaluation can be easily performed but has not yet been done.

Even the novel non-concentrating collectors have not addressed their thermal efficiency that they are achieving. One non-concentrating collector, addressed in the present study, is the double-skin sheet reactor (DSSR). It has a length of 1.4 m and height of 9.8 m. It is designed for smaller scale applications, such as house hold water cleaning. DSSR contains 30 channels in which the mixture of waste water and suspended catalyst flow through. The channels are covered by a glass sheet which is transmitting solar light. This device is connected to a reservoir of a large volume in a closed loop. A water pump forces the mixture through the collector. The volume flow, measured inductively is 11.8 L•min<sup>-1</sup> [56]. A second novel non-concentrating device is thin-film-falling-bed reactor (TFFBR), which also has not addressed its thermal efficiency. It is one of the first solar reactors to not apply a light-concentrating system. The structure of this technology consists of a sloping glass pane coated with the photocatalyst (e.g., titanium dioxide Degussa P25 or Hombikat UV100) [57]. The polluted water flows on the inclined glass pane forming a very thin film (~100 µm) and is readily decomposed by solar light. TFFBR uses a mass flow rate of 3 m<sup>3</sup>•h<sup>-1</sup>.

PTCs, CPCs and flat plate collectors for water heating consist of insulation and solar absorbers to collect the most amount of solar radiation. Flat plate collectors are utilized for solar water heating when no light concentration is needed. The utilization of solar absorbers

in these three devices has lead forth to high thermal efficiencies. The active collector surface of PTCs consists of heat absorber tubes placed in the axis of parabolic reflectors. The heat absorber tubes are thin copper absorber tubes in an evacuated glass encapsulation [58]. They provide maximum thermal efficiencies of  $\eta_{th} = 0.93$  [59] in a system using a water pump. CPCs consist of the same absorber tubes placed in the axis of compound reflectors. Variations in the reflector designs of CPCs exist in previous work in which the most common design provides high thermal efficiencies within  $0.5 < \eta_{th} < 0.60$  under  $1000 < G < 1200 \text{ W}\cdot\text{m}^{-2}$  [60]. One CPC test in previous studies, using thermosyphon/natural circulation provides  $\eta_{th} = 0.84$  [61] under this irradiance.

Flat plate collectors, the non-concentrating water heaters, provide competitive thermal efficiencies  $\eta_{th} = 0.80$  [62, 63]. The flat plate collectors are a form of non-concentrating water heating devices that constitute of copper tubes which are coated by a solar selective absorber sheets. The collector is insulated at the rear and the design provides minimum heat loss to the environment leading to maximum heat gain by the water. One of the best comparisons of the thermal efficiency of CPC, PTC and flat plate collectors is provided by Kalogirou [63]. The comparison was performed under solar light in the range of  $G = 500 \text{ W}\cdot\text{m}^{-2} - 1000 \text{ W}\cdot\text{m}^{-2}$ . Flat plate collectors provide  $\eta_{th} = 0.8$  while CPCs  $\eta_{th} = 0.7$  and PTCs give  $\eta_{th} = 0.75$ . Thus flat plate collectors are an economical and quality option for water heating. To be able to attain such high thermal efficiencies from solar photocatalytic collectors, design integration is needed. For instance, no previous work utilizes solar absorber material and thermosyphoning in solar photocatalytic collectors. This is cost effective and combines two important functions. Such a collector is absent in previous work according to the review in the present study. If it is to exist, it must meet a criterion of  $\eta_{th} > 0.7$ . It is essential that a non-concentrating collector be created since large concentrating designs are an advanced level of technology. A basic non-concentrating device that decomposes MB dye using  $\text{TiO}_2$  and collects solar light efficiently is projected to be a significant contribution to renewable energy technology, according to the present author.

### **1.3 Problem statement**

The following issues are identified through the literature review:

- i. Photovoltaic cell heating is a major issue in the presence of large solar irradiance, particularly when ambient temperatures are high and winds are under calm conditions.
- ii. The use of passive cooling approaches to dissipate PV cell heat other than PV/T is not well explored.
- iii. The use of integrated devices for simultaneous water treatment and heating is not well investigated.

## **1.4 Research hypothesis**

It is hypothesized that a cylindrical pin fin heat sink at the rear of the panel can naturally cool the panel. It has already been reviewed in previous studies that this heat sink should be within the optimum geometries as those of previous work. Since this is a down-facing heat sink, the natural convection heat transfer from it would decrease by a slight amount as compared to when it is horizontal facing (as mentioned in section 1.2.2). This is a hypothesis. Nevertheless, it is expected that the buoyancy effects from natural convection will be large and that the heat transfer from natural convection from the heat sink would surpass that of the rear of a panel without it. It is also hypothesized that a water cavity can cool this bare panel when attached to its rear. If it resembles a differentially heated problem, the buoyancy effects in the water are strong and steady and they will cool the panel by a noteworthy amount, as previous work has demonstrated. It is hypothesized that the bare panel can be cooled using a single channel at its rear. It would provide a heat transfer Nusselt number larger than those in previous works that have used multiple channels. The single channel is of a smaller aspect ratio than of previous work and its thickness is hypothesized to provide the added advantage of thermally developing flow along its length. This is expected to increase the heat transfer at the rear by a significant amount as compared to when it is thermally developed. For the last research segment of this thesis work, it is hypothesized that a fabricated non-concentrating solar photocatalytic collector can provide both functions of water cleaning and heating, with high thermal efficiency of  $\eta_{th} = 0.7$ . The design hypothesis is of a two chamber collector; one chamber absorbs the heat and transfers

it to the second chamber with the catalyst and waste water mixture. The dye is hypothesized to photo-decompose in this device.

## **1.5 Objectives**

The objectives of the present study are:

- i. To experimentally investigate various cooling configurations at the rear of a commercial PV panel
- i. To experimentally investigate the feasibility of an integrated device for simultaneous water treatment and heating using sunlight.

## **1.6 Methodology**

The above objectives are met through an experimental study conducted in a laboratory environment. Cooling of the commercial pc-Si PV panel is done using three configurations at its rear, which are assembled in the laboratory and are compared with a bare pc-Si PV panel. The irradiance source is artificial and its only purpose is to heat the panel and provide power output. Commercially available heat sinks are used in the present study. A water cavity of  $\beta^* \approx 12$  is fabricated with PVC sheets and attached at the rear of the hot panel. The cavity has a thin PVC back cover that served as the colder plate. No external cooling is provided to these standalone devices that can assist them in attaining the objectives. It was aimed to achieve natural convection in the water as that of a differentially heated cavity problem, without cooling its back side. A water channel of the lowest aspect ratio possible is created with PVC sheets and attached at the rear of the panel as the 3rd configuration. The channel is connected to a cold reservoir so that the thermosyphon effect initiates from the buoyancy differences between the hot water in the channel and the cold water at the neck of the reservoir for water circulation. These experiments are conducted in a controlled laboratory setting at Western University and initiated after a significant amount of room temperature monitoring prior to the experimental setup. The methods of experimentation were not performed without ensuring thermal equilibrium of the apparatus with the environment along with conducting the necessary safety standards of the laboratory.



## 1.7 Thesis layout

The thesis is organized in the following method:

**Chapter 1:** This chapter is a review of previous studies on photovoltaic cooling methods and photocatalytic collectors and photocatalytic-PV devices. It also contains the hypothesis, the objectives and the methodology of the present study.

**Chapter 2:** This chapter contains an experimental study of cooling a photovoltaic panel using a heat sink, a water cavity and a single channel below the PV panel. The results and discussions from the study are presented.

**Chapter 3:** This chapter consists of an experimental study on the photocatalytic collector that cleans and heats water simultaneously. The limitations of these two functions are discussed.

**Chapter 4:** This chapter discusses the research summary, the findings and the recommendations for future work on this topic.

## 1.8 References

- [1] Šúri, M., Huld, T. A., Dunlop, E. D., and Ossenbrink, H. A., 2007, "Potential of solar electricity generation in the European Union member states and candidate countries," *Solar Energy*, 81(10), pp. 1295-1305.
- [2] Green, M. A., Emery, K., Hishikawa, Y., Warta, W., and Dunlop, E. D., 2015, "Solar cell efficiency tables (Version 45)," *Progress in Photovoltaics: Research and Applications*, 23(1), pp. 1-9.
- [3] Royne, A., Dey, C. J., and Mills, D. R., 2005, "Cooling of photovoltaic cells under concentrated illumination: a critical review," *Solar Energy Materials and Solar Cells*, 86(4), pp. 451-483.
- [4] Chow, T. T., 2010, "A review on photovoltaic/thermal hybrid solar technology," *Applied Energy*, 87(2), pp. 365-379.

- [5] Duffie, J. A., and Beckman, W. A., 1980, "Solar water heating: active and passive," Solar Engineering of Thermal Processes, Wiley New York etc., New York, pp. 487-489.
- [6] Rohsenow, W. M., Hartnett, J. P., and Cho, Y. I., 1998, "Forced Convection, Internal Flow in Ducts," Handbook of Heat transfer, McGraw-Hill New York, p. 5.68.
- [7] Hashimoto, K., Irie, H., and Fujishima, A., 2005, "TiO<sub>2</sub> photocatalysis: a historical overview and future prospects," Japanese Journal of Applied Physics, 44(12R), p. 8269.
- [8] Wang, Z., Wang, Y., Vivar, M., Fuentes, M., Zhu, L., and Qin, L., 2014, "Photovoltaic and photocatalytic performance study of SOLWAT system for the degradation of Methylene Blue, Acid Red 26 and 4-Chlorophenol," Applied Energy, 120, pp. 1-10.
- [9] Sarria, V., Kenfack, S., Malato, S., Blanco, J., and Pulgarin, C., 2005, "New heliophotocatalytic-photovoltaic hybrid system for simultaneous water decontamination and solar energy conversion," Solar Energy, 79(4), pp. 353-359.
- [10] Rodriguez, S. M., Gálvez, J. B., Rubio, M. M., Ibáñez, P. F., Padilla, D. A., Pereira, M. C., Mendes, J. F., and De Oliveira, J. C., 2004, "Engineering of Solar Photocatalytic Collectors," Solar Energy, 77(5), pp. 513-524.
- [11] McEvoy, A., Markvart, T., Castañer, L., Markvart, T., and Castaner, L., 2003, "Testing, monitoring and calibration," Practical Handbook of Photovoltaics: Fundamentals and Applications, Elsevier, pp. 793-795.
- [12] Skoplaki, E., and Palyvos, J., 2009, "On the temperature dependence of photovoltaic module electrical performance: A review of efficiency/power correlations," Solar Energy, 83(5), pp. 614-624.
- [13] Tiwari, G. N., and Dubey, S., 2010, "PV array analysis," Fundamentals of photovoltaic modules and their applications, Royal Society of Chemistry, Cambridge, UK, pp. 119-121.
- [14] Rowlands, I. H., Kemery, B. P., and Beausoleil-Morrison, I., 2011, "Optimal solar-PV tilt angle and azimuth: An Ontario (Canada) case-study," Energy Policy, 39(3), pp. 1397-1409.

- [15] Hulstrom, R., Bird, R., and Riordan, C., 1985, "Spectral solar irradiance data sets for selected terrestrial conditions," *Solar Cells*, 15(4), pp. 365-391.
- [16] Emery, K., 1986, "Solar simulators and I-V measurement methods," *Solar Cells*, 18(3), pp. 251-260.
- [17] Evans, D., 1981, "Simplified method for predicting photovoltaic array output," *Solar Energy*, 27(6), pp. 555-560.
- [18] King, D. L., Kratochvil, J. A., and Boyson, W. E., 2004, Photovoltaic array performance model, United States. Department of Energy Sandia National Laboratories, Albuquerque, pp 21-28.
- [19] Herrmann, W., Wiesner, W., and Vaassen, W., "Hot spot investigations on PV modules-new concepts for a test standard and consequences for module design with respect to bypass diodes," *Proc. Photovoltaic Specialists Conference, 1997.*, Conference Record of the Twenty-Sixth IEEE, IEEE, pp. 1129-1132.
- [20] Armstrong, S., and Hurley, W., 2010, "A thermal model for photovoltaic panels under varying atmospheric conditions," *Applied Thermal Engineering*, 30(11), pp. 1488-1495.
- [21] Jones, A., and Underwood, C., 2001, "A thermal model for photovoltaic systems," *Solar Energy*, 70(4), pp. 349-359.
- [22] Fujii, T., and Imura, H., 1972, "Natural-convection heat transfer from a plate with arbitrary inclination," *International Journal of Heat and Mass Transfer*, 15(4), pp. 755-767.
- [23] Kraus, A. D., Aziz, A., and Welty, J., 2002, "Convection with simplified restraints " *Extended Surface Heat Transfer*, John Wiley & Sons., New York, pp. 6-7.
- [24] Kraus, A. D., Aziz, A., and Welty, J., 2002, "Heat Transfer considerations " *Extended Surface Heat Transfer*, John Wiley & Sons, New York, pp. 171 -172.
- [25] Luque, A., Sala, G., Arboiro, J., Bruton, T., Cunningham, D., and Mason, N., 1997, "Some results of the EUCLIDES photovoltaic concentrator prototype," *Progress in Photovoltaics: Research and Applications*, 5(3), pp. 195-212.
- [26] Natarajan, S. K., Mallick, T. K., Katz, M., and Weingaertner, S., 2011, "Numerical investigations of solar cell temperature for photovoltaic concentrator system with

- and without passive cooling arrangements," *International Journal of Thermal Sciences*, 50(12), pp. 2514-2521.
- [27] Bergman, T. L., Incropera, F. P., and Lavine, A. S., 2011, "One Dimensional, steady-state conduction," *Fundamentals of Heat and Mass Transfer*, John Wiley & Sons, New York, pp. 155-160.
- [28] Sparrow, E., and Vemuri, S., 1986, "Orientation effects on natural convection/radiation heat transfer from pin-fin arrays," *International Journal of Heat and Mass Transfer*, 29(3), pp. 359-368.
- [29] Aihara, T., Maruyama, S., and Kobayakawa, S., 1990, "Free convective/radiative heat transfer from pin-fin arrays with a vertical base plate (general representation of heat transfer performance)," *International Journal of Heat and Mass Transfer*, 33(6), pp. 1223-1232.
- [30] Bahadur, R., and Bar-Cohen, A., 2005, "Thermal design and optimization of natural convection polymer pin fin heat sinks," *Components and Packaging Technologies, IEEE Transactions on*, 28(2), pp. 238-246.
- [31] Bergman, T. L., Incropera, F. P., and Lavine, A. S., 2011, "Free Convection " *Fundamentals of Heat and Mass Transfer*, John Wiley & Sons, New York, pp. 599-624.
- [32] Catton, I., Ayyaswamy, P., and Clever, R., 1974, "Natural convection flow in a finite, rectangular slot arbitrarily oriented with respect to the gravity vector," *International Journal of Heat and Mass Transfer*, 17(2), pp. 173-184.
- [33] Arnold, J., Catton, I., and Edwards, D., 1976, "Experimental investigation of natural convection in inclined rectangular regions of differing aspect ratios," *Journal of Heat Transfer*, 98(1), pp. 67-71.
- [34] Duffie, J. A., and Beckman, W. A., 1980, "Solar water heating - Active and Passive ", *Solar Engineering of Thermal Processes*, John Wiley & Sons, New York, pp. 487-489.
- [35] Dubey, S., and Tiwari, G., 2008, "Thermal modeling of a combined system of photovoltaic thermal (PV/T) solar water heater," *Solar Energy*, 82(7), pp. 602-612.

- [36] Zondag, H., De Vries, D., Van Helden, W., Van Zolingen, R., and Van Steenhoven, A., 2003, "The yield of different combined PV-thermal collector designs," *Solar Energy*, 74(3), pp. 253-269.
- [37] Sandnes, B., and Rekstad, J., 2002, "A photovoltaic/thermal (PV/T) collector with a polymer absorber plate. Experimental study and analytical model," *Solar Energy*, 72(1), pp. 63-73.
- [38] Chow, T., He, W., and Ji, J., 2006, "Hybrid photovoltaic-thermosyphon water heating system for residential application," *Solar Energy*, 80(3), pp. 298-306.
- [39] He, W., Chow, T.-T., Ji, J., Lu, J., Pei, G., and Chan, L.-s., 2006, "Hybrid photovoltaic and thermal solar-collector designed for natural circulation of water," *Applied Energy*, 83(3), pp. 199-210.
- [40] Ji, J., Lu, J.-P., Chow, T.-T., He, W., and Pei, G., 2007, "A sensitivity study of a hybrid photovoltaic/thermal water-heating system with natural circulation," *Applied Energy*, 84(2), pp. 222-237.
- [41] Rohsenow, W. M., Hartnett, J. P., and Cho, Y. I., 1998, "Forced convection, in internal flow in ducts," *Handbook of Heat Transfer*, McGraw-Hill New York.
- [42] Konstantinou, I. K., and Albanis, T. A., 2004, "TiO<sub>2</sub>-assisted photocatalytic degradation of azo dyes in aqueous solution: kinetic and mechanistic investigations: A review," *Applied Catalysis B: Environmental*, 49(1), pp. 1-14.
- [43] Tennakone, K., Senadeera, S., and Priyadarshana, A., 1993, "TiO<sub>2</sub> catalysed photo-oxidation of water in the presence of methylene blue," *Solar Energy Materials and Solar Cells*, 29(2), pp. 109-113.
- [44] Kuo, W., and Ho, P., 2006, "Solar photocatalytic decolorization of dyes in solution with TiO<sub>2</sub> film," *Dyes and Pigments*, 71(3), pp. 212-217.
- [45] Rajeshwar, K., Osugi, M., Chanmanee, W., Chenthamarakshan, C., Zaroni, M., Kajitvichyanukul, P., and Krishnan-Ayer, R., 2008, "Heterogeneous photocatalytic treatment of organic dyes in air and aqueous media," *Journal of Photochemistry and Photobiology C: Photochemistry Reviews*, 9(4), pp. 171-192.
- [46] Houas, A., Lachheb, H., Ksibi, M., Elaloui, E., Guillard, C., and Herrmann, J.-M., 2001, "Photocatalytic degradation pathway of methylene blue in water," *Applied Catalysis B: Environmental*, 31(2), pp. 145-157.

- [47] Fuentes, M., Vivar, M., Scott, J., Srithar, K., and Skryabin, I., 2012, "Results from a first autonomous optically adapted photocatalytic–photovoltaic module for water purification," *Solar Energy Materials and Solar Cells*, 100, pp. 216-225.
- [48] Malato Rodríguez, S., Blanco Gálvez, J., Maldonado Rubio, M., Fernández Ibáñez, P., Alarcón Padilla, D., Collares Pereira, M., Farinha Mendes, J., and Correia de Oliveira, J., 2004, "Engineering of solar photocatalytic collectors," *Solar Energy*, 77(5), pp. 513-524.
- [49] Arias, F., Ortiz, E., López–Vásquez, A., Colina–Márquez, J., and Machuca, F., 2008, "Photocatalytic decolorization of methylene blue with two photoreactors," *Journal of Advanced Oxidation Technologies*, 11(1), pp. 33-41.
- [50] Malato, S., Blanco, J., Alarcón, D. C., Maldonado, M. I., Fernández-Ibáñez, P., and Gernjak, W., 2007, "Photocatalytic decontamination and disinfection of water with solar collectors," *Catalysis Today*, 122(1), pp. 137-149.
- [51] Santamouris, M., 2014, "Spectral selective material for efficient visible, solar and thermal radiation control " *Solar Thermal Technologies for Buildings: The State of the Art*, M. Santamouris, ed., Routledge, pp. 39-41.
- [52] Romero, M., Blanco, J., Sanchez, B., Vidal, A., Malato, S., Cardona, A. I., and Garcia, E., 1999, "Solar photocatalytic degradation of water and air pollutants: challenges and perspectives," *Solar Energy*, 66(2), pp. 169-182.
- [53] Minero, C., Pelizzetti, E., Malato, S., and Blanco, J., 1993, "Large solar plant photocatalytic water decontamination: degradation of pentachlorophenol," *Chemosphere*, 26(12), pp. 2103-2119.
- [54] Ajona, J., and Vidal, A., 2000, "The use of CPC collectors for detoxification of contaminated water: Design, construction and preliminary results," *Solar Energy*, 68(1), pp. 109-120.
- [55] Blanco-Galvez, J., Fernández-Ibáñez, P., and Malato-Rodríguez, S., 2007, "Solar photocatalytic detoxification and disinfection of water: recent overview," *Journal of Solar Energy Engineering*, 129(1), pp. 4-15.
- [56] van Well, M., Dillert, R. H., Bahnemann, D. W., Benz, V. W., and Mueller, M., 1997, "A novel nonconcentrating reactor for solar water detoxification," *Journal of Solar Energy Engineering*, 119(2), pp. 114-119.

- [57] Zayani, G., Bousselmi, L., Mhenni, F., and Ghrabi, A., 2009, "Solar photocatalytic degradation of commercial textile azo dyes: Performance of pilot plant scale thin film fixed-bed reactor," *Desalination*, 246(1), pp. 344-352.
- [58] Bakos, G., Ioannidis, I., Tsagas, N., and Seftelis, I., 2001, "Design, optimisation and conversion-efficiency determination of a line-focus parabolic-trough solar-collector (PTC)," *Applied Energy*, 68(1), pp. 43-50.
- [59] Hua, M., Zhang, L., Fan, L., Lv, Y., Lu, H., Yu, Z., and Cen, K., 2015, "Experimental investigation of effect of heat load on thermal performance of natural circulation steam generation system as applied to PTC-based solar system," *Energy Conversion and Management*, 91, pp. 101-109.
- [60] Kim, Y., Han, G., and Seo, T., 2008, "An evaluation on thermal performance of CPC solar collector," *International Communications in Heat and Mass Transfer*, 35(4), pp. 446-457.
- [61] Okoronkwo, C. A., Ogueke, N. V., and Nwaigwe, K. N. A., E.E 2008, "Evaluation of the thermal performance of thermosyphon water heating systems using compound parabolic solar collector " *International Journal of Engineering and Innovative Technology* 4(3), pp. 1-5.
- [62] Taherian, H., Rezaei, A., Sadeghi, S., and Ganji, D., 2011, "Experimental validation of dynamic simulation of the flat plate collector in a closed thermosyphon solar water heater," *Energy Conversion and Management*, 52(1), pp. 301-307.
- [63] Kalogirou, S. A., 2004, "Solar thermal collectors and applications," *Progress in Energy and Combustion Science*, 30(3), pp. 231-295.

## CHAPTER 2

### Experimental investigation of natural cooling of polycrystalline modules using three different configurations

#### 2.1 Abstract

Three methods to naturally cool a bare pc-Si panel in an open rack mount support frame under halogen light by increasing the heat transfer at the rear are undertaken in this work. These are done by attaching (i) a staggered arranged cylindrical pin fin heat sink to a selected prime surface of the rear of the PV panel, (ii) a water cavity of aspect ratio  $\beta^* = 12.08$  to the rear and (iii) a channel of aspect ratio  $\alpha^* = 0.08$  to the rear. Channel was connected to a cold reservoir in a closed looped system and had natural circulation of water via thermosyphoning. The essential temperatures of the configurations and power output of the pc-Si panel was experimentally determined in a controlled laboratory setting under a steady halogen light solar simulator and calm wind conditions. At steady state, the heat transfer coefficient at the rear of the bare panel is  $4.4 \text{ W}\cdot\text{m}^{-2}\cdot\text{K}^{-1}$  while using the heat sink is  $1.3 \text{ W}\cdot\text{m}^{-2}\cdot\text{K}^{-1}$  and the channel provides  $141 \text{ W}\cdot\text{m}^{-2}\cdot\text{K}^{-1}$ . The cavity is only providing cooling. Natural convection is not enhanced by the heat sink but the overall heat transfer from convection and radiation at the rear of the panel is larger than that of the bare panel. Forcing water in the channel, from thermosyphoning/natural circulation, is the best method to lower panel temperatures in this study.

**Keywords:** Natural convection; photovoltaic cooling; heat sink; PV/T collector



## 2.2 Introduction

Pc-Si (polycrystalline) PV ( photovoltaic) panels convert 11.7% of incident solar light to electrical power output ( $\eta_{el} = 0.0117$ ) [1]. The solar light is of intensity  $1000 \text{ W}\cdot\text{m}^{-2}$  and with cell temperatures of  $25^\circ\text{C}$  for this maximum conversion to occur. Traditionally, the PV panel placed on an open rack mount support frame inclined at  $\theta = 30^\circ$  from the ground.

Outdoor climate conditions are deviant from this standard test condition and the power output usually deteriorates because of cell heating [2]. This occurs when the irradiance is greater than  $1000 \text{ W}\cdot\text{m}^{-2}$  and  $0 \text{ m}\cdot\text{s}^{-1}$  wind conditions are present [3]. Such a panel will have rear temperatures exceeding  $50^\circ\text{C}$  and according to the expressions by Evans [4] ;  $\eta_{el}$  (the electrical efficiency) will drop from its maximum of 0.117 to 0.096 . This efficiency occurs when the rear temperature exceeds  $50^\circ\text{C}$ . More heating issues occur from non-uniform irradiance on the panel that leads to uneven power generation from the cells and localized hot spot regions occur. Previous work has stated that cell temperatures of hot spots may exceed  $125^\circ\text{C}$  and damage the pc-Si panel [5]. Hence such a panel must be cooled.

These pc-Si panels are opaque devices that have materials of glass/ EVA /  $\text{TiO}_2$  /pc-Si / EVA /PE-Al-Tedlar layers (from front to rear) and have been subjected to numerous studies involving the determination of their cell temperatures under various bad scenarios (shown in Figure 1-1). Pc-Si panels of such types are those in the works of Hurely & Armstrong [6] who performed thermal modelling of Siemens PV panels and studies by Tina & Abate [7] who performed thermal modelling of identical Kyocera PV panels to determine their cell temperatures when calm winds are present and the irradiance is varying. One method to cool this panel naturally is using extended surfaces at its rear.

Extended surfaces/heat sinks behind a PV panel, that provides the benefit of increasing the heat transfer via natural convection, have been implemented to concentrating photovoltaic cells only (that the author is aware of). Natural convection is attained when no wind is present. These panels are placed under  $1000 \text{ W}\cdot\text{m}^{-2}$  of solar light with longitudinal/plate fin heat sink extrusions at the rear [8]. These devices demonstrate electrical efficiency

increase when cell temperature decrease from natural convection cooling. The electrical efficiency of the panel using longitudinal heat sink increases;  $\eta_{el} = 0.143$  at  $T_{cell} = 58.14^{\circ}\text{C}$  to  $\eta_{el} = 0.165$  at  $T_{cell} \approx 25^{\circ}\text{C}$ . This has occurred when the natural coefficient of heat transfer from natural convection increases from  $7.746 \text{ W}\cdot\text{m}^{-2}\cdot\text{K}^{-1}$  to  $17.86 \text{ W}\cdot\text{m}^{-2}\cdot\text{K}^{-1}$ .

Plate fin heat sinks have also been utilized to cool a single solar cell in previous work [9] in numerical studies using Fluent ©. A  $20 \times 60$  mm cell under  $1000 \text{ W}\cdot\text{m}^{-2}$  was cooled by 3 plates each of 1 mm thickness and a plate height of 5 mm. Cell temperatures dropped from  $68.3^{\circ}\text{C}$  to  $51.3^{\circ}\text{C}$ . The heat transfer coefficient utilized in this simulation work was assumed and kept as a constant at  $h_{conv,r} = 5.8 \text{ W}\cdot\text{m}^{-2}\cdot\text{K}^{-1}$ . This coefficient was assumed in this study present and not measured prior the simulations. The natural convection heat transfer coefficient is affected by the geometry of the heat sink, the total surface area of the fins and the ambient temperatures and wind speeds. There is limited work that addresses the benefit of increasing natural convection heat transfer using cylindrical pin fin heat sinks at the rear of the panel. This heat sink has provide high natural convection heat transfer on vertical hot surfaces, i.e  $Nu = 60-100$  when the Rayleigh number signifying buoyancy effects from natural convection is between  $Ra = 0.6 \times 10^5 - 15 \times 10^5$  [10]. Similar natural convection is present using various other geometry sizes [11]. When  $Nu > 1$ , natural convection occurs while if it is less than 1, there is only condition and radiation heat transfer from this plate.

Another method to cool the PV panel using stand-alone methods as such is by attaching a water cavity attached to its rear. There is no study that has implemented this water cavity at the rear of a hot panel. Previous work has demonstrated that the heat transfer coefficient can be increased on the surface of a hot plate which is inclined at  $\theta = 30^{\circ}$  from the ground by attaching its rear end to a water cavity. The longitudinal aspect ratio criteria of the cavity; between  $1 < \beta^* < 12$ , must be met to attain natural convection. This occurs when the Rayleigh number,  $Ra$ , surpasses a critical value of  $1708/\cos\theta$  which is  $Ra = 1.107 \times 10^4$  for  $\theta = 30^{\circ}$ . The aspect ratio is the geometrical ratio between the height of the plate ( $H$ ) by the thickness of the cavity ( $L$ ) [12]. Such a problem has been experimented before in previous work by Catton *et al.* [13] who stated that a cavity with aspect ratios of  $\beta^* = 3, 5-7$  and  $10$ , inclined at  $\theta = 30^{\circ}$  from the ground, with  $Ra > 1.107 \times 10^4$  will provide natural

convection. Their studies were portrayed by the Nusselt number criteria of  $Nu > 1$ . It must be greater than 1 for natural convection to occur in this cavity. The experimental ranges for higher aspect ratio cavities ( $\beta^* = 6$ ), or thinner cavities, are  $Nu = 1 - 7$  for  $Ra = 2 \times 10^4 - 2 \times 10^6$ .

Some studies have limited natural convection to the largest aspect ratio of  $\beta^* = 12$ , inclinations between  $\theta = 15 - 60^\circ$  and criteria of  $Ra > 6 \times 10^4$  [12] that have demonstrated natural convection. Hence forth possibilities of increasing natural convection at the rear of the panel using this water cavity can be beneficial, but it is not certain if it would exceed that of using a dense heat sink.

The most accepted method of cooling a panel is by water PV/T collectors. A fraction of the solar radiation incident on the collector is converted to thermal output, in the form of hot water, which is stored in a insulated reservoir [14]. The water is transported out of the collector via the use of electrical powered pumps or by the thermosyphon phenomena; the latter which is free of cost and a trend in the last decade in these PV/T collector systems. In this phenomenon the hot, less denser fluid in the collector is replaced by the cold denser fluid in the cold reservoir tank due to buoyancy differences between these fluids, causing a circulatory flow mechanism in the system [15]. This mechanism is free of cost and expected from water PV/T collectors.

The traditional water PVT/collector is the tube and sheet collector such as that made by Dubey & Tiwari [16] and provides  $\eta_{el} = 0.11$  efficiency at  $T_{cell} = 45^\circ$ . Its cooling abilities are considerable. The collector operates at reduced temperature of  $0^\circ C \cdot m^2 \cdot W^{-1}$ , with tremendous thermal outputs of  $\eta_{th} = 0.6$ . These come with the cost of a 35-75 W DC pump. These tube and sheet collectors were compared against channel collectors which became the most popular and promising heat exchange design for passive cooling of PV panels and simultaneous hot water generation [17, 18]. At reduced temperature of  $0^\circ C \cdot m^2 \cdot W^{-1}$ , the thermal efficiencies of a tube and sheet collectors is  $\eta_{th} = 0.58$  compared to  $\eta_{th} = 0.63$  of a channel at the rear of a PV panel. This configuration provides the best cooling, judged from electrical efficiency increase of  $\eta_{el} = 0.09$  to  $\eta_{el} = 0.092$  in these numerical studies.

Experimental PV/T collectors using a channel concept consist of deploying multiple channels below the PV panel. Sandnes & Rekstad [19] investigated the energy performance 26 square-shape box-type absorber channels below a PV panel. Thermal efficiencies were  $\eta_{th} = 0.7$  in cold climate conditions and cell temperatures were cool at  $T_{cell} = 18^{\circ}\text{C}$  at ambient low ambient temperatures of  $T_a = 5^{\circ}\text{C}$ . A pump was used to drive the water in the system which is not energy conservative. Natural circulating system were later used in these collectors by Chow *et al.* [20, 21] , He *et al.* [22] and Ji *et al.* [23] without thermally conductive granules.

Chow *et al.* [20, 21] first proposed a numerical model of a multiple channel below the panel collector. Results demonstrate that the electrical efficiency dropped from  $\eta_{el} = 0.105-0.085$  and the collector gave reasonable thermal efficiencies,  $\eta_{th} = 0.58$  at zero reduced temperature. Better results were achieved without a glass cover above the panel of:  $\eta_{el} = 0.125$  and  $\eta_{th} > 0.58$ . This uncovered device was further experimented by increasing the front collector that absorbs solar radiation by He *et al.* [22] . Modifications were the addition of solar absorbers around the circumference of the panel. This had little effect on the performance of the panel since  $\eta_{th} = 0.40$  was captured at zero reduced temperature. Ji *et al.* [23] increase the water content at the rear of the panel in this collector and reported a mass flow rate of  $80 \text{ kg}\cdot\text{m}^{-2}\cdot\text{hr}^{-1}$ .

Typically the mass flow rate through tubing and channels is given in terms of flux. Hence in the present study, it is assumed that these are in values of mass flow rates per unit cross section of the channels. This provided no change in the thermal efficiency,  $\eta_{th} = 0.56$  at  $-0.000754 \text{ }^{\circ}\text{C}\cdot\text{m}^{-2}\cdot\text{W}^{-1}$  reduced temperature. For the purpose of cooling the panel, it is essential that the heat transfer at the rear of the panel is increased. If the channel is well insulated, the heat can be contained and transported out of the device to be stored. This provides higher Nusselt number at the rear of the panel as well as larger thermal efficiencies. One method to attain this is by decreasing the aspect ratio of the channel or simply experiment using a single channel at the rear of the panel. The aspect ratio  $\alpha^* = 0$  as recommended by Rohsenow *et al.*[24] should be utilized. The boundary conditions should be an upper wall heated and others adiabatic. The Nusselt number is  $\text{Nu} = 5.385$  if fully developed flow exists in this channel.

The multiple channel collectors mentioned previously have aspect ratios above 0, yielding lower values of heat transfer Nusselt number. The Nusselt number are,  $Nu = 3.61$  for  $\alpha^* = 1$ ;  $Nu = 4.11$  for  $\alpha^* = 0.5$  and  $Nu = 5.35$  for  $\alpha^* \leq 0.25$  [24]. Higher cooling using  $\alpha^* = 0$  needs to be addressed using experimental work versus the stand-alone, heat sink and cavity configuration. Furthermore it is important to optimize the single channel to attain thermally developing flow that states that  $Nu = 8.44$  at the entrance which decays logarithmically to  $Nu = 5.385$  at the exit of this optimized channel [24]. This provides the highest cooling ability using a channel at the rear of the panel to be credible for comparison to the other configurations.

The configurations missing in previous work for comparison of their cooling are; (i) cylindrical pin fin heat sink at the rear of this PV panel; (ii), water cavity at the rear of the PV panel and (iii), a single water channel at the rear of the PV panel. A comparison of cooling using these configurations is given in the present study.

### **2.3 Experimental methods**

The main components of the experimental set up consist of one bare panel and other three panels with cooling configurations all inclined at  $30^\circ$  from the ground (refer to Figure 2-1). An economical halogen light solar simulator is used to heat up the devices. A spectrometer is used to attain the spectral irradiance distribution of this light source and a pyranometer supplies the irradiance intensity values on various locations on the panel. This irradiance is the controlled variable of the study along with the fixed ambient temperatures of the laboratory. These ambient temperatures were measured using a K-type thermocouple placed at a distance from the devices. The winds speeds were assumed to be  $0 \text{ m}\cdot\text{s}^{-1}$  since the experiments were conducted in a closed environment.

The independent variables measured in the present study are the temperatures and power output of the devices. The temperature was acquired using regular and immersion temperature and a non-contact infra-red temperature reader.

The power was acquired using a resistor circuit attached parallel to the panels. Before using these resistors, the maximum power output of the panel was measured using a 20 ohm

variable load resistor is used in parallel to the bare panel on an open rack mount. The power output was acquired from the voltages attains using ohms law. The resistance of the panel was determined and four ceramic resistors were used in parallel with this panel in all the devices for the comparison study.

Two data acquisition consoles convert the analog data signals from the temperature sensors and the voltage from the resistors to digital output, which are recorded on two personal computers and reduced to average temperature and power output using LABVIEW. A jacketed cold reservoir is connected to channel/configuration 3 (Figure 2-1). It was placed directly above its top edge. The reservoir and the channel are connected by polyethylene tubing and form a closed loop system. The inlet temperatures of the channel are kept constant (controlled) during experiments by using dry ice packets in the reservoir tank.

### **2.3.1 The setup**

i. Bare panel:

This is a 20 W KYOCERA® pc-Si PV panel purchased from MATRIX ENERGY of size  $W \times H = 0.352 \times 0.52$  m and 36 cells. This opaque device contains glass/EVA/TiO<sub>2</sub>/Si/EVA/PE-Al-Tedlar layers (from front to rear) [6]. The total measured thickness of this device is  $4.5 \times 10^{-3}$  m and it rests on an open rack mount inclined at 30° from the ground (Figure 2-1). All configurations were inclined at this angle. The protective aluminum frame at the sides of the panel was removed, since this component was not utilized with the attachments of the configurations. The open rack was created by Aluminum and the angle of inclination of this panel was measured using Boschtool DLR130K laser distance device.

ii. Panel with heat sink at rear/configuration 1:

197 aluminum (clear anodic plated) pin fin heat sink, of base dimensions  $0.127 \times 0.127$  m is attached to a prime surface of the panel's rear while the remaining panel is insulated with polyurethane foam (Figure 2-1). The exposed area of the front is equal to that of the base. Only 4 cells were exposed at the front in this configuration. The rear of the panel and the heat sink is joined together with ARTIC SILVER adhesive. The geometry of pins are  $d = 4.35 \times 10^{-3}$  m,  $l = 6.67 \times 10^{-3}$  m and they

are spaced in a staggered form with spacing  $S = 9.01 \times 10^{-3}$  m between each other. These values are kept constant and are not modified in this research. The base of the heat sink is  $10 \times 10^{-3}$  m thick. It has a fin population density of  $1.22 \text{ fins}\cdot\text{cm}^{-2}$ . The heat sink was attached at this specific location because the bare panel was near uniform temperature when exposed to halogen light. Thus the location was arbitrary.

iii. Panel with water cavity at rear/configuration 2:

The cavity was created with PVC. It's sides were  $6.35 \times 10^{-3}$  m thick and served as the adiabatic side walls, selected on the basis of the low thermal conductivity of  $2.72 \text{ W}\cdot\text{m}^{-2}\cdot\text{K}^{-1}$  (specified by vendor 3M™). The back cover of this cavity is  $3.25 \times 10^{-3}$  m thick also made from PVC. It is aimed that it would lose heat to the surroundings and remains cooler than the rear to provide a differentially heated cavity problem. The water cavity thickness is  $L = 25 \times 10^{-3}$  m. After fabrication, the measured width of the cavity was  $W = 0.295 \times 10^{-3}$  m making the aspect ratio  $\beta^* = 12.08$ . This is the minimum aspect ratio of the cavity that could be achieved without breaking the body of PVC from water weight.

iv. Panel with water channel at rear/ configuration 3:

A PVC water channel of thickness  $L = 2.5 \times 10^{-3}$  m is attached directly to the rear of the panel. There is no top glazing cover over the panel. The side walls are  $25 \times 10^{-3}$  m thick made from PVC. The back cover of the channel is  $3.25 \times 10^{-3}$  m thick made from PVC as well. Inlet and outlet holes are drilled into the channel sides to allow water to flow through it. Polyester tubing is used to connect this channel to a jacketed cold reservoir tank. The tank is placed on level with the top edge/leading edge of the inclined channel. This channel is placed on an open rack mount support frame, as are all the other configurations. The channel was measured for its dimensions after fabrication. The thickness of the channel was kept constant at  $L = 0.025$  m as that of the cavity. It was expected that the flow would develop along its length from strong enough flow rates arising from the thermosyphon effect between the collector and cold reservoir.

**Legend**

1. Kyocera Pc-Si Panel
2. Configuration 1
3. Polyurethane insulation foam
4. 197 Cylindrical pin fins
5. Configuration 2
6. PVC adiabatic water cavity , thickness 25 mm
7. Insulated cold water reservoir
8. Configuration 3
9. Adiabatic channel
10. Insulated tubing ,  $d = 6.35$  mm
11. Inlet zone

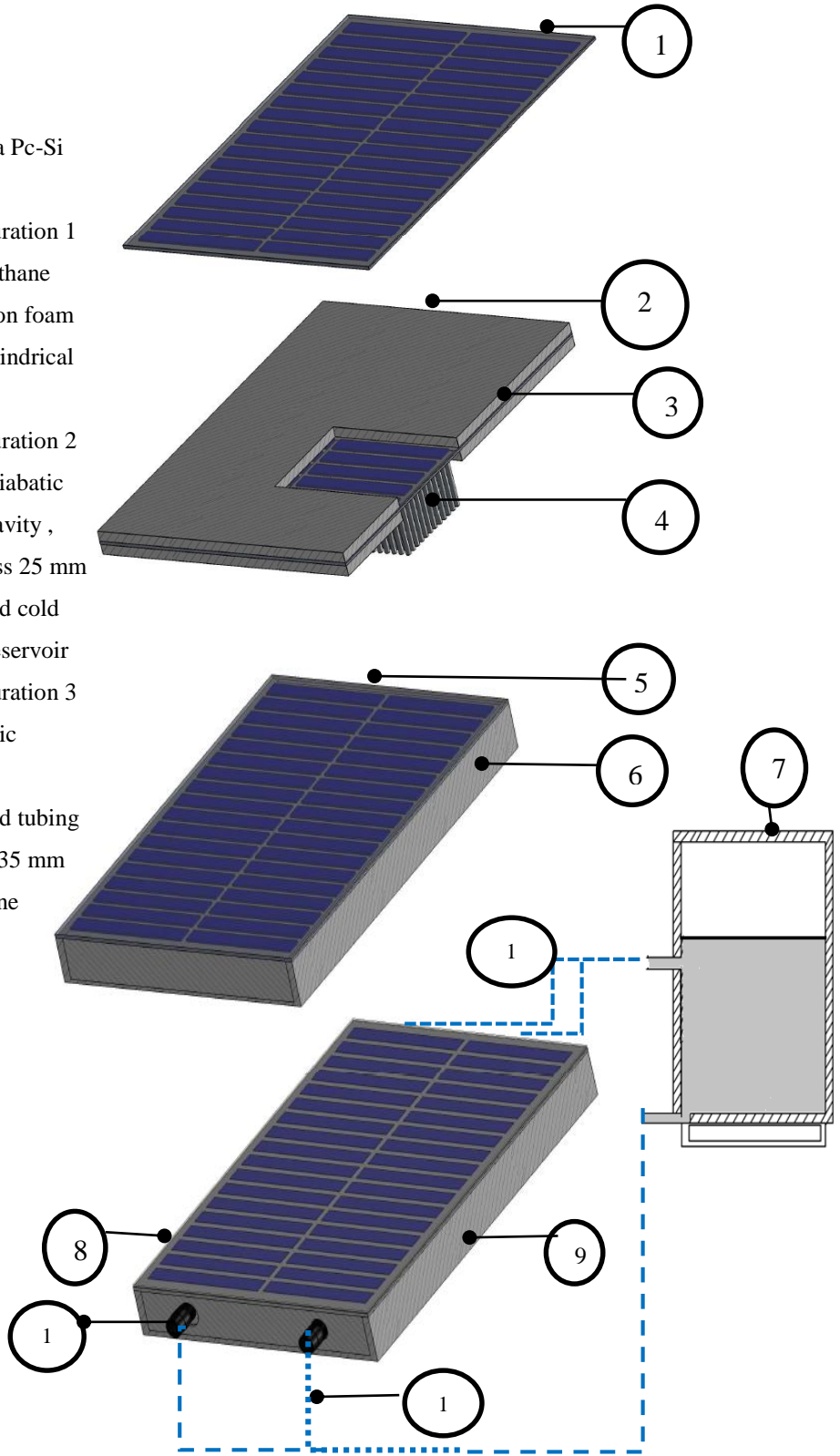


**Figure 2-1: The four devices under investigation; the Kyocera 20 Watt pc-Si solar panel and the three configurations with cooling devices at the rear of this panel**



Previous work has assumed constant mass flow velocities through their channels of value  $\dot{m} = 76 \text{ kg}\cdot\text{m}^{-2}\cdot\text{hr}^{-1}$  [17], with channel length of thickness of 0.005 m with aspect ratios of  $\alpha^* = 0$  (cross section not reported) and for channels of thickness 0.01 m with aspect ratio of  $\alpha^* = 0.025$  (with natural circulation in the system) [21]. This is the mass flow rate of 76 kg of water per hour per  $\text{m}^2$  cross section of the channel assumed in the present study. These works assume their Nusselt number arising from these fixed mass flow rates. Any system with forced circulation or natural circulation should provide measured mass flow rates. However, it is assumed that the system in the present study should provide high enough mass flow rates as well of  $76 \text{ kg}\cdot\text{m}^{-2}\cdot\text{hr}^{-1}$ . According to this value, the channel of the present study of cross section  $0.352 \text{ m} \times 0.025 \text{ m}$  must have a flow Reynolds number above 17 (calculation of this value demonstrate in the analysis segment of the present study). For higher flow rates, the Reynolds number would be greater and the flow would develop along the channel. A Reynolds number of  $\text{Re} = 60$ , is the minimum value needed to attain thermally developing flow along this channel for  $\text{Nu} = 8.44$  at the entrance and  $\text{Nu} = 5.35$  at the exit, only according to theory [22].

### **2.3.2 The solar simulator**

Four 500 W, 240 V, halogen lamp flood lights are placed at  $0.475 \pm 0.25 \text{ m}$  normal distance from a wood surface. Wood is chosen because it was assumed that it's reputedly low thermally conductive material would provide local temperatures which are not influenced from one another. For instance, the local temperature in one location determined on the wood surface would not be influenced by a neighboring location if the irradiance intensities on these locations are different from one another. This proved to be a good assumption since the irradiance values between the locations on wood were very deviant from one another.

The wood surface under the halogen lamps served as a test subject to determine; i) the UV light (Ultra Violet), VIS light (Visible light) and NIR radiation (Near infra-red radiation) intensities and ii), the spatial irradiance distribution. Cooling of the halogen lights via a pedestal fan provided temporal stability in the spectral distribution peak, since shift towards the right of the spectrum to higher wavelengths can occur at higher bulb temperature.

The procedure to determine the uniformity of irradiance was done by first determining uniform temperatures over a wood surface of area  $A = 0.274 \pm 0.002 \text{ m}^2$ , by a non-contact infra-red temperature reader on 84 locations. The temperatures of the wood surface under the halogen lamps demonstrate a non-uniformity of 6.81% on a surface area of  $A = 0.274 \pm 0.002 \text{ m}^2$ . This surface area was reduced to  $0.183 \text{ m}^2 \pm 0.002 \text{ m}^2$  with a spatial non-uniformity of 4.81% in temperature. Spatial non-uniformity is the ratio of the mean temperature of the wood by the difference between the maximum and minimum temperatures measured [25].

50 locations were selected on this surface for spectral distribution measurement (spectrum in Figure 2-2) and irradiance distribution (bar chart in Figure 2-2). The halogen spectrum provides information about the intensities and non-uniformity of UV (ultra violet), VIS (visible) light and NIR (near infra-red) radiation from a basic data reduction, described in a later text of this section. To determine the spectral distribution, an OCEAN OPTICS USB 2000+ RAD spectrophotometer (range  $\lambda = 200\text{-}900 \text{ nm}$ , accuracy;  $0.03\text{-}10.0 \text{ nm}$  of the full width at half maximum of the spectrum) was used. The measurements were performed over 5 hours. It was concluded that no light in the range of  $\lambda = 0\text{-}300 \text{ nm}$  is present. This is a significant portion of UV light. The spectral distribution was only achieved for a wavelength range of  $\lambda = 300\text{-}894 \text{ nm}$ . This distribution remained steady in this period of time, an important quality for any steady simulator to possess.

The maximum spatial non-uniformity (in a.u) over 50 locations is 16.1% in the visible light range. It demonstrates the only non-uniformity from the spectrum attained. It was assumed that visible light was contributing to the total irradiance as well since is the most abundant light from the halogen lamps.

UV light and NIR radiation did not demonstrate any non-uniformity as judged from the spectrum. The irradiance from the halogen light is one of the controlled variables and was averaged from the distributions in Figure 2-2 (bar charts). This figure demonstrates how non-uniform this simulator was over the configurations front surface/ the PV panels.

These irradiances were measured using a TES pyranometer 1333R (ranges;  $G = 0\text{-}2000 \text{ W}\cdot\text{m}^{-2}$  and  $\lambda = 400\text{-}1100 \text{ nm}$ , accuracy;  $\pm 1.0 \text{ W}\cdot\text{m}^{-2}$ ). This is a hand held device that

contains a lens which records the incident irradiance and a digital display displays the irradiance value in  $\text{W}\cdot\text{m}^{-2}$ . The total irradiance measurement over these locations demonstrates non-uniformity. The total intensity is of spatial non-uniformity 16.5% which is close to that of VIS light.

From the irradiance distribution in Figure 2-2, it is judged that maximum irradiance is  $G = 1450.1 \text{ W}\cdot\text{m}^{-2}$  while the minimum  $G = 1250.2 \text{ W}\cdot\text{m}^{-2}$  from this simulator. The maximum irradiance is present near the top edge of the test plane (trailing edge of the panel) while lower intensities are near the bottom edge of the test plane (leading edge of the panel). The average irradiance in the present study is calculated to be  $G = 1378.4 \pm 23.5 \text{ W}\cdot\text{m}^{-2}$ . This irradiance level is extremely high.

From these measurements, it was not possible to predict what the cell temperatures would be under this particular type of light source. Relations are present in literature that provide that cell temperature by means of known irradiance, ambient temperature and wind speed values under solar light only [1]. Thus using this intensity of halogen light only served the purpose of attaining experimental panel temperatures that can yield analytically determined cell temperatures, which may be within  $60 < T_{\text{cell}} < 125^{\circ}\text{C}$ . This represents a bad operating scenario of a PV panel. Thus the simulators purpose is only defined by panel temperatures it can provide an not from its ability to be matched with solar light and used in future studies to demonstrate factory rated panel outputs. This is due to its deviation in UV, VIS light and NIR radiation as compared to solar light.

It is important to place this halogen light source in a class of simulators as that in previous studies [26], to make this claim. It is essential that the normalized percentages of UV, VIS light and NIR radiation and compared to the spectrum of AM ( Air Mass) 1.5 [27] and Global irradiance spectrum of solar light [28], as done in previous studies on solar simulators. This is because a lot of misconception can be present when dealing with economical indoor simulators. It cannot be assumed that if a panel is providing power output from the light source that the light source is of solar light. The comparison of the simulator used in the present study with respect to solar light is demonstrated in Table 2-1.

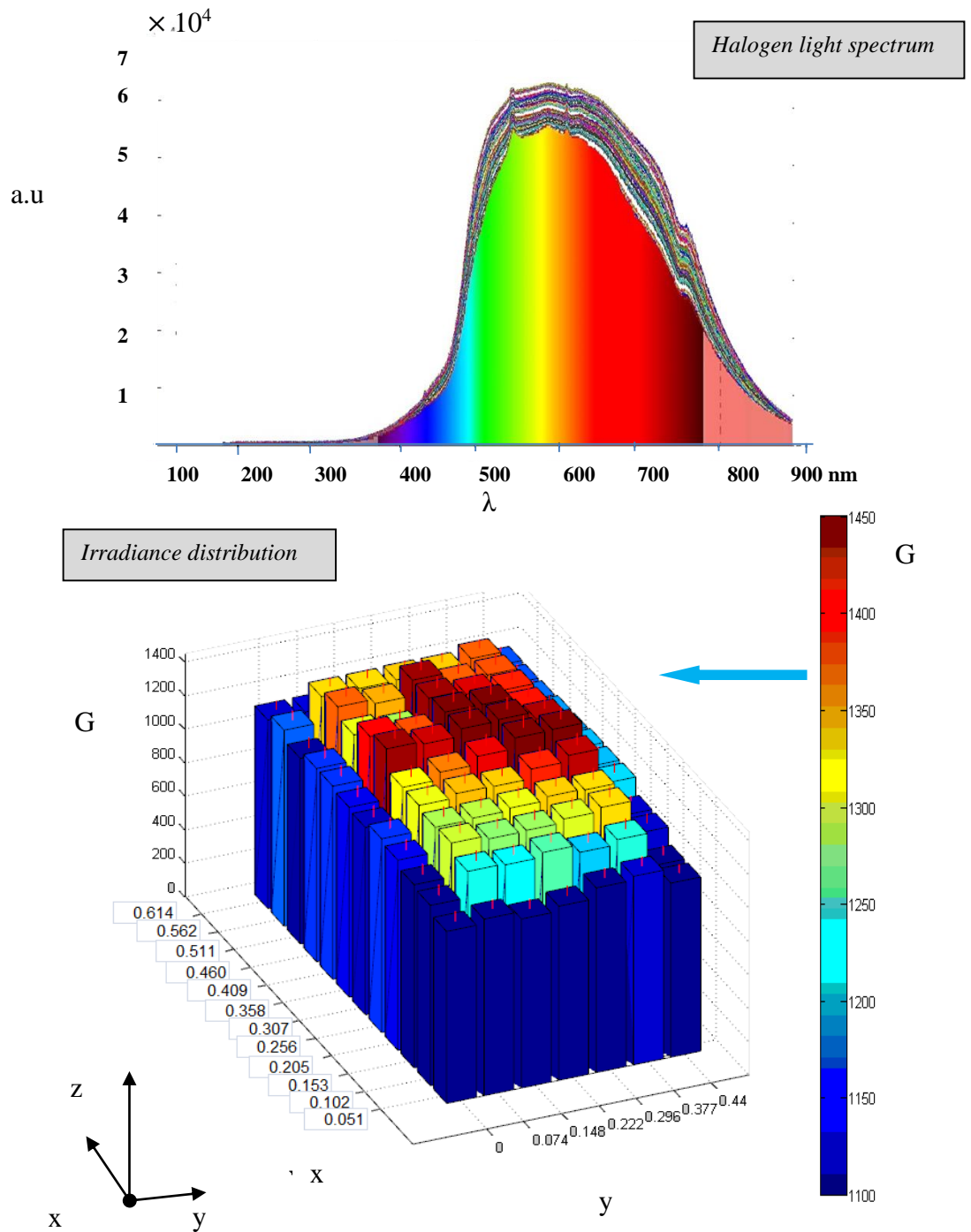


**Figure 2-2: The Halogen light spectral distribution (above) and irradiance distribution (below) on the devices**

**Table 2-1: Percentage reference spectrums normalized for the 300 - 1100 nm compared to Halogen light**

$\lambda$ (nm)	Global	AM1.5	Halogen Simulator
300-400	N/A	N/A	$\approx 0.7$
400- 500	18.9 [27]	18.5 [28]	$\approx 7.6$
500- 600	21 [27]	20.1 [28]	$\approx 33.1$
600- 700	17.5 [27]	18.4 [28]	$\approx 33.3$
700- 800	14.8 [27]	14.8 [28]	$\approx 19.6$
800- 900	11.5 [27]	12.3 [28]	$\approx 7.1$
900-1100	16.3 [27]	16 [28]	N/A

To attain the normalized percentages provided in this table, a wavelength range is selected, i.e UV light between  $\lambda = 300-400$  nm and then spectrum is then integrated between these wavelengths and divided by the total integrated area of the spectrum. In this table, halogen UV light is between  $300 < \lambda < 400$  nm, VIS light is within  $400 < \lambda < 700$  nm and NIR radiation is between  $700 < \lambda < 1100$  nm.

Extensive reference is made to AM 1.5 spectra of solar light in reporting panel performance in any previous studies. The global and AM 1.5 spectrum is from a sun-facing collector surface tilted  $37^\circ$  from the horizontal (chosen to represent an average latitude in the continental United States) and has been used adequately for many solar simulators [24]. The Global irradiance is also selected which is commonly simulated to test PV panel indoors [25]. Judging from this comparison table, the halogen simulator is abundant in VIS light, which comprises of 74% of the irradiance as compared to the 54.2% of VIS light of the Global and AM 1.5 spectra. Halogen light is deficient in NIR radiation which comprises of 26.4% of the irradiance as compared to 42.85% of NIR radiation of the Global and AM 1.5 spectra. UV light is inadequate in the present study but still present of approximately 0.7% of the irradiance. Over all, the entire simulator is different from solar light.

It is concluded that the simulator cannot be placed in any class of an indoor solar simulator. Class of simulators require very small non-uniformity (<1%) as well as lower irradiance of  $1000 \text{ W}\cdot\text{m}^{-2}$ , close to that of solar light [26]. In the present study, UV light is calculated to be  $9.6 \text{ W}\cdot\text{m}^{-2}$  incident on the panels. The works in Table 2-1 do not contain the percentage of UV light in their spectra. This is mainly due to the lack of UV light present from the sun. It is also calculated in the present study that a large amount of VIS light of intensity  $1020.0 \text{ W}\cdot\text{m}^{-2}$  is available from halogen lamps. This surpasses that VIS light present from solar light. NIR radiation is of intensity  $367 \text{ W}\cdot\text{m}^{-2}$  from the simulator in the present study which is nearly equal to the amount that would be present under  $1000 \text{ W}\cdot\text{m}^{-2}$  of solar light, that is of value  $373 \text{ W}\cdot\text{m}^{-2}$ .

### **2.3.3 Temperature and power measurement**

The measurement setup to attain values of temperatures and power output from the panels is demonstrated in Figure 2-3. These two are the independent variables of the study. They provided the comparative heat transfer coefficients at the rear of the panel in all the configurations as well as the performance of the heat sink and the channel. These temperatures are influenced by the controlled variable; the irradiance and the ambient conditions of the laboratory. Even though the simulator is not of solar light, the power outputs must be determined from the PV panel in this study. An MTP 1328 infra-red temperature reader (range  $20^\circ\text{C} < T < 170^\circ\text{C}$ , resolution  $0.1^\circ\text{C}$  and accuracy  $\pm 1^\circ\text{C}$ ) is used to acquire the front temperatures of the glass over the 36 cells of the pc-Si PV panels. Each cell has a width of  $0.163 \text{ m}^2$ ; this area is too large for a multitude of temperature measurements. Hence the front surface temperature was measured via the infra-red temperature reader, by moving the device over the glass covering the cells. This provides the front surface temperature of the panel, which are the glass temperatures. This method was used for all the other configurations. Ambient temperatures are measured constantly during the experiment, below and above these configurations and were recorded using a K-type thermocouple (range  $5^\circ\text{C} < T < 150^\circ\text{C}$  and accuracy  $\pm 1^\circ\text{C}$ ).

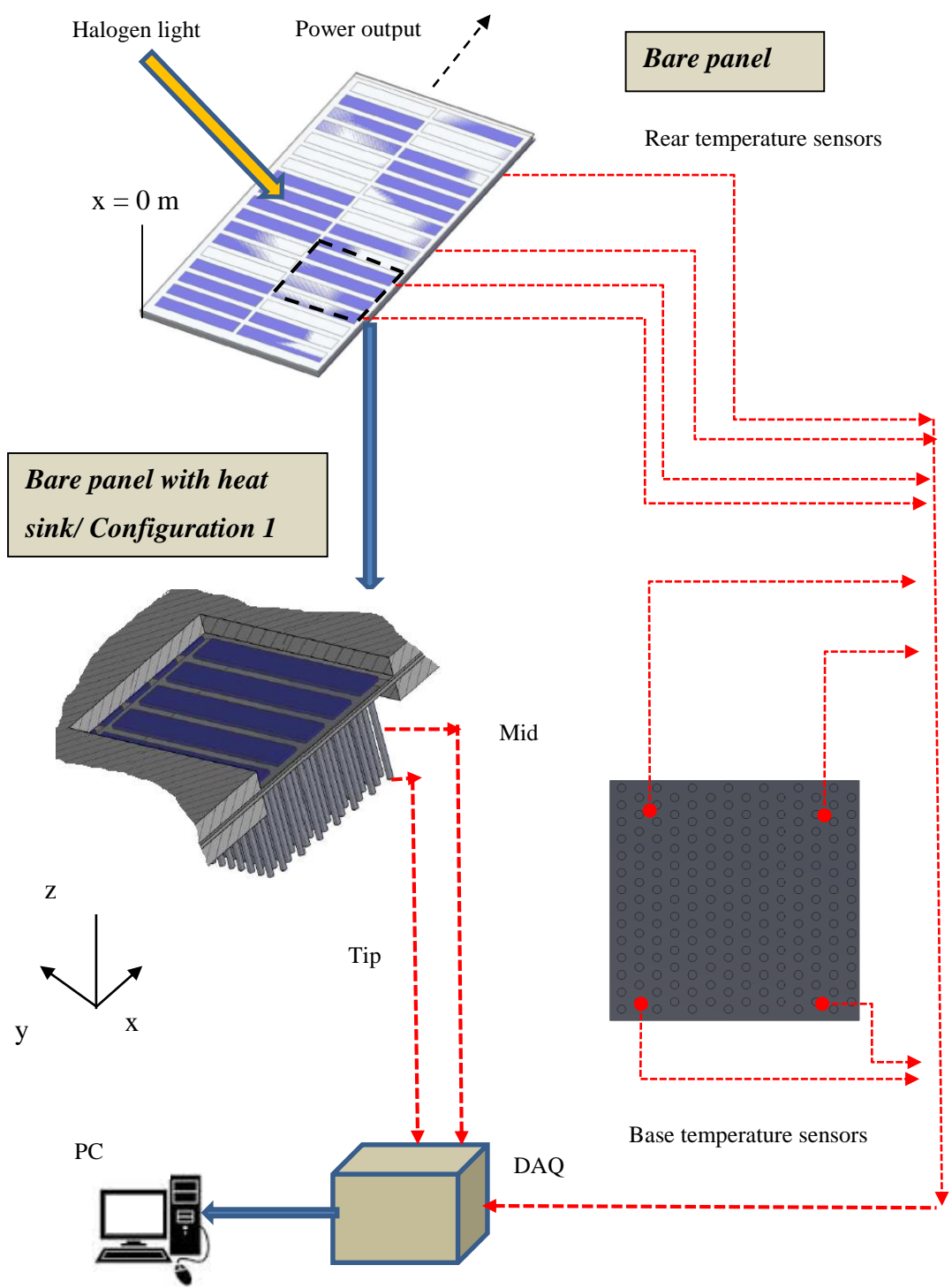


**Figure 2-3: Experimental setup of the bare pc-Si panel and the pc-Si panel with heat sink**

For the bare panel, the rear temperatures,  $T_r$ , were acquired locally. The temperature reader was initially utilized to attain the rear temperatures of the panel and determine where the curtail points to measure the transient temperatures are located. The rear surface temperature does not provide any transverse or longitudinal deviance in its values (only  $\pm 0.5^\circ\text{C}$  deviation over the entire rear surface). The surface is isothermal. Hence the center of the panel was subjected to temperature measurements only on four locations using four K-type thermocouple sensors (range  $5^\circ\text{C} < T < 150^\circ\text{C}$  and accuracy  $\pm 1^\circ\text{C}$ ) at locations of  $x = 0.052\text{ m}$ ,  $0.190\text{ m}$ ,  $0.330\text{ m}$  and  $0.471\text{ m}$  from the bottom edge (see Figure 2-3). They are mounted directly on the surface using thermally conductive adhesive tape. This method was deemed as sufficient to acquire the panel temperatures over time. Analysis was utilized to attain the cell temperature. The panel with the heat sink at the rear/configuration 1 is read for temperatures of the glass over 4 cells only. This area was the subject to all the temperature measurements in this configuration. The remaining surfaces of the panel were insulated from the environment using polyurethane foam as shown in Figure 2-2. Figure 2-3 represents the area selected for temperature measurement. The covered area of the panel at the front and rear is regarded as insulated.

Figure 2-4 demonstrates the experimental setup for the cavity/configuration 2 and the channel/configuration 3. Both these configurations have the same geometry (channel thickness, height and width). Thus they were utilized in the same setup. The cavity was operated with the shut-off valves closed and the channel was utilized with these valves open. For the channel setup, the inlet and outlet temperatures were acquired, unlike that of the cavity. J-type immersion thermocouples (range  $10^\circ\text{C} < T < 650^\circ\text{C}$  accuracy  $\pm 1^\circ\text{C}$ ) are used to attain the rear temperature,  $T_r$ , center cavity/channel water temperatures,  $T_w$ , as well as the temperatures of the back cover,  $T_c$ . The locations of these thermocouples are the same as those at the rear of the bare panel. Ambient temperatures are measured constantly during the experiment below and above these configurations. The front surface temperature of the cavity and the channel were recorded using the infra-red temperature reader with the same method as that of the bare panel. The inlet temperature,  $T_{in}$  and outlet temperature,  $T_{out}$  of the channel/configuration 3 are acquired using immersion K-type thermocouple probes at the center of the insulating tubing attached to the channel (range  $5^\circ\text{C} < T < 150^\circ\text{C}$  and accuracy  $\pm 1^\circ\text{C}$ ).



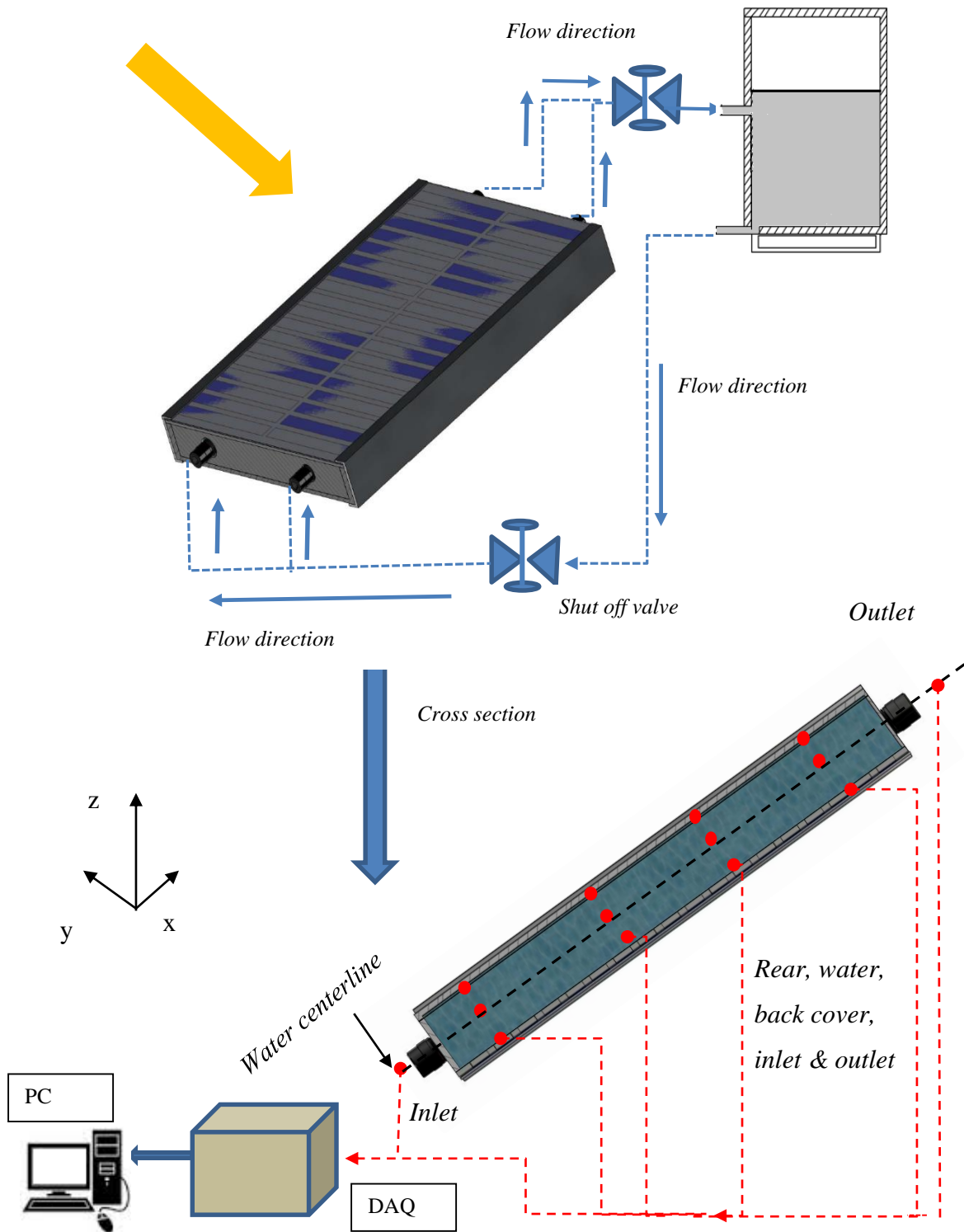


**Figure 2-4: Experimental setup of the cavity and channel at rear of pc-Si panel**

These inlet and outlet thermocouples are placed  $5 \times 10^{-2}$  m from the walls of the channel. The side walls of the channel and cavity are read for their surface temperatures and were compared to the ambient temperature so that they may be assumed to be adiabatic if their temperatures match.

Similarly the outer surface of the reservoir tank, which is only present when operating the channel/configuration 3 experiment, was read for its surface temperature to ensure that it is equal to the ambient temperature and can be assumed to be adiabatic. The tank temperatures were not important since they were not utilized in any of the analysis of the dependent variable, the convective heat transfer coefficient at the rear of the panel. The second dependent variable is the power output of the panel. Pre-determined ceramic power resistors are placed in parallel to the panels to acquire their voltages which are converted to power output using ohms' law on LABVIEW. To acquire the maximum power output of the panel, the maximum power point tracking technique was applied. A 100 ohm 100 Watt power resistor (resolution of  $\pm 1\%$  of reading) is connected in parallel with the bare panel under the halogen light which demonstrates that its maximum power is equal to 12.2 Watts during  $t = 0 - 140$  minutes.

Fluke multi-meters (Model 87-5, resolution  $\pm 0.05\%$  of voltage) provided the current and the voltage to determine this maximum power. The total resistance needed to monitor power over time is calculated to be 19.4 ohms using Ohms law. This resistance is divided into a four power resistors which are attached the panels in this setup to attain the power output over time. The resistors were soldered together and their power rating was 15 Watts each. Maximum power point determination is not done during the transient power acquisition of these panels. The resistors have values of 4.905 ohms, 5.058 ohms, 3.940 ohms and 4.965 ohms (true values attained using a YOKOGAWA model 7556 digital multi-meter). These resistors were chosen based on their ability to withstand high temperatures and their power rating. It was essential to utilize ceramic material for the present study. The experiments to attain the temperatures and power were conducted over a course of time that provided steady state values of these independent variables, after which the experiments were stopped. A cooling unit was placed near the power resistors and the halogen light simulator during this course of time. Each variable was measured

three times to provide enough data for analysis and the errors associated with the experiments.

#### **2.3.4 Calibration of sensors and data acquisition system**

The equipment was calibrated prior to usage and installation. The USB 2000 spectrophotometer came pre-calibrated by the vendor OCEAN OPTICS hence the spectral intensity reported in Figure 2-3 is assumed to be accurate ( resolution of 1-10 nm and accuracy  $\pm 1\%$  of a.u reading provided by vendor between  $\lambda = 300-894$  nm) . The spectrum of halogen light was mapped on Spectra Suite® software installed on a personal computer. The calibration of the TES pyranometer for irradiance measurement was performed against a SSL-52 solar meter (accuracy of  $\pm 1 \times 10^{-3} \text{ W}\cdot\text{m}^{-2}$ ). There was a linear relationship between the measured and true value and no adjustment to the data were performed. An MTP 1328 infra-red temperature reader (range  $20^\circ\text{C} < T < 170^\circ\text{C}$  and accuracy  $\pm 1^\circ\text{C}$ ) was used to determine front surface temperatures. It was calibrated against a K-type digital 1312A thermometer and it involved a tedious procedure. The calibration procedure consisted of a hot plate with a masking tape. The temperature of this masking tape was read by the infra-red temperature detector and compared to the surface mounted k-type thermocouple (range  $5^\circ\text{C} < T < 150^\circ\text{C}$  and accuracy  $\pm 1^\circ\text{C}$ ) which was mounted on the masking tape. The temperature of the reader was only accurate when its emissivity was adjusted to  $\epsilon = 0.92$ . This provided the true temperatures, which is the agreement between the k-type thermocouple output and those displayed on this device. The IR temperature reader was able to measure temperatures for the range of  $20^\circ\text{C} < T < 150^\circ\text{C}$  with an accuracy of  $\pm 1\%$  of the reading, determined from this calibration process. The surface mount K-type thermocouples at the rear of the panel and those on the heat sink and the immersion J-type thermocouples in configuration 2 & 3 were calibrated against a K-type digital 1312A thermometer (accuracy of 0.3% of the reading and resolution  $0.1^\circ\text{C}$ ) in a hot water bath. The water in the bath was allowed to cool down and data was recorded at different bath temperatures. The J-type thermocouples used in the cavity and channel were calibrated by placing them in an insulated hot water bath along with a high accuracy thermometer (Kessler-2150, 76 mm immersion, range  $T = -36-154^\circ\text{C}$ ) which was used as the reference. The water in the bath was allowed to cool down and data was recorded at

different bath temperatures. Calibration equations were obtained for all the thermocouples and were incorporated in the LabVIEW program when obtaining the temperatures in the experiments. Two National Instruments data acquisition system cards (NI-cDAQ-9211, 4 channels) were used to acquire the signal for the temperature sensors. These cards were mounted on a chassis (NI-cDAQ-9711) to connect to the LabVIEW software (Signal express edition 2012) on a PC. The data acquisition card had a built in cold junction compensation device and hence no temperature adjustments to the sensor output were required. All the DAQ's were 18 bit systems.

## **2.4 Experimental results**

Few issues faced were that the temperatures at the front PV panel surface of the cavity kept rising. Its temperatures do not provide any steady state values. Also, no power output was measured from the panel with the heat sink. This is because the whole panel was not illuminated by halogen light in this configuration. The power output of four cells was too low to monitor using the present setup. This is because the bare panel power output, which will be demonstrated later, was at less than half of its full power rating under the halogen light. Decreasing the cell coverage from 36 cells to four cells using polyurethane foam for the heat sink configuration further decreased this power output which was too low to be recorded with the present equipment.

The temperatures in Figure 2-5 demonstrate the cooling witnessed at steady state on the front of the panels. These are glass temperatures. Steady state is assumed in the present study to be reached when the temperatures of the devices are constant and their deviation is  $< 5\%$  from the mean. The temperature of the devices reached steady state at different times. At  $t = 140$  minutes, three of the device are at steady state. The bare panel is assumed to reached steady state temperatures at approximately  $t \approx 20$  minutes, with a heat sink, at  $t \approx 32$  minutes, with the cavity no steady state was achieved and with a channel at  $t \approx 100$  minutes. The bare panel is at a temperature of  $83.78 \pm 1.5^\circ\text{C}$  near trailing edge (top of the panel) and  $85.2 \pm 1.2^\circ\text{C}$  at the center and  $68.5 \pm 1.5^\circ\text{C}$  near the leading edge (at the bottom of the panel). The maximum longitudinal deviation in temperature at the front is  $15.8 \pm 1.5^\circ\text{C}$ .

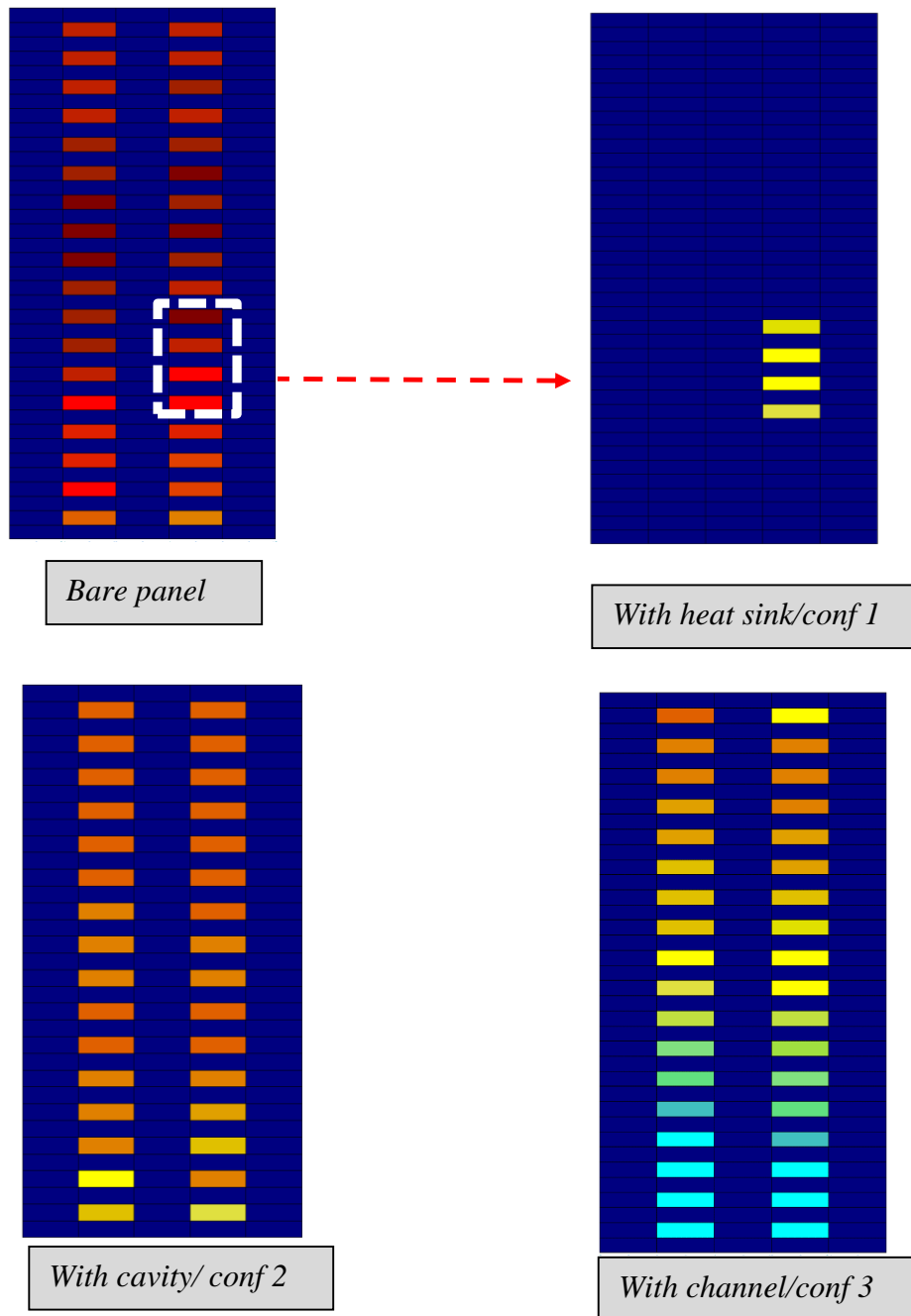
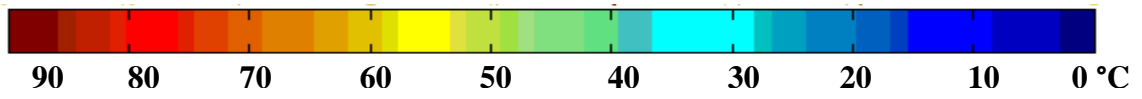


**Figure 2-5: Front surface/glass temperatures over 36 cells of Kyocera Pc-si panel under  $G = 1378.2 \text{ W}\cdot\text{m}^{-2}$  with different configurations at the rear**

This deviation is contributed the most between the temperatures of the panel at 2<sup>nd</sup> row from the bottom. These temperatures are influenced by the irradiance distribution only. No local hot locations were witnessed. There is low irradiance present on the bottom rows near the leading edge of the panel of value  $G = 1021 \text{ W}\cdot\text{m}^2$  which provides a front surface temperature of temperature  $68.5 \pm 1.5^\circ\text{C}$ . The irradiance is much higher at the center of the panel. The temperatures increase from  $70^\circ\text{C}$  to  $90^\circ\text{C}$  at the center, following the distribution of irradiance. The center row is under an irradiance intensity of  $1450 \text{ W}\cdot\text{m}^2$ . Over all, the front surface of the bare panel surface can be taken at an average from surface temperature of  $T_f = 83.7 \pm 1.4^\circ\text{C}$  with a temperature distribution over the surface with deviation of  $\pm 11.1^\circ\text{C}$  from this mean. Comparatively, the surface temperatures of the panel's front with the heat sink attachment demonstrate that the areas that were between  $70$  and  $80^\circ\text{C}$  were lowered in temperature to  $63.2 \pm 1.3^\circ\text{C}$ . This is the temperature of the glass over the four cells under which the heat sink is attached. This surface had no spatial non-uniformity.

The remaining of the panel was at ambient temperature of  $T_a = 21.5^\circ\text{C}$ . The front surface of the heat sink is regarded as isothermal at average temperature of  $T_f = 63.2 \pm 1.3^\circ\text{C}$ . The front of the cavity shows temperature in Figure 2-5 at  $t = 140$  minutes which are not of steady state value. They are increasing but shown for the same of comparison. At this moment in time there is a gradient rise in temperature from the leading edge of the cavity to the trailing edge. Temperature increases from  $42.3 \pm 1.2^\circ\text{C}$  to  $73.7 \pm 2.42^\circ\text{C}$ . These temperatures have no significance for the present study since the goal of achieving steady state was not achieved in this device. Hence it can only be mentioned that the device is providing lower temperature compared to the bare panel at this time only at  $T_f = 64.5^\circ\text{C}$ . The reasoning why steady state was not achieved in this cavity was not only judged from the front surface temperatures but also from the temperatures inside the cavity at  $t = 140$  minutes. All the temperatures, at the rear, the back cover of the cavity were rising. Hence no steady state achievement is a good assumption in this configuration.

The front surface temperatures of the channel show the lowest temperatures amongst all the panels. The glass near edge is extremely cool at  $31.5 \pm 1.2^\circ\text{C}$  and at the trailing edge the temperature is  $72.6 \pm 1.42^\circ\text{C}$ . The temperatures of the leading edge to the trailing edge

increase almost linearly. There are no transverse variations in the temperature of this surface. The irradiance distribution on the channel does not play a role in influencing its front surface temperature. The thermosyphon effect was established in this setup. The water flowed into the device at the inlet in Figure 2-4 and exited from the two nozzles placed at the outlet. The water circulated from the cold reservoir tank. The inlet temperature was kept constant at  $T_{in} = 14.56 \pm 0.4^\circ\text{C}$  which exits that collector at  $T_{out} = 66.5 \pm 2.5^\circ\text{C}$ . The inlet temperature is assumed to be the reason why the channel is at extremely low temperature near the leading edge (near bottom of the panel in Figure 2-5). The steady state temperature rise is at nearly  $50^\circ\text{C}$ . Since, this is a traditional PV/T collector setup, reporting the temperature gain by water is customary at the conditions tested is customary as per the review of previous collectors. The reduced temperature of this device is the ratio of the difference between the inlet water temperature and ambient air temperature by the irradiance on the panel. In this setup, this channel was operated at  $-0.007^\circ\text{C}\cdot\text{m}^2\cdot\text{W}^{-1}$  reduced temperature. Its thermal efficiency would be analyzed/ along with the mass flow rates.

The thermosyphon effect in the channel configuration was monitored using dye tracing in this collector after it was identified that the effect does not initiate right away. It took approximately 21 minutes for the thermosyphon effect to initiate water circulation in the system. After this time, the experimental results of this channel can be established. From these results, it can only be concluded that the channel and heat sink at the two working cooling methods of the present study. However, the natural convection heat transfer coefficient would be analyzed to assert this claim. The other variables measured, such as the rear surface temperature of the panel provides better justification of this assumption.

The rear temperature of this panel reached steady state at  $t = 20$  minutes as seen in Figure 2-6. This rear temperature is the average of the four local rear temperatures of the panels. These temperatures were nearly equal and the surface was regarded as an isothermal surface and it was not influenced by the distribution of irradiance on the panel. The rear temperature is at an isothermal value of  $T_r = 88.6^\circ\text{C}$  for the bare panel. This temperature increases from the room temperature drastically between  $t = 0$ -20 minutes to a steady state value. There are no temperature variations seen after 20 minutes.

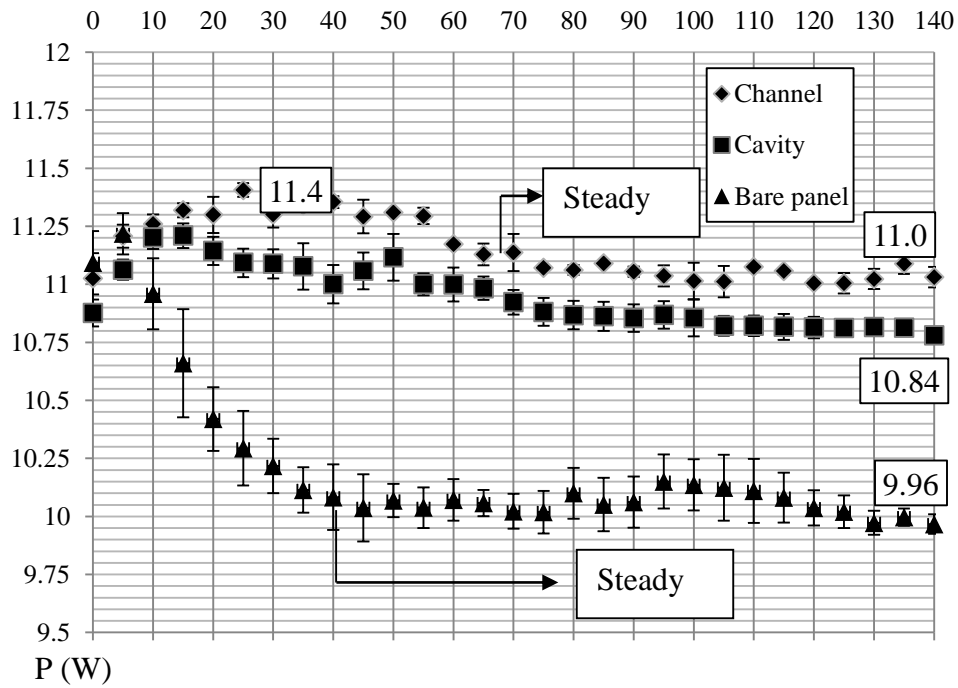
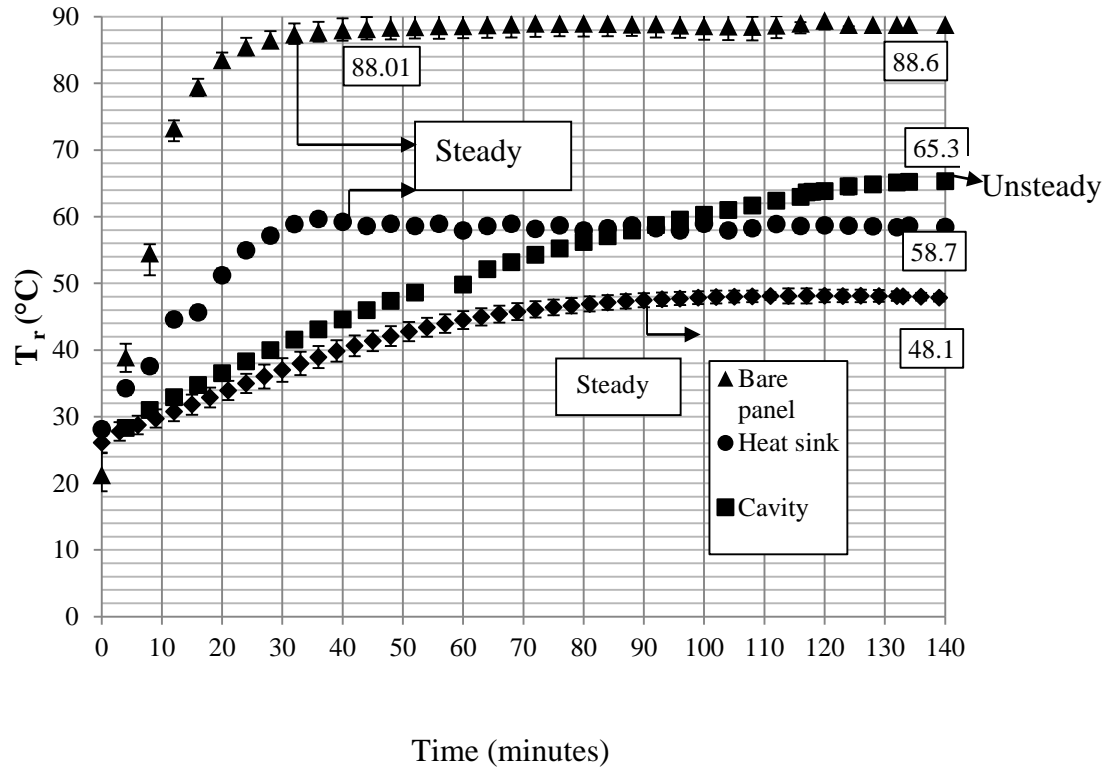


**Figure 2-6: Rear temperatures of the pc-Si panel in bare state, with heat sink, water cavity and channel and its rear and its corresponding power output**



The average base temperature of the heat sink is compared to this reference high temperature during 0-140 minutes as shown in Figure 2-6. The rear of the panel of the heat sink was not measured. The base temperature of the heat sink was utilized as the representation of the rear of this panel. The rear temperature locations represented in Figure 2-6 are using the heat sink average base temperature of the four temperatures in Figure 2-3.

The temperatures are steady at  $58.7^{\circ}\text{C}$ , while the mid is at  $52.3^{\circ}\text{C}$  and tip at  $49.5^{\circ}\text{C}$ . The fin surface did not have uniform temperature. These steady state temperatures are when 28 minutes had passed. It is constant at this value for the remaining period of the experiment. The front temperature remained  $3\text{-}5^{\circ}\text{C}$  higher than that of the base of the heat sink/rear of Configuration 1 during 0-28 minutes, after which, the temperatures difference was  $1.2^{\circ}\text{C}$  higher. Temperatures of the rear of the panel in the cavity are rising but they are lower than the bare panel during the experiment as seen from Figure 2-6. The temperatures at the rear of the panel are not uniform. They are averaged in the data represented in the present study. The average rear temperature is  $T_r = 63.3^{\circ}\text{C}$ , well above that of the heat sink, but lower than that of the bare panel. Over time it increases from room temperature to this value. No steady state is evident in this device judging from the temperatures.

The rear temperatures of the panel with the channel were the lowest in comparison to the others. The rear temperatures demonstrate that the channel reaches steady state at  $t = 100$  minutes. At steady state the average temperature of the rear is  $T_r = 48.1^{\circ}\text{C}$ . The rear of the panel reveals a gradient of temperature rise from leading edge to the trailing edge with the channel. The local rear temperatures of the panel are very different from one another. The profile of temperatures is nearly linear in nature.

Four locations were measured at  $x = 0.052\text{ m}$ ,  $0.190\text{ m}$ ,  $0.330\text{ m}$  and  $0.471\text{ m}$  of the bare panel, the cavity and the channel. The temperatures corresponding at these locations at the rear of the bare panel are  $89.1^{\circ}\text{C}$ ,  $91.1^{\circ}\text{C}$ ,  $88.2^{\circ}\text{C}$  and  $92.0^{\circ}\text{C}$  while that of the channel are  $27.1^{\circ}\text{C}$ ,  $43.4^{\circ}\text{C}$ ,  $58.8^{\circ}\text{C}$  and  $62.0^{\circ}\text{C}$ . The difference between the local rear temperatures of the bare panel and channel are nearly constant over the time period of 0-140 minutes. Hence the experiments have justified cooling using the channel device, is the best among the methods.

To attain the heat transfer coefficient, other temperatures in the channel were acquired as shown in Figure 2-4. The water temperatures are 16°C, 37.1°C, 52°C and 61°C at steady state, not much different from the rear and remain at these differences over time. However, the back cover temperatures are much cooler. Its temperatures are 16.1°C, 31°C, 49°C, 59°C at steady state and maintain a constant difference from the rear during the period of the experiments.

The light source type reflects the power output of the panel. In Figure 2-6, the bare panel outputs an initial power of approximately 11.1 Watts. This value is measured at room temperature of 21.6°C. Thus the halogen light source provides a decrease of 9.9 watts of power from its STC rating of 20 watts when experimented under solar light. Over time the power deteriorates with rising temperature. At steady state the power output of the bare panel is 9.96 Watts. The power output of Configuration 1/ heat sink was not attained as mentioned previously. The power output of the channel remained at a constantly high value of above 11 Watts and reached a maximum at  $t = 25$  minutes at 11.4 Watts. This is the maximum power recorded in the present study from this panel. With increasing temperatures, this power deteriorates to 11.03 Watts at steady state when the temperature of the rear are  $T_r = 48.1^\circ\text{C}$ . It is assumed that the power output over time reflects the temperatures of the rear of the panel in the bare state and with the channel attachment.

The water cavity's panel provided power output that is higher than that of the bare panel due to its relatively cooler temperatures as well. Its maximum power measured is 11.25 Watts at  $T_r = 38.1^\circ\text{C}$  at a time of 20 minutes. This power also deteriorates with increasing temperatures. However, no steady power output was achieved in this device and it is best left out of discussions.

These variables are utilized to determine the best cooling method from calculating the convective heat transfer coefficient at the rear of the panel, the dependent variable. Furthermore, it is uncertain what the applicability is of the heat sink judging from the temperatures alone. Thus the heat transfer coefficient from the heat sink cannot be demonstrated without the evaluation of its effectiveness and its efficiency as done in previous work [29].

These two parameters are important to evaluate when claiming any sort of cooling from extended surfaces as discussed in the review of this thesis. Furthermore, the channel device mimics traditional PV/T collectors with modification of the channel's aspect ratio in the present study. Its heat transfer coefficient cannot be evaluated without determining the parameters of thermal efficiency, the Nusselt number and the cell temperatures achieved. Hence, these heat transfer coefficient brings forth the comparison of cooling using configurations at the rear and the evaluated parameters serve as a tool for analyzing their practical usage.

## 2.5 Data analysis

The data analysis is performed on the experimental results to attain the convective heat transfer coefficient, the effectiveness and efficiency of the heat sink and the thermal efficiency of the water channel and cell temperatures. All the data represented in the previous section has been subjected to uncertainty analysis, i.e, the front temperatures, rear temperatures and the power output. Uncertainty analysis provides the error of these variables from the equipment and the experimental repetitions. The errors associated with these variables are then propagated into the determination of the heat transfer coefficient and the parameters to be determined.

### 2.5.1 Uncertainty calculation

The errors of the average front and rear temperature and the power output contain the resolution error of the temperature sensors and the DAQ attaining the voltages from the resistors. The error from repeating the experiment is computed using a 95% confidence interval and thus, 95% of the data is within the population mean reported or in other terms, there is 0.95 probability that the data acquired is equal to the mean values mentioned in the present study [30]. The total uncertainty of temperature or voltage is attained by:

$$e = \left[ (\zeta)^2 + \left( \frac{t_{95} \times Std}{\sqrt{n}} \right)^2 \right]^{0.5} \quad (2-1)$$

Here  $\zeta$  is the instrument error (the resolution of the voltage and temperature readers) and  $t_{95} = 2.72$ , is the student-t value based on a 95% confidence interval of the mean of  $n = 3$

samples repetitions. Symbol, Std is the standard deviation of the measured local temperatures or the voltage for 3 samples. Once the uncertainties of these measured quantities are established it is used in the propagation of uncertainty formula to determine the total errors associated with the independent variables reported in Figure 2-5 and Figure 2-6. The total error from the average rear temperature or front temperature or power is attained from [30] :

$$e_{\gamma} = \left[ \sum \left( \frac{\partial \phi}{\partial \gamma} \right)^2 (e_{\gamma})^2 \right]^{0.5} \quad (2-2)$$

Here  $\partial \phi / \partial \gamma$  is the differential of the reported independent variable by the measured variable. For instance the average power output shown in Figure 2-6 is attained from:

$$e_{T_r} = \sqrt{\left( \frac{\partial P}{\partial V} \right)^2 (e_V)^2} \quad (2-3)$$

After evaluation of the total errors it is concluded that there is confidence in the experimental data after and is precise within 5% error in repeatability. The uncertainty reduction brought forth confidence in the difference in the front temperatures of the panels, the rear temperatures and the power output. The error bars associated with this data represented in Figure 2-5 and 2-6 do not overlap and hence are assumed to represent differences from one another. The evaluation of  $h_{conv,r}$  is conducted after attaining this confidence. The error in the coefficient is also attained from utilizing the uncertainty formula Eq (2-2) by:

$$e_{h_{conv,r}} = \sqrt{\left( \frac{\partial h_{conv,r}}{\partial \gamma} \right)^2 (e_{\gamma})^2} \quad (2-4)$$

Here  $\gamma$  are the variables which  $h_{conv,r}$  is a function of.

## 2.5.2 Comparative heat transfer coefficient

The comparison of cooling is done via calculation of the convective heat transfer coefficient at the rear of the panels over a time period of 140 minutes. Heat transfer relations from literature and heat transfer modelling are used to perform this evaluation. The values reported in this analysis are with the associated errors. The values are within

95% confidence interval of their statistical mean and have within 5% error in repeatability from three experiments. Prior to attaining the heat transfer coefficients, the applicability of heat transfer correlations used in this analysis was verified. The correlations are used in the heat transfer models to attain the convective heat transfer at the rear of the panel. The relations of heat transfer were verified by equating bare panel heat losses and power consumption to the irradiance on the panel, as done in previous work [31]. For this process it is assumed that the irradiance on the panel is equal to the sum of the convective heat loss, radiation heat loss and the electrical power output of the bare panel under (heat transfer modes shown in Figure 1-1). It is assumed that the transmittance of the glass is equal to unity of this state of the art pc-Si panel as judged from previous work [18]. The transmission of light through the Pyrex glass cover of the panel is dependent on the angle of the solar light on its surface. The transmission of solar light is taken as 1 when the angle between the glass and incident light is 90°, from the data collected by Zondag *et al.* [18]. The pyranometer in the present study measures the normal light on the surface only and it was placed normal to the test plane for irradiance measurements. Hence it is assumed that all the light from the lamps is normal to the surface of the panel and thus it is transmitting through without being reflected. The equation below provides the applicability of the convective heat transfer coefficients that will be used in this study. It is assumed that they are correct when the R.H.S (Right Hand Side) of the equation below will agree with the L.H.S (Left Hand Side):

$$G(1 - \eta_{el}) = q''_{conv,f} + q''_{conv,r} + q''_{rad,f} + q''_{rad,r} \quad (2-5)$$

The electrical efficiency  $\eta_{el}$  is calculated by the ratio of power output by the product of the irradiance and area of the panel. The above equation is derived from the heat transfer model in Figure 1-1 of Chapter 1. It is assumed that the irradiance which is not converted to power is absorbed by the cells. These cells generate heat which is dissipated to the surrounding via the front surface and rear surface of the panel. The convective heat flux,  $q''_{conv,f}$  is calculated from the Nusselt number relation of previous work. It is the amount of energy (in Watts) being dissipated per unit meter square from this surface by natural convection.

The Nusselt number is needed to attain the flux at the front, and is acquired from the relation of Churchill & Chu [32] :

$$Nu_{(x)} = 0.14 \left[ (Ra_{(x)} \cos\theta)^{\frac{1}{3}} - (Ra_{cr})^{\frac{1}{3}} \right] + [0.57(Ra_{cr} \cos\theta)]^{\frac{1}{4}} \quad (2-6)$$

$Nu_{(x)}$  is the local Nusselt number on the front surface and  $Ra_{(x)}$  is the local Rayleigh number. It is assumed that the above relations are applicable to isothermal wall boundary conditions as they are for isoflux walls [33]. The Rayleigh number is attained by:

$$Ra_{(x)} = \frac{\beta L^3 (T_{f/r(x)} - T_a)}{\alpha \nu} \quad (2-7)$$

The characteristic length, L, is equal to the height of the panel,  $H = 0.520$  m,  $\beta$  is the thermal expansion coefficient of the adjacent fluid and  $\alpha$  and  $\nu$  are its thermal diffusivity and kinematic viscosities. These are calculated at the average temperature of the surface and the quiescent fluid. The Eq (2-5) can be used for Rayleigh number range of  $10^7 < Ra_{(x)} \cos\theta < 10^{11}$  and  $15^\circ < \theta < 75^\circ$  and  $0 < Pr < \infty$ . When  $Ra_{cr} > 2 \times 10^9$ , turbulent natural convection occurs. Laminar natural convection was present when  $Ra < Ra_{cr}$ .

The term  $q''_{conv,r}$  is attained by the Nusselt number correlation by Fuji & Imura [34]:

$$Nu_{(x)} = 0.670 Ra_{(x)} \cos\theta^{\frac{1}{4}} / \left[ 1 + \left( \frac{0.437}{Pr} \right)^{\frac{9}{16}} \right]^{\frac{4}{9}} \quad (2-8)$$

This equation is used for isoflux wall conditions and is valid to within 1% accuracy to be used for isothermal wall conditions in the range of  $10^5 < Ra < 10^9$  and for fluids with  $Pr > 0.74$  and inclinations of  $\theta < 60^\circ$ . The Prandtl number is the ratio of the kinematic viscosity and thermal diffusivity of the adjacent fluid. The Rayleigh numbers at the front and rear have the same correlation as in Equation (2-7), using the same characteristic length. The heat transfer coefficient from convection at the front or rear is attained by [35]:

$$h_{conv,f/r(x)} = \frac{Nu_{(x)} k}{L} \quad (2-9)$$

Here  $h_{conv,f/r(x)}$  is integrated over  $x$ , from 0 - 0.520 m to attain the average convective heat transfer coefficient. This coefficient is used to attain the convective heat flux in Eq (2-5), by using Newton's law of cooling equation [36]:

$$q_{conv f/r(x)} = h_{conv f/r(x)}(T_{f/r(x)} - T_a) \quad (2-10)$$

The total front and rear convective heat flux is integrated over the height of the panel. The second form of heat dissipation is by radiation and attained from the radiation heat transfer equation in previous work, where it is assumed that the radiation emissivity of glass of the panel (at the front) is  $\varepsilon = 0.90$  and rear EVA is  $\varepsilon = 0.85$  [36]. It is assumed that radiation heat flux, needed in Eq (2-5) is the sum of that radiation emitted to the ambient air and the ground. This is attained by multiplying the view factor of the front/rear to the radiation heat transfer terms calculated from the Stefan Boltzmann law [6]:

$$q''_{rad,f/r} = F\sigma (T_{f/r}^2 - T_a^2)_{air} + F\sigma (T_{f/r}^2 - T_a^2)_{ground} \quad (2-11)$$

Here  $F$  is the view factor either from the surface to the air (first term on right hand side of the above equation) and from the surface to the ground (second term on the right hand side). View factor equations are given in previous work [6], and for  $\theta = 30^\circ$  these equate to  $F = 0.93$  at the front and  $F = 0.066$  at the rear. Symbol  $\sigma$  represents the Stefan Boltzmann constant equal to  $5.67 \times 10^{-8} \text{ W}\cdot\text{m}^{-2}\cdot^\circ\text{C}^{-1}$ . After applying the values of all the heat losses, it is concluded that there is only 2.6% difference between the values of R.H.S (right hand side) and the L.H.S (left hand side) of Eq (2-5). Thus the assumptions and relations used in this analysis are acceptable.

Figure 2-7 illustrates various modes of heat transfer involved in the overall energy balance for each configuration. These energy balances were used to estimate the convective heat transfer coefficient.

These heat transfer modes are used for transient calculations of this coefficient so that a comparison of cooling of these devices can be illustrated over a time period of 0-140 minutes. They are also used to determine the parameters of the heat sink and channel. The heat transfer coefficient at the rear of the bare panel is attained by Eq (2-8).

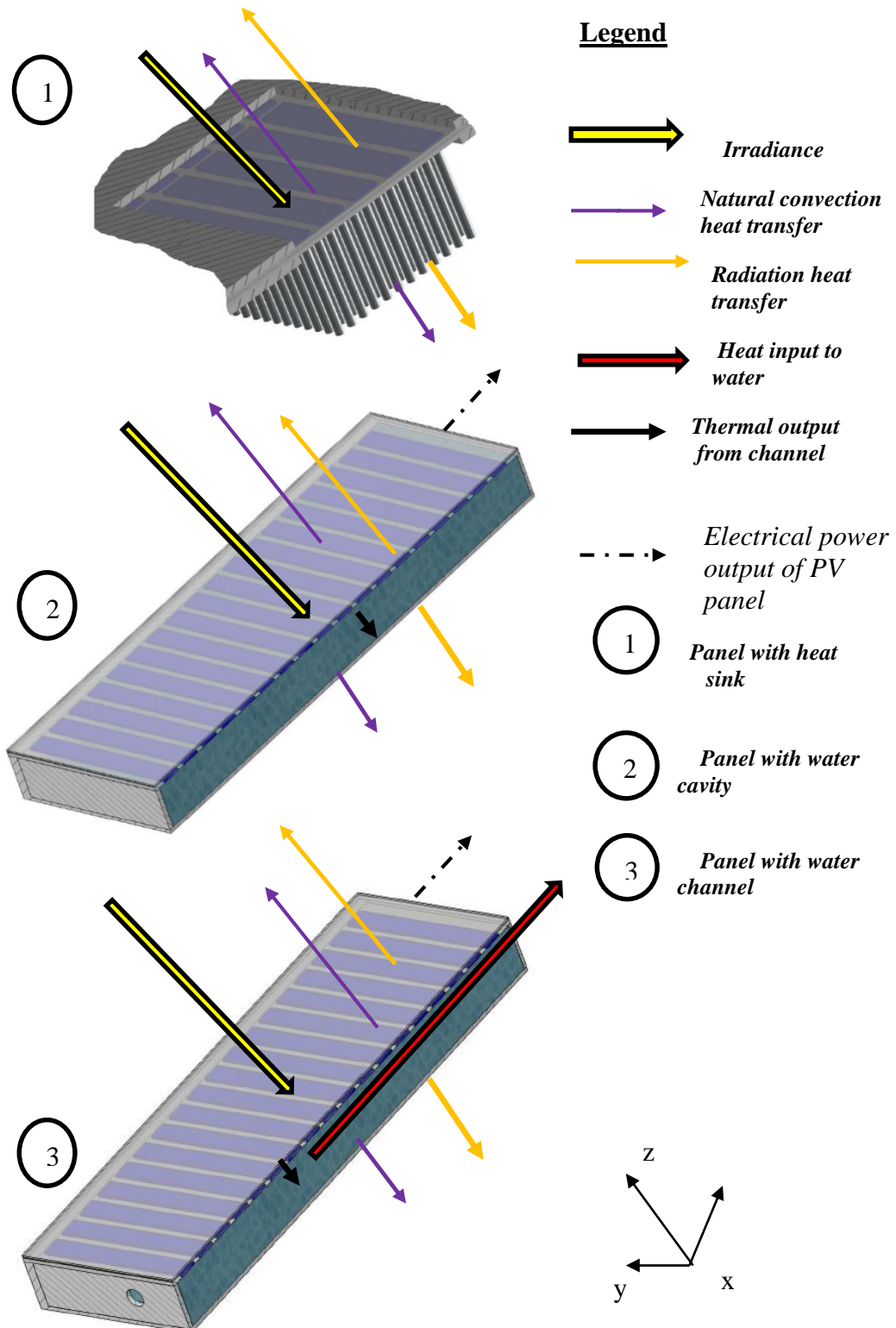


**Figure 2-7: Illustration of various heat transfer modes present in the configurations considered in the present study**



That heat transfer coefficient at heat sink is attained by:

$$h_{conv,r} = \frac{GA - (q''_{conv,f} + q''_{rad,f})A_f - q_{rad,r}}{(T_{avg} - T_a)(A_{fins} + A_{base})} \quad (2-12)$$

The equation states that the heat losses are by convection and radiation from the front and the rear. In this equation,  $T_{avg}$ , is the average temperature of the heat sink (base and fin). The base is at 58.7°C, while the mid is at 52.3°C and tip at 49.5°C, making the average temperature equal to 53.5°C. The irradiance,  $G$  is experimentally attained and  $A_f$  is the front exposed area of the panel with heat sink, equal to 0.016 m<sup>2</sup>. The convective heat flux at the front is attained from Eq (2-10). This is acquired using the height of the heat sink as the characteristic length of natural convection heat transfer,  $H = 0.127$  m. The radiation heat transfer flux at the front of the heat sink is attained from Eq (2-11). Area of the fins is  $A_{fin} = 0.176$  m<sup>2</sup> and the base is  $A_{base} = 0.0139$  m<sup>2</sup>. The heat sink radiation heat transfer rate is calculated in and used in the above equation. The rate is the product of the flux and the heat transfer surface area (area of the heat sink). Previous work has demonstrated that highly populated fins must account for the radiation heat transfer as the secondary mode of heat transfer after convection [11], by the formula which is the average radiation heat transfer by the base and fin surfaces of the heat sink:

$$q_{rad,r} = \varepsilon [ab^2 + 2l(b^2)](T_{fin}^4 - T_a^4) \quad (2-13)$$

This value is highly dependent on the material finish of the heat sink. The finish of the commercially purchased heat sink in the present study is clear coated smooth finish and no surface roughness values are provided by the vendor. The emissivity of the heat sink is influenced by the pin population and is calculated to be  $\varepsilon = 0.99$  attained from formula in previous work [11, 37]. The convective heat transfer rate from the fins in Eq (2-13) is attained from:

$$q_{conv,fin} = GA - (q''_{conv,f} + q''_{rad,f})A_f - q_{rad,r} - q''_{conv,base} \cdot A_{base} \quad (2-14)$$

The heat transfer flux from the base  $q''_{conv,base}$  is attained by Eq (2-10) and the heat transfer coefficient at the base of the heat sink is attained from Eq (2-9). The Rayleigh number at the

base is attained by using Eq (2-7), with  $H = 0.127$  and the Nusselt number is attained by Eq (2-8). To understand if natural convection was achieved by the heat sink, its Nusselt number was calculated from substitution in Eq (2-9). The characteristic length of heat transfer in this equation for the heat sink only, is attained from previous work and equal to  $L = 0.084$  m from [33]:

$$L_{heat\ sink} = (N - 1) S + d \quad (2-15)$$

In this equation,  $N$  is the number of fins in one row of the heat sink,  $S$  is the spacing and  $d$  is the diameter of the fins. The third convective heat transfer coefficient is attained at the rear of the panel with the water cavity. This method is adapted from the works of Bar-Cohen [38], which provide the following formula to acquire this coefficient for a certain time:

$$h_{conv,r} = \frac{\left[ M C_w \left( \frac{dT_w}{dt} \right) + q_b \right]}{(T_b - T_w) A_f} \quad (2-16)$$

Here the mass of water is  $M = 4.75$  kg (measured in the laboratory),  $q_b$  is the heat transfer rate from the back PVC cover (from convection and radiation), and  $dT_w$  is the temperature change of the water during the time interval  $dt$ . This formula is derived from their heat transfer model which is represented in Figure 2-7. It is assumed that the rate of heat input into the water is lost from the back cover of the cavity. The heat input into the water is term  $MC_w \left( \frac{dT_w}{dt} \right)$  and the heat lost at the back of the cavity is given by  $q_b$ . The heat transfer in this cavity is between the rear of the panel and the water.  $A_f$  is the front or rear area of the panel,  $C_w$  is the specific heat capacity of the water taken as  $4181 \text{ J}\cdot\text{kg}^{-1}\cdot\text{K}^{-1}$ . The heat transfer into the water is calculated for an interval of 3 seconds using the change in temperature of the water,  $dT_w$ , attained from experimental data. The water temperatures of the device over time were 3-4 degrees lower than the rear during the experiment. The rate of heat loss from the back cover of the cavity,  $q_b$ , is the average heat loss between time  $t$  and  $t + dt$ .

Since the evolution of temperature was slow on the back PVC cover of the cavity, it is fair to assume that there was initial phase of conduction heat transfer from this surface. This provides realistic values of  $q_b$ . The Nusselt number at the back surface is attained from [39]:

$$Nu^n(x) = \frac{1}{H} \int_0^H Nu(x) dx = \frac{1}{n+1} \left( \frac{\pi}{4\alpha t} \right)^{\frac{n}{2}} H^{n+1} \left( \frac{Ra(x)}{10 \left[ 1 + \left( \frac{0.437}{Pr} \right)^{\frac{9}{16}} \right]^{\frac{16}{9}}} \right)^{\frac{n}{4}} \quad (2-17)$$

In this formula  $n = 6$ , which used for fluids with  $Pr > 0.01$  and situations in which  $Ra < 10^9$ . Time step is  $dt = 3$  seconds. After decreasing this time step, no change in the heat transfer coefficient was witnessed and thus it was the minimum time step needed to attain the results.

The last phase of this data reduction segment is determining the convective heat transfer coefficient at the rear of the panel in the channel/configuration3. A heat transfer model was used as shown in Figure 2-7. Initially the panel is absorbing heat while it is emitted heat via its front and the rear. Heat entering the water is partially carried forward to the cold reservoir and some of it is lost to the back cover. The heat transfer coefficient is the ratio of the heat input into the water by the difference between the rear of the panel,  $T_r$  and the back cover  $T_b$ . The heat transfer into the water channel is attained by:

$$q''_{conv,r} = G(1 - \eta_{el}) - \frac{C_{pv}\Delta T_{pv}}{\Delta t} - q''_f \quad (2-18)$$

Here  $\Delta T_{pv}$  is the temperature change of the panel, calculated from the average of the back and front surface between  $\Delta t$ ,  $q''_f$  is the total convective and radiation heat loss from the front. The panel temperature,  $T_{pv}$  is taken as the average of the front and rear.

The heat capacity of pc-Si panel is  $C_{pv} = 1003.57 \text{ J}\cdot\text{K}^{-1}$  [31], acquired from previous work. The time step  $\Delta t = 1$  second is used for this analysis. Lower time steps demonstrated no difference in the values  $q''_{conv,r}$  in the above equation. The coefficient  $h_{conv,r}$  is calculated from substitution in Eq (2-10) using the value of  $q''_{conv,r}$  calculated above.

The determination of these coefficients has been done via many assumptions. It is assumed that the ambient and ground temperatures remain constant. It is assumed that only natural convection is the mode of convective heat transfer in the closed laboratory room and no forced convection was present. It is assumed that during the experimental time period, the irradiance on the panels remains constant. It is assumed that there are no panel power output measurement discrepancies from the heating of the ceramic power resistors.

In the heat transfer coefficient determination of the cavity, the procedure negates the use of the front surface convective and radiation heat loss and the heat absorbed by the panel over time. The thermal model was utilized as such to negate their usage. The average temperature of the panel,  $T_{pv}$ , in Configuration 3 is assumed in this study to be equal to the mean of the front and the rear. In the experiments, the front of the panel was recorded to be of value  $3.8^{\circ}\text{C}$  higher than the rear in this configuration.

### 2.5.3 Evaluation of heat sink performance

The heat sink must meet a certain criteria of applicability. This is  $E > 2$  and  $\eta = 1$ . The effectiveness  $E$  is calculated via:

$$E = \frac{q_r | \text{configuration 2}}{q_r | \text{bare panel}} \quad (2-19)$$

Here  $q_r$  is the sum of the convection and radiation heat transfer rate from either the heat sink/Configuration 1 or the bare panel. The above equation states that the effectiveness is the ratio of heat transfer rate by the heat sink to that without the heat sink (bare panel). Term  $q_r$  for the heat sink is attained by the subtraction of the front surface convection and radiation heat transfer rate from the rate of light on the four cells. Term  $q_r$  for the bare panel is attained by subtraction of the front surface convection and radiation heat transfer rate over four cells of the bare panel from the rate of light over  $0.127 \times 0.127$  m only and not the entire panel.

The efficiency of the fins is the ratio of heat transfer rate from the heat sink, to its maximum potential heat transfer rate. The maximum potential heat transfer rate is calculated based on assuming the entire fins would be at the same temperature as that of the base. A

temperature gradient along the fins exists in the present study that is deviant from this idealization. The efficiency of the fins is then:

$$\eta = \frac{q_{fins | experimental}}{h_{fins}(T_{base}-T_a)A_{fins}} \quad (2-20)$$

Here  $h_{fins}$  is the heat transfer coefficient at the fins. It is assumed in this study that the heat transfer coefficient at the fins is constant between the experimental and ideal conditions and thus the above equation reduces to the ratio of the difference between the fin and ambient temperature to the difference of the base and ambient temperature.

It is important to attain the heat transfer coefficient at the fins, to demonstrate the negative impact of using the fin array and compare it to the heat transfer coefficient at the base of this heat sink. At the fins the coefficient is attained from:

$$h_{fins} = \frac{q_r - h_{base} A_{base} (T_{base} - T_a)}{T_{fins} - T_a} \quad (2-21)$$

In this equation rates of heat transfer are utilized.

#### 2.5.4 Evaluation of channel performance

The channel is hypothesized to have thermally developing flow and provide significantly high cooling. It was initially hypothesized that a competitive mass flow rate as that of previous work could exist or be stronger to provide  $Re > 60$ , which yields the thermally developing flow along the channel length. The Nusselt numbers in this channel from experimental work are compared to hypothetical values that should have been attained from the flow strength of the channel in the present study and also to the values of previous work. The local Nusselt numbers at the rear are evaluated from the heat transfer model:

$$Nu_{(x)} = \frac{(G - \eta_{el}A) - q_{f(x)}}{T_{r(x)} - T_{w(x)}} \quad (2-22)$$

All local values are used in this equation. The local Nusselt numbers of this channel are compared to those of the local Nusselt numbers when  $Re > 60$  and those which should be from the Reynolds number in the present study. The Reynolds number in the present study is calculated from [40]:

$$Re = \frac{4 \dot{m}}{\mu 2L} \quad (2-23)$$

where  $\dot{m}$  is the mass flow rate,  $\mu$  is the dynamic viscosity equal to  $8.94 \times 10^{-4} \text{ kg} \cdot \text{m} \cdot \text{s}^{-1}$  and  $L$  is the channel spacing equal to  $25 \times 10^{-3} \text{ m}$ .  $Re < 2300$  represents laminar flow in the channel. The mass flow rate in the above equation is calculated via the following equation attained from the heat transfer model of the channel :

$$\dot{m} = \frac{q''_{in} A_f - q''_b A_f}{(T_{out} - T_{in}) C_{water}} \quad (2-24)$$

Here  $A_f = 0.162 \text{ m}^2$  and  $C_{water} = 4182 \text{ kJ} \cdot \text{kg}^{-1} \cdot \text{K}^{-1}$ . Data is present in previous work that provide values of  $Nu_{(x)}$  vs  $x^*$ , the non-dimensional distance from the leading edge of the channel according to the flow Reynolds number and channel thickness and fluid Prandtl number. This data reduction is needed to attain the local Nusselt numbers that should arise from the flow strength of the present and that when  $Re > 60$ . The non-dimensional distance,  $x^*$  from previous work is simply converted to the local distance  $x$  of the channel in the present study by using the formula [24]:

$$x = Re \cdot Pr \cdot 2L \cdot x^* \quad (2-25)$$

Hence,  $Nu_{(x)}$  is plotted against  $x$  in the present work. The present work is also compared to previous PV/T collectors using channels with Nusselt number of  $Nu = 3.61$  for  $\alpha^* = 1$  channel,  $Nu = 4.11$  for  $\alpha^* = 0.5$  with boundary conditions of all walls heated at constant temperature and  $Nu = 5.385$  for  $\alpha^* = 0$  when the boundary condition of upper channel wall dissipating uniform heat flux while others are adiabatic. The thermal efficiency of the channel configuration is calculated and compared to these collectors as well. This is simply the ratio of the heat flux out of the channel by that entering the water. Lastly, since this was the best method to cool the panel, its cell temperatures must be verified.

The process of determining the cell temperature is vital in research work comprising of panel cooling. The analytical cell temperature is thus determined in the present study for the bare panel and compared with that with the channel.

In any claims of cooling, it is essential to validate the cell temperature of the panel, rather than reports on the measured surface temperatures. In the present study,  $T_{cell}$  is achieved via analysis utilizing the thermal conductivity properties and geometry of the pc-Si panel in previous work [6] and the heat transfer coefficients (over all heat transfer coefficients from natural convection and radiation) attained from the experimental work.

A one-dimensional conduction heat transfer model with energy generation is used to determine this value. The heat losses from the surfaces of the panel are assumed to be in one direction only and not along the height of the panel. This assumption is made based on the fact that the heat was being dissipated normal to the hottest surfaces of the panel, being the front and the rear. Thus the heat transfer is in the z-direction only of Figure 1-1 of the bare panel and z-direction of the panel with the channel in Figure 2-7.

The model assumes that the irradiance that is not converted to electricity is generated as heat from the center of the cell. This heat is dissipated at the front and the rear of the panel as shown in Figure 1-1. The one dimensional heat transfer model with energy generation as the cell center in a channel is adapted from previous work [41]:

$$T_{cell} = \frac{G(1-\eta_{el})\delta^2}{2k} + \frac{q''_f R_{cell-a}|_{front} + T_a + q''_{conv,r} R_{cell-a}|_{rear} + T_a}{2} \quad (2-26)$$

The thickness of the cell is  $\delta = 225 \times 10^{-6}$  m and the conductivity of the cell is  $k = 1.48 \text{ W}\cdot\text{m}\cdot\text{K}^{-1}$  and symbol R is the thermal resistance of heat transfer.  $R_{cell-a}$  is the thermal resistance from the cell center to the fluid at the front or the rear. It is the ambient air for the bare panel on both surfaces at temperature  $T_a$ . The thermal resistance concept of different layers attached in series to one another, is rigorously explained in previous work [41]. The thermal resistance is represented by:

$$R = \frac{\delta_i}{k_i} + \frac{1}{h_{f/r}} \quad (2-27)$$

Symbols  $\delta_i$  and  $k_i$  are the thickness and thermal conductivities of the  $i_{th}$  layer adjacent to the center travelling to the front or the rear. Eq (2-26) can be utilized to attain the cell temperature of the bare panel in Figure 1-1 by calculating the respective resistances and replacing the last term on the R.H.S,  $T_a$  by  $T_w$ .

## 2.6 Discussion

The analysis provides critical information about cooling the panel using these three configurations. The average convective heat transfer coefficients at the rear of the panel using the three configurations are compared to that of the bare panel in Figure 2-8. The bare panel absorbs heat till  $t = 1.72$  minutes after which it dissipates heat via natural convection and radiation from its rear and front. The heat sink is demonstrating weak convective heat transfer while also emitting heat via radiation, while the cavity stops cooling via natural convection after  $t = 140$  minutes and conduction is the mode of heat transfer. The channel initially provides a high cooling that decreases to a moderate value. Thermosyphon effect provides forced flow of water through this channel after  $\approx 21$  minutes into the experiment after which the convective heat transfer coefficient is attained. Prior to this time, it is unrealistic to report this coefficient since it represents extremely large values according to the data reduction procedure in the present study.

The heat transfer coefficient at the rear of the bare panel is  $h_{\text{conv,r}} = 4.4 \text{ W}\cdot\text{m}^{-2}\cdot\text{K}^{-1}$ . It is initially lower at  $h_{\text{conv,r}} = 3.5 \text{ W}\cdot\text{m}^{-2}\cdot\text{K}^{-1}$  at  $t = 1$  minutes and increases due to higher surface temperatures. The heat losses are by natural convection and are laminar in nature judging from  $Ra = 5.55 \times 10^8$  at  $Pr = 0.714$  and  $Nu = 64.4$  at the front, while  $Ra = 2.2 \times 10^8$  at  $Pr = 0.711$  and  $Nu = 83.3$  at the rear once steady state is achieved. The critical Rayleigh number to onset natural convection is  $Ra > 1.97 \times 10^4$  which has been surpassed by the bare panel. The critical Rayleigh number to onset turbulent natural convection at the rear is  $Ra_{\text{cr}} > 2 \times 10^9$  which is not the case. The radiation heat transfer from the panel is very significant. The total convective heat loss from the panel is 36.4% of the irradiance while the radiation heat loss is 63.38%. The front and rear of the panel are dissipating equal amount heat; 53.1% of the irradiance at the rear 46.9% at the front. These percentages remain nearly constant throughout the experiment. Comparatively the rear of the heat sink provides a low convective heat transfer coefficient. The convective heat transfer coefficient at the base of the heat sink is  $h_{\text{conv,base}} = 3.58 \text{ W}\cdot\text{m}^{-2}\cdot\text{K}^{-1}$  while at the fins is  $h_{\text{conv,fin}} = 1.02 \text{ W}\cdot\text{m}^{-2}\cdot\text{K}^{-1}$  making the overall value  $h_{\text{conv,r}} = 1.3 \text{ W}\cdot\text{m}^{-2}\cdot\text{K}^{-1}$ . Initially the overall coefficient for the entire heat sink is  $4.5 \text{ W}\cdot\text{m}^{-2}\cdot\text{K}^{-1}$ . This is the heat transfer coefficient when the front surface is not at the high temperatures as those at steady state in Figure 2-5.



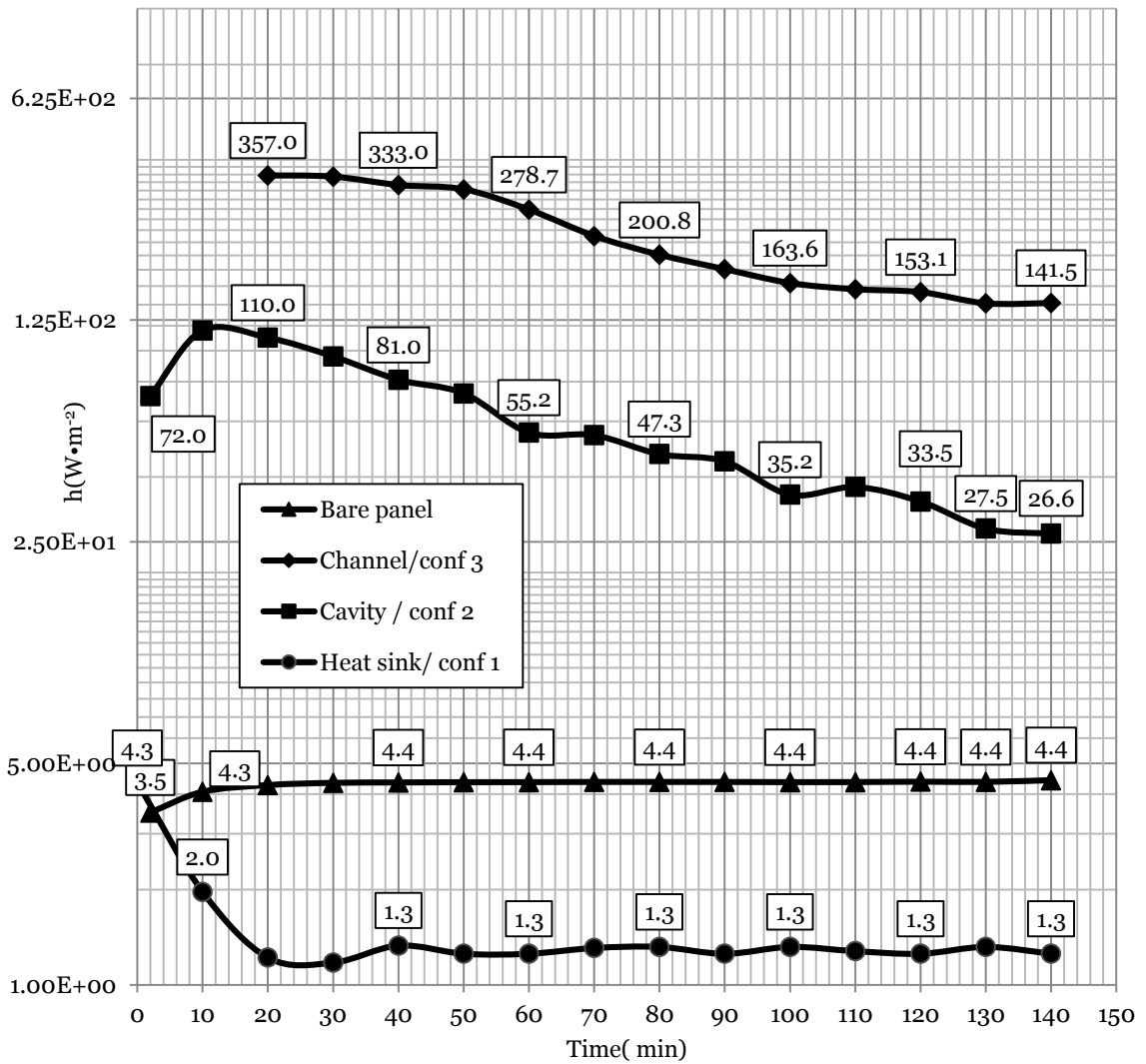


**Figure 2-8: Convective heat transfer coefficients at the rear of the panel**

Once the panel with the heat sink has gained heat and is dissipating it to the surrounding, when the temperature of the heat sink base rises to 59.68°C, the heat transfer coefficient becomes very small. This is because of the negative influence of the population of the pins. Majority of the heat is lost via radiation from the heat sink. The natural convection at the heat sink is weak, as judged from the low Rayleigh number value of  $Ra = 8.26 \times 10^5$  and

$Nu = 16.39$  at  $Pr = 0.713$  at the base. The Nusselt number of the heat sink is  $Nu = 2.0$  which signifies weak natural convection. Radiation heat transfer is 68.1% of the total heat transfer at the heat sink while the remaining amount is from natural convection. It is important to compare how much over all cooling was achieved from the heat sink. To do so, the effectiveness is calculated. The effectiveness is the increase in heat transfer with the heat sink than without the heat sink on the hot surface under study.

The effectiveness is calculated to be equal to  $E = 1.53$  for an area of  $0.127 \times 0.127$  of the panel and the fin efficiency is  $\eta = 0.69$ . This means that the heat transfer (convection and radiation) was not enhanced by twice the amount of that of the bare panel. Also, although it is impossible to attain an ideal  $\eta = 1$ , the efficiency of 0.69 means that the ideal conditions were not met.

The heat transfer in the cavity decays from  $h_{conv,r} = 115.2 \pm 2.5 \text{ W}\cdot\text{m}^{-2}\cdot\text{K}^{-1}$  at  $t = 10$  minutes to  $h_{conv,r} = 27.5 \pm 1.0 \text{ W}\cdot\text{m}^{-2}\cdot\text{K}^{-1}$  at  $t = 140$  minutes shown in Figure 2-8. The heat transfer is not steady and the heat loss from the front increases drastically over time. The cavity loses too much heat to the surrounding via laminar natural convection at the front and the back cover i.e. at  $t = 10$  minutes,  $Ra = 1.13 \times 10^7$  at the front while at back cover it is  $Ra = 1.01 \times 10^7$ . It also loses heat via radiation heat transfer to the surrounding. Strength of natural convection in the cavity was evaluated by attaining the Rayleigh numbers at specific instances using the correlation for differentially heated cavities in previous work [33]. This Rayleigh number is attained from Eq (2-7), using the thickness of the cavity as the characteristic length. The Rayleigh numbers from previous work of aspect ratio  $\beta^* = 12$  displays very weak natural convection for inclinations of  $\theta = 15^\circ - 60^\circ$  when  $Ra > 6 \times 10^4$  [12] as discussed in the introduction of this chapter. In the present study, instantaneous numbers are  $Ra = 2.94 \times 10^4$  at  $t = 10$  minutes which decays to  $1.1 \times 10^4$  at  $t = 140$  minutes which do not signify any significant natural convection and hence this configuration will not be discussed further.

Initial cooling in the channel/configuration 3 is large (see Figure 2-8) due to the fact that initiation of the thermosyphon flow is occurring and the heat losses from the collector are minimal. Over time, laminar natural convection is increasing on the front and the back cover of the channel. The front heat losses from natural convection increase from  $Nu =$

22.2 to 46.1 from  $t = 21-140$  minutes and from back cover of the channel from  $Nu = 42.3$  to 63.9. These are high laminar natural convection heat losses where  $Ra = 4.60 \times 10^7 - 2.178 \times 10^8$  during this time period. The heat transfer coefficient decays from  $357 \text{ W}\cdot\text{m}^{-2}\cdot\text{K}^{-1}$  to  $141 \text{ W}\cdot\text{m}^{-2}\cdot\text{K}^{-1}$  at the rear of the panel. The heat transfer at the rear of the panel is from convection and accounts for 61% of the heat loss from the panel when at steady state. The rest is via the front from natural convection and radiation. Figure 2-8 clearly depicts that traditional PV/T collector designs are the best for cooling the panel under the conditions used in the laboratory. This channel's  $Nu_{(x)}$  values are 5.94, 5.57, 5.36 and 5.13 at the rear locations where the temperatures were measured. The Reynolds number in this device is  $Re = 12.1$ . Figure 2-9 provides a comparison of these experimental values. The current mass flow should provide the local Nusselt number values of  $Re = 12.2$  for an  $\alpha^* = 0$  channel. Its local Nusselt number trend should be that depicted in this Figure. The values of local Nusselt numbers attained in this work are too few for a solid comparison to claim thermally developing flow.

Hypothetical values from  $Re = 60$  in the channel and the constant values in previous work are also compared. For the flow to be thermally developing along the channel height, the profile of  $Re = 60$  should be attained in such a channel. This demonstrates the optimum local Nusselt numbers for cooling the panel rear using a single channel, in which the rest of the walls of the channel are adiabatic. The walls of the channel in the present study were not adiabatic. This Number would surpass those of previous work if it is attained and demonstrated in Figure 2-9. As seen from Figure 2-9,  $Nu_{(x)}$  values are higher for  $Re = 60$  in the single channel of aspect ratio of  $\alpha^*=0$  than those from previous work that assume constant values of  $Nu = 5.385$  of Zondag *et al.*[18] , while those of Chow *et al.*[20]& Ji *et al.*[23] and Sandes & Rekstand [19] who assumed  $Nu = 4.11$  and  $Nu = 3.68$ . He *et al.*[22] utilized a  $\alpha^* = 0.2$  channel which translates to  $Nu = 5.35$  according to Rohsenow [24]. These values of Nusselt numbers in previous work have not been measured or evaluated. They have been assumed from literature. The previous PV/T collectors have used a maximum irradiance of solar light between  $800-900 \text{ W}\cdot\text{m}^{-2}$  at  $0 \text{ C}^\circ \cdot \text{m}^{-2} \cdot \text{W}^{-1}$  reduced temperatures. Their thermal efficiencies are higher than the channel device of the present study as given in Figure 2-9. The present study provides a PV/T collector of thermal

efficiency of  $\eta_{th} = 0.51$ . Using this channel brings forth  $T_{cell} = 87.5 \pm 1.2^\circ\text{C}$  to  $63.8 \pm 1.2^\circ\text{C}$  by enhancing the heat transfer coefficient.

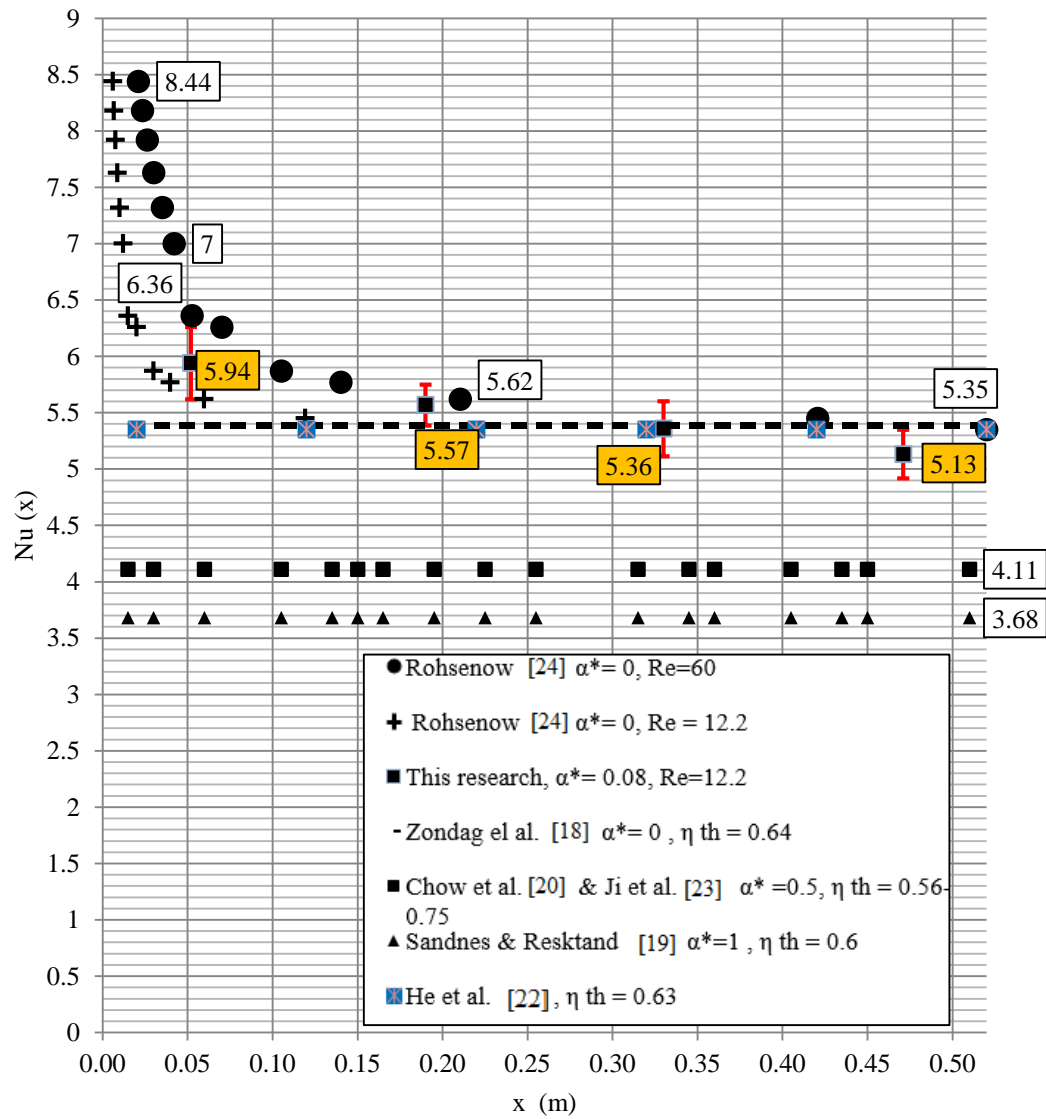


**Figure 2-9: Local Nusselt numbers along the channel in the present study compared to previous work and hypothetical scenarios**

## 2.7 Conclusion

This work is performed under halogen light, controlled ambient temperatures and  $0 \text{ m}\cdot\text{s}^{-1}$  wind speeds. The independent variables of the study were the temperatures of the panel and the power output. These were utilized to understand the dependent variable, the heat transfer coefficient at the rear of the panel when using three configurations. This heat transfer coefficient comparison serves as a datum for future reference of using these types of device such as their geometries and materials for cooling the panel, if needed.

The hot panel is demonstrated on an open rack mount inclined at  $\theta=30^\circ$  from the ground under halogen light irradiance of  $1378.4 \pm 23.5 \text{ W}\cdot\text{m}^{-2}$  to simulate high temperatures. This work is suitable for referring various methods to cool a panel at front surface temperatures of  $T_f=81.7 \pm 2.3^\circ\text{C}$  and rear temperatures of  $90.7 \pm 2.3^\circ\text{C}$  when no winds are present and ambient temperatures are  $T_a = 23.5^\circ\text{C}$ . Cell temperature of this panel cannot be claimed since it was not measured but analytically calculated.

The heat sink and the channel were determined to be the best methods of cooling, while the channel was more superior. A water cavity attachment to the rear does not reach steady state and is not recommended to be used. The surface area enhancement using 197 cylindrical pin fin heat sink brings forth an effectiveness of  $E = 1.53$  and the fin efficiency of  $\eta = 0.69$ . Heat sink needs to cover the entire rear surface of the panel for more comprehensive results. Applicability of heat sinks to any hot surface must meet an effectiveness of greater than 2. It is concluded that although it cooled the panel, judging from a lower front temperature of  $T_f = 53.2 \pm 1.5^\circ\text{C}$ , it provides weak natural convection with the current method of experimentation only. Most of the heat loss is by radiation from the heat sink. It is recommended that optimized cylindrical pin fin geometry is needed to attain stronger natural convection, or different types of heat sinks should be trailed under these experimental conditions to compare it to the hot bare panel. For a more comprehensive comparison, varying experimental conditions should be used.

The channel configuration is identical to the design of PV/T collectors in previous work and differs in using a single channel at the rear of the panel. It is connected to a cold

reservoir in a closed loop. Water circulation from the thermosyphon effect began at a later stage in the experiment, at  $\approx 20$  minutes. The initial heat transfer coefficient at the rear of the panel was large which decayed to a steady state value of  $141.1 \text{ W}\cdot\text{m}^{-2}\cdot\text{K}^{-1}$ . The local Nusselt numbers at the rear of the panel with this channel were evaluated and compared to the hypothesis and previous work.

Over all the Nusselt number in the channel is  $\text{Nu} = 5.67$  but more values are needed to assure this average. Furthermore, it is recommended to measure mass flow rates arising from thermosyphon effect since it is a more accurate way of determining the thermal efficiency of such setups.

## 2.8 References

- [1] Skoplaki, E., and Palyvos, J., 2009, "On the temperature dependence of photovoltaic module electrical performance: A review of efficiency/power correlations," *Solar Energy*, 83(5), pp. 614-624.
- [2] Jazayeri, M., Uysal, S., and Jazayeri, K., "Analysis of effects of sun's position in the sky on solar radiation and solar panel output power," *Proc. AFRICON, 2013, IEEE*, pp. 1-7.
- [3] King, D. L., Kratochvil, J. A., and Boyson, W. E., 2004, "Determination of cell temperature during testing" *Photovoltaic array Performance model*, United States Department of Energy Sandia National Laboratories, Albuquerque, pp 21-28
- [4] Evans, D., 1981, "Simplified method for predicting photovoltaic array output," *Solar Energy*, 27(6), pp. 555-560.
- [5] Herrmann, W., Wiesner, W., and Vaassen, W., "Hot spot investigations on PV modules- new concepts for a test standard and consequences for module design with respect to bypass diodes," *Proc. Photovoltaic Specialists Conference, 1997., Conference Record of the Twenty-Sixth IEEE, IEEE*, pp. 1129-1132.
- [6] Armstrong, S., and Hurley, W., 2010, "A thermal model for photovoltaic panels under varying atmospheric conditions," *Applied Thermal Engineering*, 30(11), pp. 1488-1495.

- [7] Tina, G., and Abate, R., "Experimental verification of thermal behaviour of photovoltaic modules," Proc. Electrotechnical Conference, 2008. MELECON 2008. The 14th IEEE Mediterranean, IEEE, pp. 579-584.
- [8] Luque, A., Sala, G., Arboiro, J., Bruton, T., Cunningham, D., and Mason, N., 1997, "Some results of the EUCLIDES photovoltaic concentrator prototype," Progress in Photovoltaics: Research and Applications, 5(3), pp. 195-212.
- [9] Natarajan, S. K., Mallick, T. K., Katz, M., and Weingaertner, S., 2011, "Numerical investigations of solar cell temperature for photovoltaic concentrator system with and without passive cooling arrangements," International Journal of Thermal Sciences, 50(12), pp. 2514-2521.
- [10] Sparrow, E., and Vemuri, S., 1986, "Orientation effects on natural convection/radiation heat transfer from pin-fin arrays," International Journal of Heat and Mass Transfer, 29(3), pp. 359-368.
- [11] Aihara, T., Maruyama, S., and Kobayakawa, S., 1990, "Free convective/radiative heat transfer from pin-fin arrays with a vertical base plate (general representation of heat transfer performance)," International Journal of Heat and Mass Transfer, 33(6), pp. 1223-1232.
- [12] Arnold, J., Catton, I., and Edwards, D., 1976, "Experimental investigation of natural convection in inclined rectangular regions of differing aspect ratios," Journal of Heat Transfer, 98(1), pp. 67-71.
- [13] Catton, I., Ayyaswamy, P., and Clever, R., 1974, "Natural convection flow in a finite, rectangular slot arbitrarily oriented with respect to the gravity vector," International Journal of Heat and Mass Transfer, 17(2), pp. 173-184.
- [14] Anis, W., Mertens, R., and Van Overstraeten, R., "Calculation of solar cell operating temperature in a flat plate PV array," Proc. Photovoltaic Solar Energy conference. 5, pp. 520-524.
- [15] Duffie, J. A., and Beckman, W. A., 1980, "Solar water heating - Active and Passive " Solar Engineering of Thermal Processes, Wiley New York New York, pp. 487-489.
- [16] Dubey, S., and Tiwari, G., 2008, "Thermal modeling of a combined system of photovoltaic thermal (PV/T) solar water heater," Solar Energy, 82(7), pp. 602-612.

- [17] Zondag, H., De Vries, D. D., Van Helden, W., Van Zolingen, R., and Van Steenhoven, A., 2002, "The thermal and electrical yield of a PV-thermal collector," *Solar Energy*, 72(2), pp. 113-128.
- [18] Zondag, H., De Vries, D., Van Helden, W., Van Zolingen, R., and Van Steenhoven, A., 2003, "The yield of different combined PV-thermal collector designs," *Solar Energy*, 74(3), pp. 253-269.
- [19] Sandnes, B., and Rekstad, J., 2002, "A photovoltaic/thermal (PV/T) collector with a polymer absorber plate. Experimental study and analytical model," *Solar Energy*, 72(1), pp. 63-73.
- [20] Chow, T. T., Pei, G., Fong, K., Lin, Z., Chan, A., and Ji, J., 2009, "Energy and exergy analysis of photovoltaic–thermal collector with and without glass cover," *Applied Energy*, 86(3), pp. 310-316.
- [21] Chow, T., He, W., and Ji, J., 2006, "Hybrid photovoltaic-thermosyphon water heating system for residential application," *Solar Energy*, 80(3), pp. 298-306.
- [22] He, W., Chow, T.-T., Ji, J., Lu, J., Pei, G., and Chan, L.-s., 2006, "Hybrid photovoltaic and thermal solar-collector designed for natural circulation of water," *Applied Energy*, 83(3), pp. 199-210.
- [23] Ji, J., Lu, J.-P., Chow, T.-T., He, W., and Pei, G., 2007, "A sensitivity study of a hybrid photovoltaic/thermal water-heating system with natural circulation," *Applied Energy*, 84(2), pp. 222-237.
- [24] Rohsenow, W. M., Hartnett, J. P., and Cho, Y. I., 1998, "Forced Convection, Internal Flow in Ducts," *Handbook of Heat Transfer*, McGraw-Hill, New York, p. 5.68.
- [25] Victoria, M., Herrero, R., Domínguez, C., Antón, I., Askins, S., and Sala, G., 2013, "Characterization of the spatial distribution of irradiance and spectrum in concentrating photovoltaic systems and their effect on multi-junction solar cells," *Progress in Photovoltaics: Research and Applications*, 21(3), pp. 308-318.
- [26] Emery, K., 1986, "Solar simulators and I–V measurement methods," *Solar Cells*, 18(3), pp. 251-260.
- [27] Hulstrom, R., Bird, R., and Riordan, C., 1985, "Spectral solar irradiance data sets for selected terrestrial conditions," *Solar Cells*, 15(4), pp. 365-391.



- [28] Emery, K., 1986, "Solar simulators and I-V measurement methods," *Solar Cells*, 18(3), pp. 251-260.
- [29] Bergman, T. L., Incropera, F. P., and Lavine, A. S., 2011, "One Dimensional, steady-state conduction," *Fundamentals of Heat and Mass Transfer*, John Wiley & Sons, New York, pp. 155-160.
- [30] Holman, J. P., 2010, "Analysis of Experimental Data" in *Experimental methods for Engineers*, McGraw-Hill, pp. 110-113
- [31] Jones, A., and Underwood, C., 2001, "A thermal model for photovoltaic systems," *Solar Energy*, 70(4), pp. 349-359.
- [32] Churchill, S. W., and Chu, H. H., 1975, "Correlating equations for laminar and turbulent free convection from a vertical plate," *International Journal of Heat and Mass Transfer*, 18(11), pp. 1323-1329.
- [33] Bergman, T. L., Incropera, F. P., and Lavine, A. S., 2011, "Free Convection " *Fundamentals of Heat and Mass Transfer*, John Wiley & Sons, New York, pp. 599-624.
- [34] Fujii, T., and Imura, H., 1972, "Natural-convection heat transfer from a plate with arbitrary inclination," *International Journal of Heat and Mass Transfer*, 15(4), pp. 755-767.
- [35] Bergman, T. L., Incropera, F. P., and Lavine, A. S., 2011, "one-dimensional steady-state heat conduction " *Fundamentals of Heat and Mass Transfer*, John Wiley & Sons, pp. 164-171.
- [36] Notton, G., Cristofari, C., Mattei, M., and Poggi, P., 2005, "Modelling of a double-glass photovoltaic module using finite differences," *Applied Thermal Engineering*, 25(17), pp. 2854-2877.
- [37] Matsumoto, N., Tomimura, T., and Koito, Y., 2014, "Heat Transfer Characteristics of Square Micro Pin Fins under Natural Convection," *Journal of Electronics Cooling and Thermal Control*, 4(03), p. 59.
- [38] Shaukatullah, E., Storr, W. R., Hansen, B. J., and Gaynes, M., "Design and optimization of pin fin heat sinks for low velocity applications," *Proc. Semiconductor Thermal Measurement and Management Symposium, 1996. SEMI-THERM XII. Proceedings.*, Twelfth Annual IEEE, IEEE, pp. 151-163.

- [39] Bar-Cohen, A., and Herman, A., 1977, "Experimental investigation of transient natural convection heat transfer in vertical enclosures (constant heating)," *Letters in Heat and Mass Transfer*, 4(2), pp. 111-118.
- [40] Okiishi, M. Y., Munson, B., and Young, D., 2006, "Dimensional analysis, similitude and modelling," *Fundamentals of Fluid Mechanics*, John Wiley & Sons, New York, p. 347.
- [41] Kothandaraman, C., 2006, "Conduction with heat generation," *Fundamentals of Heat and Mass Transfer*, New Age International, New Delhi, pp. 99-100.

## CHAPTER 3

### **A two-chamber integrated photocatalytic and solar-thermal system for water heating and cleaning**

#### **3.1 Abstract**

Water heating systems that can maximize the usage of solar energy and provide water cleaning are highly desired. There are studies missing that report the thermal efficiency of their non-concentrating solar photocatalytic collector, or they are incapable of providing an efficient water heating design. A novel two-chamber solar photocatalytic collector that integrates photocatalytic water cleaning and efficient solar-water heating is reported in the present study. The system utilizes the thermosyphon effect to circulate the mixture in the system and negates the use of water pumps utilized in previous works. Methylene blue dye in de-ionized water was used as a model pollutant against AEROXIDE<sup>®</sup> TiO<sub>2</sub> P90. An irradiance of 1004.7 W•m<sup>-2</sup> was used on the front of this collector to power these two functions. Simulated solar light provided this irradiance using four 500 W halogen bulbs. The indoor experimental conditions were kept at 0 m•s<sup>-1</sup> wind speeds and constant ambient temperatures so that the preliminary behaviour of this device could be determined.

**Keywords:** Solar photocatalytic collectors; natural circulation/ waste water cleaning

## 3.2 Introduction

Natural resources such as solar energy provide a large potential alternative from immense expenditure on earth extraction mechanisms [1], and it is inexhaustible and free. It is being utilized for energy conversion to electricity with lower irradiance and is subjected to immense growth in the future [2]. Along with electrical power conversion, there is a growing demand of solar collector devices for hot water production, for the combination of hot water and electrical power production [3], and the combination of electrical power production and water cleaning [4]. These devices, of the types that are the focus of the present study, have a flat plate design which utilizes the direct and diffuse component of solar radiation.

Utilization of UV-VIS light and some portion of NIR radiation are done by photovoltaic panels for the production of electrical energy, while photovoltaic-thermal collectors provide heat collection using mostly VIS light and NIR radiation [5]. Photovoltaic-photocatalytic devices utilize UV-VIS light and NIR radiation to produce electrical energy. The UV light is required to photoactive semiconductor oxides which are suspended in contaminated waste water in these devices, such as textile dye waste water [6]. Photocatalytic collectors utilize UV light specifically to clean the waste water. These collector designs are either concentrating types with reflective parabolic surfaces or are present without these surfaces and termed non-concentrating devices [6]. They are not designed for hot water production. These photocatalytic collectors are protégés of solar thermal collectors that are made for the sole purpose of producing hot water efficiently. There is work missing from these renewable energy devices; a photocatalytic-solar thermal technology to provide both functions of water cleaning and efficient production of hot water.

The advanced oxidation using  $\text{TiO}_2$  can be used to degrade the complex residue up to a certain level of toxicity in solar photocatalytic collectors beyond which the conventional methods can be successfully used for further degradation [7]. One poisonous textile waste is MB dye.  $\text{TiO}_2$  P25 in suspension form has been used in great multitudes against MB dye under solar light because the catalyst responds to UV light,  $\lambda < 388 \text{ nm}$ , and the dye

responds to larger wavelengths ( $\lambda > 388 \text{ nm}$ ) of VIS light [8]. The reaction is a combination of photocatalysis and photosensitization of dye that provides adequate decomposition under artificial UV light and VIS light.

However, solar photocatalysis is a weak cleaning method. Indoor experiments by Houas *et al.* [9], have demonstrated the best results of decomposing MB dye against TiO<sub>2</sub> P25 catalyst with an indoor Pyrex glass reactor with 125 W mercury lamps . They report full decomposition of MB dye within 110 minutes of initial concentration of  $\approx 22 \text{ ppm}$  using  $2.5 \text{ g}\cdot\text{L}^{-1}$  of TiO<sub>2</sub> P25. Outdoor collectors cannot decompose MB dye as well as indoor reactors because of the lower amounts of UV light present from the sun. However, MB dye versus TiO<sub>2</sub> is a popular combination to test the performance of and immersing technologies such as the combined PV-photocatalytic devices.

Recent combined designs such as the Solwat receiver [10] and the new –helio-photovoltaic [11]. MB dye in waste water is decomposed against a UV activated photocatalyst of type TiO<sub>2</sub> P25 in these works. TiO<sub>2</sub> P25 particles are suspended in a solution of Methylene blue dye and de-ionized water which flow over a 14 Watt pc-Si panel. It takes a certain amount of time (50–120 minutes depending on the catalyst concentration) for decomposition to be completed [12]. These devices provide electrical energy and clean water. However, the pc-Si panel outputs 4 W prior to the water being clean. 10 Watts are being utilized by a pump to push the mixture over the pc-Si panel. Approximately 20-30% of solar light within  $700 < \lambda < 1100 \text{ nm}$  is absorbed by the catalyst, glass cover and water over the panel. Thus, placing any VIS light absorbing dye with even low concentrations of catalyst, such as  $0.2 \text{ g}\cdot\text{L}^{-1}$  of TiO<sub>2</sub> P25 will yields low power output. The author claims that there are low PV panel outputs from these devices and hence traditional solar photocatalytic collectors should be resorted to, if water cleaning is needed.

Two non-concentrating collectors, which clean water but do not generate electricity, are the double-skin sheet reactor (DSSR), which has a length of 1.4 m and height of 9.8 m. It is designed for smaller scale applications, such as house hold water cleaning. DSSR contains 30 channels in which the mixture of waste water and suspended catalyst flow through. The channels are covered by a glass sheet which is transmitting solar light. This device is connected to a reservoir of a large volume in a closed loop and a water pump

forced the mixture through the collector [13]. Similarly another device is the thin-film-falling-bed reactor (TFFBR). It is one of the first solar reactors not applying a light-concentrating. It consists of a sloping glass pane coated with the photocatalyst (e.g., titanium dioxide Degussa P25 or Hombikat UV100) as per the design of Zayani *et al.* [14]. The polluted water flows on the inclined glass pane forming a very thin film ( $\sim 100 \mu\text{m}$ ). These devices are more effective in cleaning waste water using solar light than combined devices and hence PV panels must be separated from solar photocatalytic devices.

One of the best results from the decomposition of MB dye versus  $\text{TiO}_2$  P25 under solar light using CPCs (Compound parabolic collector) and tubular collectors (CPCs without light concentration, non-concentrating collectors) are by Arias *et al.* [15] who reported the photocatalytic de-colorization of 10 ppm MB dye within 315 minutes. These best results were attained including hydrogen peroxide and oxygen bubbles as the supporting reducing and oxidizing agents. Outcomes showed 5 ppm of initial concentration of MB degrading to 70.8% using the CPC ( $0.44 \text{ g}\cdot\text{L}^{-1}$  of  $\text{TiO}_2$  P25), in contrast to tubular collectors; 63.46% degradation ( $0.38 \text{ g}\cdot\text{L}^{-1}$  of  $\text{TiO}_2$  P25).

These collectors do not utilize PV panels and are the best methods for solar water cleaning. CPCs, PTCs (Parabolic trough collector) and these mentioned non-concentrating collectors are the best option for water cleaning. Their categorization is: (i) non-concentrating, low concentration or low temperature systems (up to  $150^\circ\text{C}$  hot water output); (ii) medium concentrating, or medium temperature systems (from 150 to  $400^\circ\text{C}$ ); (iii) high-concentrating or high temperature systems (over  $400^\circ\text{C}$ ) [6]. These collectors are protégés of their water heating versions. Their versions for water cleaning are created to provide significant amount of transmittance of solar light to the mixture of catalyst and waste water. Their thermal efficiencies, the conversion of solar light to thermal energy in the form of hot water output has not been given much consideration. Thus low temperature systems are hence more commonly utilized for small scale operations such as the DSSR, TFFBR and TC.

This is because PTCs for water cleaning contain large parabolic trough mirrors on which concentrate light on borosilicate glass (in which the mixture of waste water and catalyst is present) running along its axis [16]. They concentrate light up to 50 times the incident

sunlight and are medium to high temperatures systems. CPCs are present as a flatbed design, smaller in size as compared to PTCS, with borosilicate tubes running along the compound parabolic reflectors. An array of this set is placed on the bed without any insulation to contain the heat [17]. The device is commonly for low or medium temperature applications and concentrates light up to 1.5 times the irradiance. Tubular collectors are CPCs without light concentration. These three leading collectors do not contain any insulation, which is needed to contain the heat. Also they lack solar thermal absorbers to absorb VIS light and NIR radiation to gain heat. Their thermal efficiencies, which are the amount of conversion of solar light to thermal output, have thus not been evaluated in one study. The water heating versions are excellent for the purpose of efficiency hot water generation. The active collector surface of PTCs for water heating consists of parabolic reflectors and heat absorber pipe which is placed parallel to the axis of rotation of these reflectors. The heat absorber tubes are thin copper absorber tubes in an evacuated glass encapsulation [18]. This is a sophisticated absorber design and absent in water cleaning collectors. A glass encapsulation is outside the copper absorber tubes to contain the heat in the water [18]. The PTCs for water cleaning are commonly utilized for very high temperature output in large scale applications and sometimes are used for steam generation. They provide maximum thermal efficiencies of  $\eta_{th} = 0.93$  [19] in a system using forced circulation of water (water pump). CPCs consist of the same absorber tubes placed on the axis of compound reflectors which are attached to a flat bed. The CPCs provide low to medium temperature outputs and have yielded significantly high thermal efficiencies within  $0.5 < \eta_{th} < 0.60$ , in the most recent study, where high irradiance is present between  $1000 < G < 1200 \text{ W}\cdot\text{m}^{-2}$  [20]. While one setup, using natural circulation/thermosyphoning provides  $\eta_{th} = 0.84$  [21] under the same irradiance range.

Non-concentrating water heating devices are commonly the flat plate collectors. They provide near similar thermal efficiencies  $\eta_{th} = 0.80$  [22, 23], while are easier to design and install. The flat plate collectors constitute of copper tubes which are coated by a solar selective absorber sheets. The collector is insulated at the rear and the design provides minimum heat loss to the environment and maximum thermal heat gain by the water. These are the most economical solar collection devices.

One of the best comparisons of the thermal efficiency of CPC, PTC and flat plate collectors for water heating is provided by Kalogirou [23]. The comparison was performed for solar light in the range of  $G = 500 \text{ W}\cdot\text{m}^{-2} - 1000\text{W}\cdot\text{m}^{-2}$ . Flat plate collectors provide  $\eta_{\text{th}} = 0.8$  of the irradiance while CPCs  $\eta_{\text{th}} = 0.7$  and PTCs  $\eta_{\text{th}} = 0.75$ . Thus non-concentrating flatbed type water heaters are a better option and should have an integrated design for water cleaning, which is not present in previous work, which the present author is aware of. Such a device would possess adequate thermal absorption, while also providing a transparent section that contains the mixture of catalyst and waste water for the incident light to provide photo-activated decomposition of a model pollutant in water. If any non-concentrating collector that provides an integration of water cleaning and heating is created, it must contain a solar absorber and maximize the thermal efficiency from its design and material selection to meet criteria of  $\eta_{\text{th}} > 0.7$ . Thermosyphoning can provide the means of mixture circulation in the collection system to conserve energy. The present study addresses the methods to attain such a device and the results that are attained. It addresses its limitations for MB dye water cleaning and its thermal efficiency under no/calm winds and fixed ambient temperatures. .

### **3.3 Experimental setup**

The devices for solar photocatalytic water cleaning which do not concentrate light have a flatbed design with transparent glass containers that and are attached to a cold reservoir in a closed loop as discussed. The collectors for solar thermal water heating, of the non-concentrating types reviewed in chapter 1 are also of a flatbed design but have a sophisticated solar thermal absorber material and heat exchanger design. Thus, to integrate these two functions of water cleaning and water heating, one chamber of the collector in the present work had to be a heat absorber and transfer heat to a chamber containing the illuminated waste water and catalyst. Hence forth, in the present work, a two chamber collector is fabricated and attached to a cold reservoir in a closed loop without a water pump. This method is adapted from the review in this thesis. The reservoir is placed above the collector. The thermosyphon effect circulates the mixture in the system. The flow setup is shown in Figure 3-1.



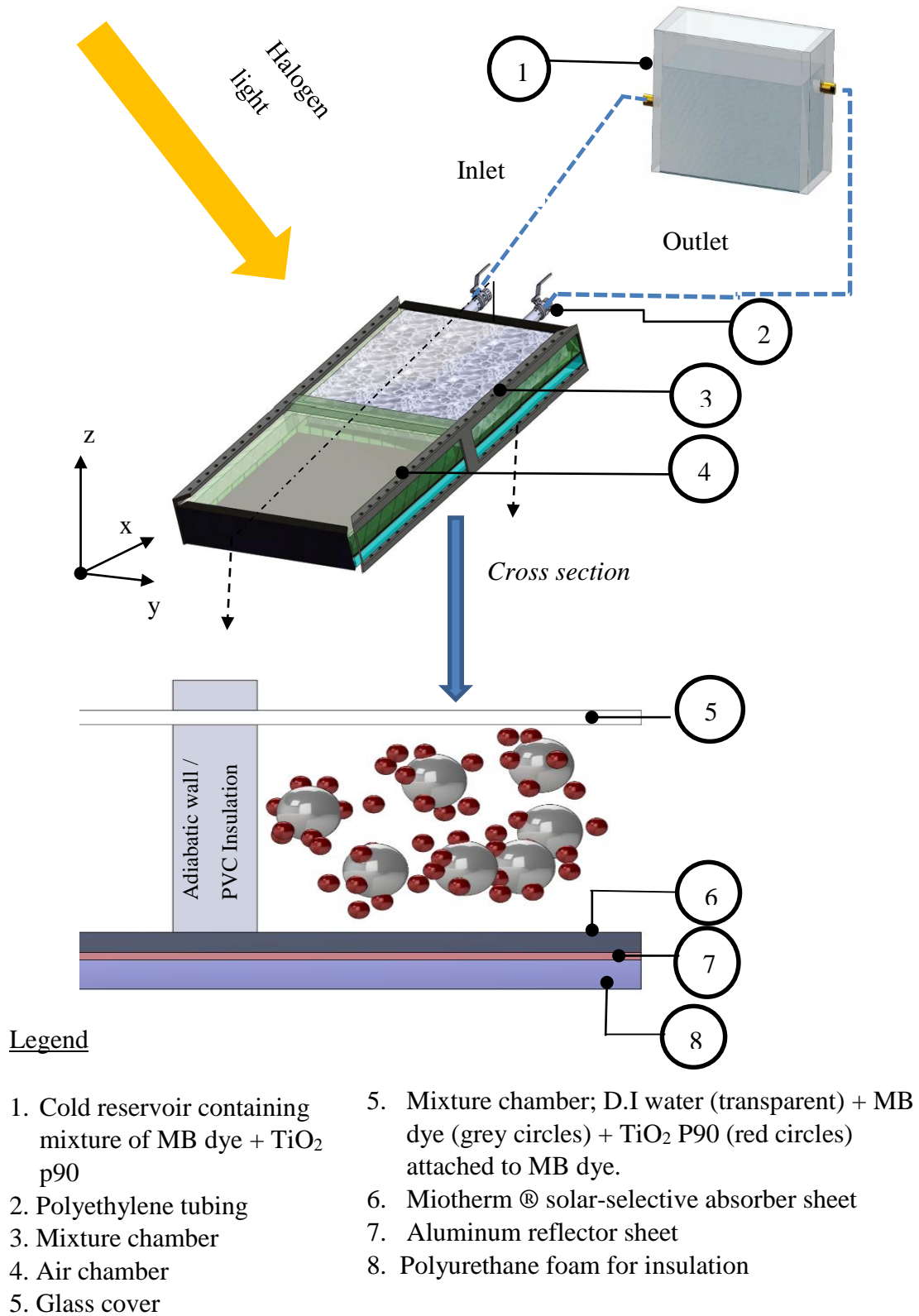


**Figure 3-1: The solar collector and the flow setup**

Halogen lamps are used as the light source on this collector. The heat gain by one chamber is transferred to the mixture chamber, while this mixture chamber also gains heat from the incident light. The irradiance on the collector is carefully characterized for the available UV, VIS light and NIR radiation that it was providing and its intensity on different locations on the surface of the collector.

In the present study, TiO<sub>2</sub> P90 catalyst is required to adsorb MB dye and decompose it from light activated photocatalysis. MB dye is also expected to undergo photo-sensitization under the abundant VIS light from the simulator used. MB dye is chosen as the model pollutant from its plentiful utilization in previous works. It is well known that researchers have diverted to using TiO<sub>2</sub> P90, where they have commended upon its larger reaction surface area of 104 m<sup>2</sup>•g<sup>-1</sup> as compared to 51 m<sup>2</sup>•g<sup>-1</sup> of the TiO<sub>2</sub> P25 [24, 25]. AEROXIDE® TiO<sub>2</sub> P90 (surface area = 90 ± 20 m<sup>2</sup>•g<sup>-1</sup>, non-porous particles of average diameter = 14 nm) was used against the MB dye. These values are reported by the manufacturer. The surface adsorption of the dye was recorded separately from the results of photodecomposition using the catalyst (photosensitization and photocatalysis) in the present work using dark conditions.

Temperatures of the collector were detected on the front and inside the chambers, while the inlet and outlet mixture temperatures are also attained. These provide the analytical determination of the mass flow rates and the thermal efficiencies. The mass flow rate in the present study was not measured.

The controlled variables of the present study are the irradiance on the collector, the ambient temperatures and the wind speeds (no wind), the inlet mixture temperatures and the inlet concentration of MB dye and the dosages of TiO<sub>2</sub> P90 catalyst used. Various dosages of this catalyst were used in the dye solution to determine its mass effects on the decolourization of MB dye via photocatalysis. The limitations of the device for water cleaning was addressed by using one concentration of MB dye for all the experiments while varying the dosages of TiO<sub>2</sub> P90 that provide the minimum catalyst needed to onset photocatalysis and the maximum that would provide the highest amount of decomposition.

The irradiance, the ambient temperatures and  $0 \text{ m}\cdot\text{s}^{-1}$  wind speeds are kept constant by conducting the experiments indoors. The inlet temperature is kept constant to attain an operating condition of  $0 \text{ }^\circ\text{C}\cdot\text{m}^2\cdot\text{W}^{-1}$ . Thermal efficiencies of previous solar water heaters are evaluated at this reduced temperature, as mentioned in the introduction of this chapter. The independent variables of the present study are the outlet concentration of MB dye and the temperatures of the collector. The dependent variables of the present work are the % decomposition of MB dye,  $D$ , and the second dependent variable is the thermal efficiency of the device,  $\eta_{\text{th}}$ . The dependent variable,  $D$ , is changing with time while the thermal efficiency is evaluated at one condition and provided as a single value in this chapter.

The experiments are carried out in an indoor facility. The main apparatus are a halogen light solar simulator, the collector, a cold reservoir, an open rack support frame (on which the device rests), thermocouples and an IR temperatures sensor to attain front surface temperatures, a spectrophotometer to acquire the absorbance of MB dye (converted to concentration using calibration curve).

The open rack mount was constructed from 2090 grade aluminum to hold the device and perform safe experimental work. The back side of the mount was open to allow any probable heat losses from the collector. The orientation of the collector was  $\theta = 30^\circ$  from the ground to conform to the methods of solar harvesting technology to gain the maximum amount of sunlight in a day, as mentioned in Chapter 1. An angle of  $\theta = 30 \pm 1.1^\circ$  was measured from the ground to the back of the collector in this chapter (using Bosch tool DLR130K laser distance measurement device of accuracy  $\pm 6.35 \text{ mm}$ ).

### **3.3.1 The solar photocatalytic collector**

The design method of this collector was based on the aim of maximizing thermal heat gain into the mixture from absorbance of halogen light while also indirectly gaining heat from a neighboring hot air chamber. The collector contains two rectangular chambers separated using a PVC wall. The thickness of this wall was  $52 \times 10^{-3} \text{ m}$  and polyurethane foam was placed on its outer surface to make it adiabatic (see Figure 3-1). One chamber contains a closed volume of air and the other is an open volume containing the mixture of dye and catalyst in de-ionized water. Both chambers were of equal volume, as measured after

fabrication. The chambers are measured to be each of  $1.84 \pm 0.01$  L. One borosilicate glass sheet was placed on top of the chambers. It was regular tempered borosilicate glass with a slight green tinge (visually inspected) of thickness  $3 \times 10^{-3}$  m. The optical properties of the tempered glass were not known and hence experimentation was performed to determine its transmittance of halogen light, which was the type of light used for the simulator. This was carried out by orienting the glass  $\theta = 30^\circ$  from the horizontal on an open rack mount support frame and measuring the incident light on its surface and then the transmitted light behind it on 50 locations (via the TES pyranometer 1333R). The laboratory determined transmittance was  $\tau = 0.71 \pm 0.05$  while the reflectance was  $\rho = 0.22$  after the glass had reached steady state. This transmission is for the wavelength range of the pyrometer of  $\lambda = 300 - 1100$  nm which constitutes UV light, VIS light and NIR radiation.

Inlet and outlet ports are present at the side wall of the mixture chamber. They are connected to a cold reservoir placed at the edge of this port wall. The ports are connected with insulated tubing to a cold reservoir tank (refer to Figure 3-1). The collector is of surface dimensions  $0.52 \times 0.32$  m, which is equal to the same dimensions of the most uniform light over 50 locations on a test plane that was used to characterize the solar simulator. Its characterization will be discussed in the preceding section.

The side clamps of the collector were created from aluminum. The clamps covered a portion of the exposed top glazing surface to decrease the front glazed (glass covered) area to  $0.495 \times 0.327$  m. Total collector area exposed to halogen light is  $0.162 \pm 0.02$  m<sup>2</sup> in this collector. The height of the chambers is  $25 \times 10^{-3}$  m. These clamps were necessary to press the assembly together.

A solar selective absorber sheet was purchased from Alonod Solar © and layered under the chambers without segmentation. This is a dark aluminum base solar absorber sheet, commercially available by the name Miotherm®. This is a multilayer selective absorber which has spectral selective coatings that exhibit a very high absorption coefficient,  $\alpha = 0.95 \pm 0.02$  over the entire wavelength range of solar radiation while allowing minimum emission of long wavelength radiation,  $\varepsilon = 0.03$  (in the range  $\lambda = 2 \mu\text{m} - 20 \mu\text{m}$ ) [26]. With a high thermal conductivity of  $k = 210 - 220$  W•m<sup>-2</sup>•K<sup>-1</sup> of the absorber, the heat is predicted to be transferred adequately from its body at the air chamber to its cooler body

under the mixture. Below the absorber is an aluminum foil sheet of which's purpose was to reflect the heat that may be lost from the chambers to the ambient air at the rear. Below this reflector was  $25.4 \times 10^{-3}$  m polyurethane foam to serve as the insulation material.

It was predicted that the heat absorbed by the solar absorber in the air chamber would be transfer to its body under the mixture chamber from this design method. The irradiance on the mixture chamber would provide more heat gain to the fluid. There would be heat losses from the glass surface but it was aimed that maximum heat would be transported out of the collector and into the cold reservoir via thermosyphoning. The irradiance on the collector plays a significant part in the mechanism of this device and was characterized according to its availability of UV, VIS light and NIR radiation and its total intensity from an experimental method.

### **3.3.2 The solar simulator**

The halogen light solar simulator was setup according to identical method of those mentioned in section 2.3.2 of this thesis. The difference in the setup was the distance of the halogen lights from the collector surface. The lamps were placed at  $0.371 \pm 0.25$  m normal distance from the collector. 4.81% spatial uniformity of temperature (the ratio of the average deviance between the maxima the maxima value of temperature on the wood test plane used in Chapter 2) is present on an area of  $0.164 \pm 0.002$  m<sup>2</sup>. A TES pyranometer 1333R (ranges;  $G = 0-2000$  W•m<sup>-2</sup> and  $\lambda = 400-1100$  nm, accuracy;  $\pm 1.0$  W•m<sup>-2</sup>) was used to acquire the irradiance on 84 locations. Only 50 locations were providing uniformity in light and the rest 34 locations had to be neglected for the study.

OCEAN OPTICS USB 2000+ RAD spectrophotometer (range  $\lambda = 200- 900$  nm, accuracy;  $\lambda = 0.03 - 10.0$  nm of the full width at half maximum of the spectrum) provides the distribution spectrum as that of Figure 2-2 in Chapter 2. The maximum irradiance measured is  $G = 1054.1$  W•m<sup>-2</sup> while the minimum is  $G = 853.2$  W•m<sup>-2</sup>. The average intensity from halogen light that is incident on the collector is  $1004.7$  W•m<sup>-2</sup>. These are illustrated in Figure 3-2.

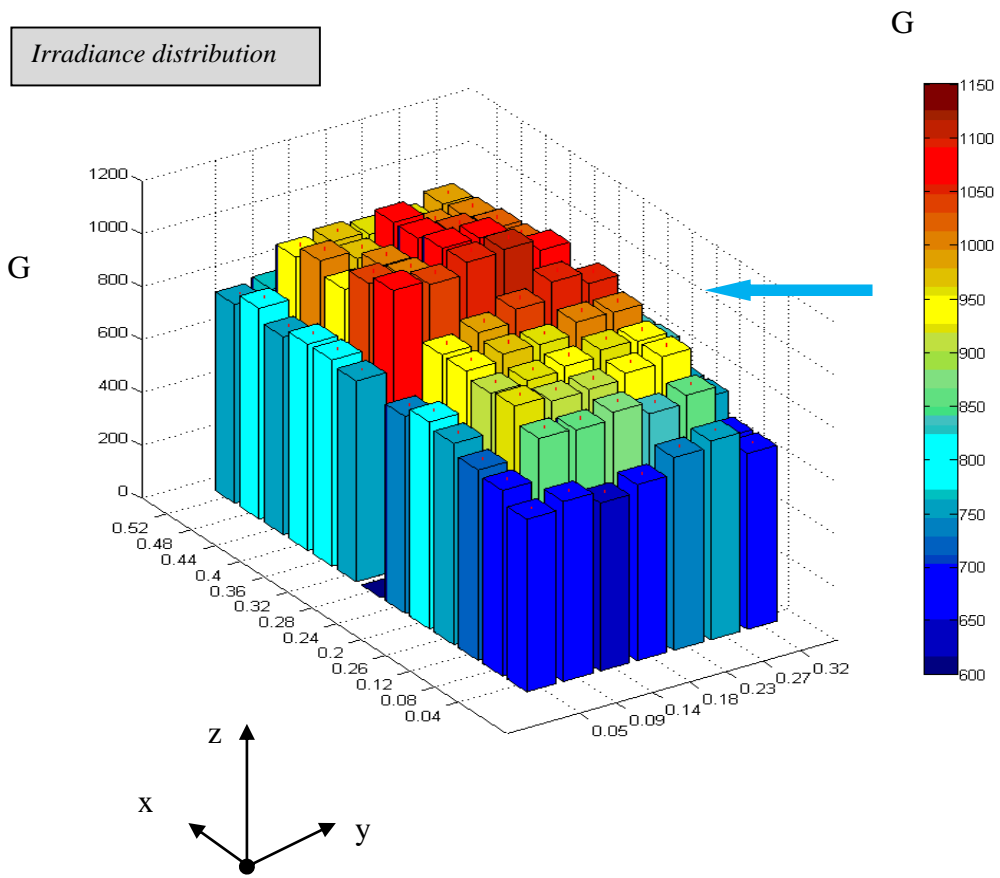


**Figure 3-2: Halogen light spectral distribution and spatial irradiance distribution on the collector**

There is 16.1% spatial non-uniformity of irradiance over the collector. This is a large non-uniformity. The gap between the bars in Figure 3-2 is the partitioning wall of the collector, between the chambers. The irradiances at  $x = 0.24$  m was not measured which is where this partitioning wall is placed in the collector.

The amount of UV, VIS light and NIR radiation from this simulator remained the same as those utilized in Chapter 2 and are addressed in Table 2-1 and compared to the reference spectra of AM 1.5 and Global irradiance. The intensity of UV light was calculated from the percentages in Table 2-1 and the average irradiance, and it was determined to be of intensity  $7 \text{ W}\cdot\text{m}^{-2}$  while,  $741.5 \text{ W}\cdot\text{m}^{-2}$  of VIS light intensity is present and  $71.3 \text{ W}\cdot\text{m}^{-2}$  of NIR radiation is available. These are very large as compared to the intensities that would be present under  $1004.7 \text{ W}\cdot\text{m}^{-2}$  of solar light of the AM 1.5 spectrum or Global irradiance. Conclusions about the simulator remain the same as those discussed in section 2.3.2 of this thesis.

### **3.3.3 Dye concentration and temperature measurement**

Methylene blue 319112 (empirical formula:  $\text{C}_{18}\text{H}_{18}\text{C}_1\text{N}_3\text{S}$ ) 0.05 wt. % in  $\text{H}_2\text{O}$  and light absorbance peak at  $\lambda = 665$  nm was purchased from SIGMA ALDRICH. Its extinction coefficient varies by concentration ( $70,000 \text{ mol}^{-1}\cdot\text{cm}^{-1}$  at 2.5 ppm in DI water) and hence forth a calibration curve of its concentration versus VIS light absorbance was experimentally determined prior to using it in the experiments.

Different concentrations of MB dye were prepared and its absorbance was recorded at  $\lambda = 665$  nm using a VRAIAN CARY<sup>®</sup> UV-VIS-NIR spectrophotometer. One, 1 cm thick Pyrex plastic container was used to contain the solution of MB dye, which was placed in the spectrophotometer for absorbance measurements. The catalyst dosage mixed with MB dye solution in the system was initially measured in a high precision weighing scale (resolution of 0.1 mg). This mixture was poured into the system shown in Figure 3-1. To attain the concentrations at the inlet and outlet during the experiments, a 15 mL suction syringe was inserted at these locations to extract a sample of the mixture to measure the MB dye concentrations. Since this solution contained catalyst, the separation of the  $\text{TiO}_2$  P90 catalyst from these mixture samples was performed. The separation was done by

centrifuging the sample at 8000 rpm for 60 minutes in 15 mL centrifuge tubes. The dye solution with no catalyst particles was then read for its absorbance value in the spectrophotometer. The absorbance was converted to concentration using a calibration curve. The calibration curve was created by making various known concentrations of MB dye solution and measuring the absorbance from the spectrophotometer. The curve was almost linear in nature. This curve was used to attain all the concentrations reported in the present study. Absorbance of the MB dye at  $\lambda = 665$  nm is not reported.

With these methods, the initial concentration and the final concentration of MB dye were acquired. These were respectively, at the inlet and outlet port in Figure 3-1. The outlet concentration read decreased from the influence of adsorption of MB dye on the catalyst, photosensitization and from photocatalysis. All three were measured in this study.

Experiments using MB dye in de-ionized water with various dosages of TiO<sub>2</sub> P90 were performed in the dark to attain the amount of dye adsorbed on this catalyst. These experiments were performed using a beaker of solution of MB dye with de-ionized water with various dosages of TiO<sub>2</sub> P90 suspended in it. The beaker was covered with opaque material which simulated dark conditions. Significant agitation of the mixture was provided. Concentrations of MB dye were measured at different times until the amount of concentration decrease remained steady.

To understand the amount of photosensitization, an experiment was performed using MB dye solution in the collector system without catalyst. This experiment consisted of pouring a homogenous solution of MB dye in the collector system in Figure 3-1 and turning the halogen lights on. The solution was allowed to circulate in the system by the thermosyphon effect. The concentrations at the inlet and outlet were compared over time for this experiment and the results from photosensitization were recorded. After these two experiments, MB dye in water was used against various concentrations of TiO<sub>2</sub> P90 to attain the photodecomposition results.

The front surface/front glass temperature of the collector during these experiments was measured from non-invasive infra-red temperature on 50 locations. These provide the analytically determined front surface heat loss from natural convection and radiation,



assumed to be occurring in this setup with relevance to the stagnant wind conditions. The surface temperatures of the side walls of the collector were measured and compared to ambient temperature in-order to assume they were adiabatic. The total heat gain by the mixture is attained by analytical methods which require the temperatures inside the collector and at the inlet and outlet.

Temperatures inside the collector constituted of acquiring the inner glass temperature, fluid (air and water) and the absorber temperature using four temperature sensors in each chamber (J-type thermocouples, accuracy  $\pm 0.1^\circ\text{C}$ ), as shown in Figure 3-3. These are customized in a 3.2 mm diameter aluminum probe (1/8" probe specified by McMasterCarr, the supplier), so that they may withstand the water pressure and temperature and bend adequately to ensure their tips are in contact with the hot surfaces. Over all, there are 24 locations in the device that are measured for temperature. The placements of these thermocouples are shown in Figure 3-3. They are placed at a distance from the leading edge of the collector, which is at  $x = 0$  m in Figure 3-3. The locations are  $x = 0.025$  m,  $x = 0.123$  m,  $x = 0.213$  m and  $x = 0.247$  m at the air chamber. No thermocouples are present at the partitioning wall. The mixture chamber has thermocouples at  $x = 0.273$  m,  $x = 0.298$  m,  $x = 0.369$  m and  $x = 0.495$  m. In order to determine the temperature gain of the mixture the inlet and outlet temperatures of the collector are measured using two K-type thermocouples. These are placed at the center of the insulated tubes spaced 25 cm from the port wall. The inlet temperature of the mixture was controlled using packet ice in the insulated cold reservoir tank. The mass flow rate was not measured in this setup and is analytically determined in this thesis work.

All of the temperatures are read over time till steady state. Different days are chosen for each experimental runs. The flow movement via thermosyphoning was monitored prior to conducting water cleaning experiments. This was done with clear water in the system and injecting dye at the inlet port. The results show that the direction of the flow in the system is as demonstrated in Figure 3-3. There are no claims about the type of flow in the mixture chamber in the present study. It is simply flowing through the chamber and to and from the cold reservoir. It is also crucial to mention that the mass flow rates were not measured in this system as those in previous works on solar collectors.

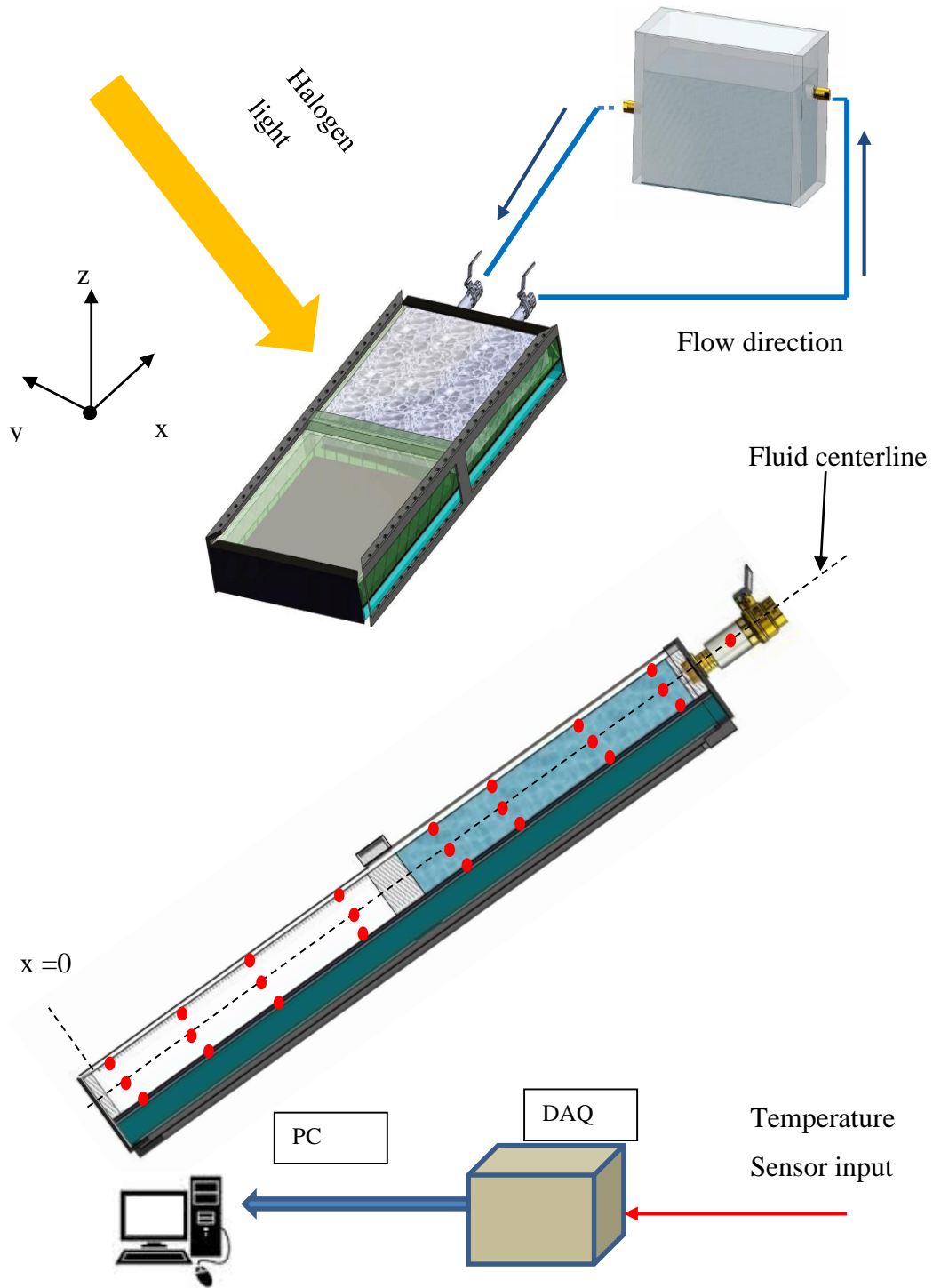


**Figure 3-3: Experimental setup layout and placement of temperature sensors inside the collector and the system**

### 3.3.4 Calibration of equipment and data acquisition system

The infra-red digital temperature reader was calibrated against a K-type digital 1312A thermometer (accuracy of 0.3% of the reading and resolution 0.1°C). The calibration procedure is explained in section 2.3.4. The calibration and accuracies of the pyrometer, the accuracy of the spectrometer and the calibration of the thermocouple probes are also provided in this section of this thesis. All the calibration curves for the thermocouples provided almost linear relationships with very small bias errors. Two National Instruments data acquisition system cards (NI-cDAQ-9211, 4 channels) was used to acquire the signal for the temperature sensors. These cards were mounted on a chassis (NI-cDAQ-9711) to connect to the LabVIEW software (Signal express edition 2012). The data acquisition card had a build in cold junction compensation device and hence no temperature adjustments to the sensor output were required. The VARIAN-UV spectrophotometer was calibrated for MB dye absorbance by first reading the absorbance of clear de-ionized water and making it the zero value.

## 3.4 Experimental results

The steady state temperatures in the mixture occur after a substantial amount of time,  $t = 150$  minutes. The inlet in this collector was successfully maintained at  $T_{in} = 22.3 \pm 1.5^\circ\text{C}$  that provided an outlet temperature of  $T_{out} = 60.4 \pm 1.7^\circ\text{C}$  during steady state. This yields an operation of this collector at reduced temperature of  $0^\circ\text{C}\cdot\text{m}^2\cdot\text{W}^{-1}$  under  $G = 1004.7 \text{ W}\cdot\text{m}^{-2}$  of halogen light. The rear and the side walls of the collector were at room temperature ( $T_a = 21.5 \pm 1.1^\circ\text{C}$ ) throughout the experimentation, thus they were assumed to not lose heat to the surrounding and were adiabatic. The only exterior heated surface was the front glass. Front temperatures of the collector at the air chamber was  $T_f = 66.2 \pm 1.5^\circ\text{C}$  was lower than that at the mixture chamber,  $T_f = 58.39 \pm 1.5^\circ\text{C}$  from the first observation. After 150 minutes the system was allowed to run for a substantial amount of time. The water was circulating to and from the cold reservoir throughout the experiment. The inlet temperature was kept cool using ice packs. After 150 minutes the temperatures of the air chamber were measured and compared to that of the mixture chamber. They were different and the air chamber temperatures were rising.

The air chamber reached steady state at  $t = 190$  minutes. This is well after when the mixture chamber reached steady state. Thus the steady state temperatures which will provide the analytical thermal efficiency is at  $t = 190$  minutes. Fluctuations in the mixture chamber occurred after 150 minutes, which were slight, i.e  $\pm 3-4^{\circ}\text{C}$  higher than those reported in Table 3-1 between 150-190 minutes. Hence they were not to be concerned with. The mean mixture temperature remained steady. Later analysis would demonstrate that the steady state in the air chamber was achieved due to a steady heat transfer to the mixture and that to the glass covering.

The spatial distribution of the temperature at the air side dictates that they were mostly even in value (not more than  $\pm 1.3^{\circ}\text{C}$  spatial deviation from the mean). However, the water side temperatures varied along the surface (at locations  $x = 0.273$  to  $x = 0.495$  m in Figure 3-3). This suggested a temperature difference of  $3.03 \pm 1.1^{\circ}\text{C}$  from the mixture partition to the inlet and outlet zone. There are no transverse variations to report on the front surface of glass. These temperatures differed by a maximum of  $\pm 1.5^{\circ}\text{C}$ . Over all the front of the collector was at high temperatures that yield a possibility of significant heat loss to the environment which are evaluated via analysis. The temperatures inside the device dictate that the air chamber temperatures were significantly higher than that of the mixture chamber. This does not provide information about the amount of heat transfer from the absorber sheet. Data analysis provides this information and had to be conducted.

The data in Table 3-1 also suggests that heat losses within the air chamber must be accounted for. This is because the absorber sheet at the air chamber is substantially higher than the temperature of the glass covering it. Thus there can be significant heat transfer between the absorber and the glass surface in the air chamber. This decreases the possibility of maximum heat transfer to the mixture chamber. There was no significant temperature difference in the mixture body. The water flowing into the mixture chamber from the inlet was heated up instantaneously judging from the temperatures. There is no mixing in this chamber and the flow will not be quantified. The temperatures of the various thermocouples in the mixture chamber are near equal. Thus the only evaluation needed of this device is the thermal efficiency.

**Table 3-1: Front glass and inside chamber temperatures of the collector under  $G = 1004.7 \text{ W}\cdot\text{m}^{-2}$  of halogen light at steady state**

x (m)	Air chamber				Mixture Chamber			
	0.025 8	0.1235	0.2213	0.2471	0.273	0.298	0.369	0.495
$T_f$	$68.3 \pm 1.1$	$67.5 \pm 1.2$	$66.3 \pm 1.3$	$65.3 \pm 1.4$	$60.6 \pm 1.2$	$61.3 \pm 1.5$	$62.1 \pm 1.6$	$63.5 \pm 1.2$
$T_g$	$76.23 \pm 1.2$	$73.58 \pm 1.2$	$72.5 \pm 1.5$	$69.2 \pm 1.5$	$58.2 \pm 1.2$	$59.2 \pm 1.0$	$60.2 \pm 1.0$	$61.2 \pm 1.2$
$T_{\text{Fluid}}$	$80.2 \pm 1.4$	$78.22 \pm 1.6$	$84.9 \pm 1.5$	$72.8 \pm 1.2$	$57.58 \pm 1.6$	$58.26 \pm 1.2$	$60.1 \pm 1.3$	$58.25 \pm 1.1$
$T_{\text{abs}}$	$85.2 \pm 1.3$	$89.2 \pm 1.5$	$90.2 \pm 1.2$	$87.5 \pm 1.8$	$57.25 \pm 1.0$	$58.26 \pm 1.0$	$59.8 \pm 1.1$	$58.28 \pm 1.1$

The thermal efficiency of the collector can only be claimed by analytical methods but the % decomposition of MB dye is attained without detailed analysis. The results of water cleaning are for the time duration of 360 minutes and shown in Figure 3-4. This is the time needed for the dye to not demonstrate any more decomposition, regardless of the concentration of TiO<sub>2</sub> P90 utilized. Steady state temperatures are reached prior to 360 minutes for all the results shown in Figure 3-4. The % decomposition, from the data in this Figure is attained by:

$$\%D = \frac{[C]_{t=0} - [C]_{t=360}}{C_{t=0}} \quad (3-1)$$

Here C is the concentration in ppm units. The results also given to demonstrate the adsorption of MB dye with varying dosages of TiO<sub>2</sub> P90 for duration of 300 minutes to understand the level of adsorption. This data is plotted before the origin of time on the graph (at 0 minutes). Results claim that the highest dosage of TiO<sub>2</sub> P90 was adsorbing an insignificant amount of MB dye. Over all, adsorption of the dye on the catalyst was very low regardless of the amount of catalyst used. The amounts do not need to be mentioned

since they are very low as compared to the decomposition results when the lights are turned on in Figure 3-4.

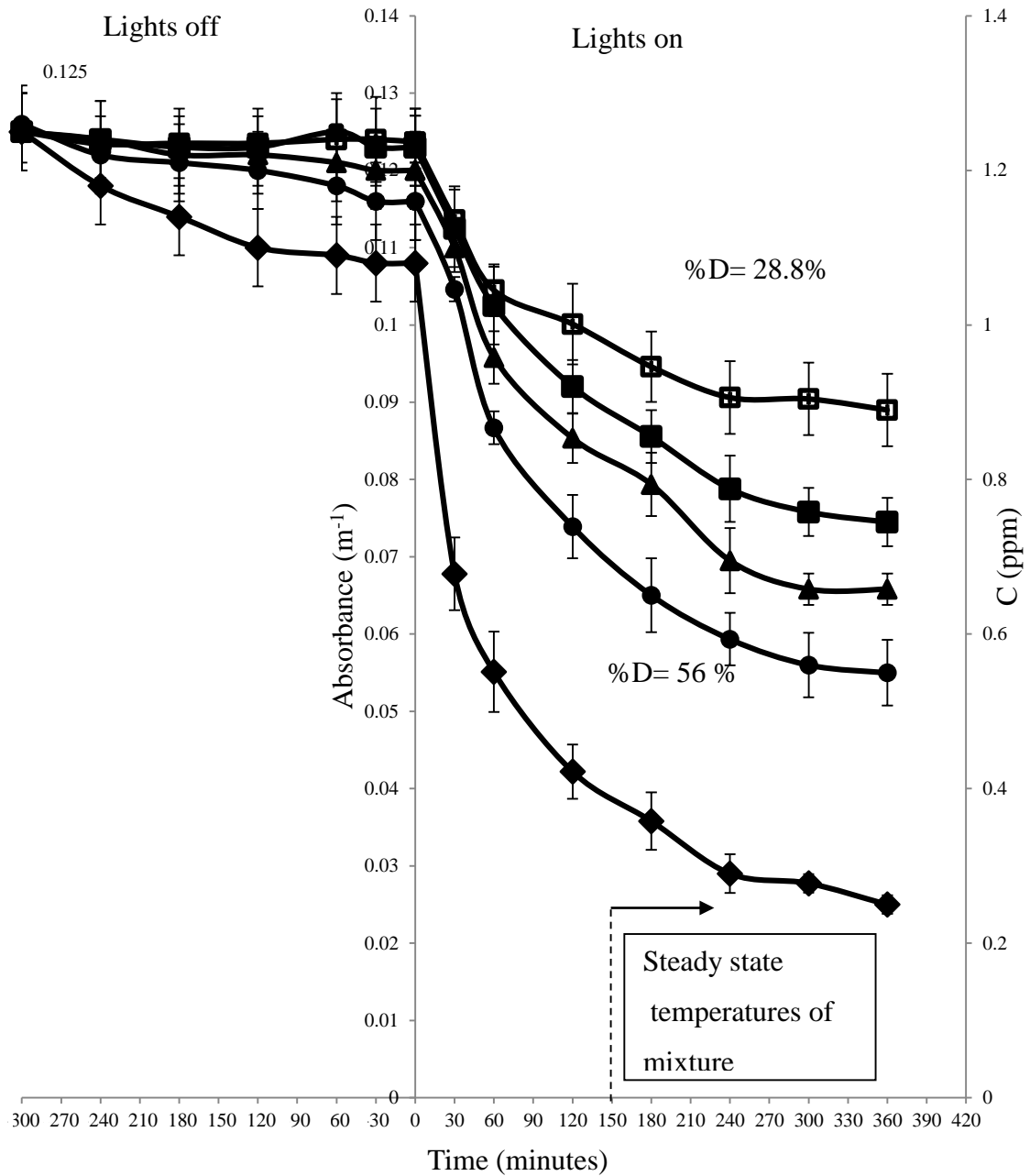


**Figure 3-4: Decomposition of Methylene blue dye ( $C_{18}H_{18}ClN_3S$ ) under  $G = 1004.7$   $W \cdot m^{-2}$  of Halogen light ( $7.0$   $W \cdot m^{-2}$  of UV light in  $\lambda = 300-400$  nm) without hydrogen peroxide and oxygen using ( $\square$ ),  $12.7$   $mg \cdot L^{-1}$ ; ( $\blacksquare$ ),  $25.7$   $mg \cdot L^{-1}$ , ( $\blacktriangle$ )  $50.9$   $mg \cdot L^{-1}$ , ( $\bullet$ )  $76.9$   $mg \cdot L^{-1}$  and ( $\blacklozenge$ )  $127.4$   $mg \cdot L^{-1}$  of  $TiO_2$  P90**

When the lights are turned on, it can be seen that the results are not merely from adsorption. The lowest dosage of TiO<sub>2</sub> P90, 12.7 mg•L<sup>-1</sup> was used against 1.2 ppm of MB dye and research shows 28.8% decomposition. Lowering the catalyst dosage beyond this value shows no change. Using no catalyst has identical results. This result is the % decomposition achieved with the effects of photosensitization of MB dye in the collector. Regards to the possibility of thermal decolourization of the dye, it is demonstrated that each data curve on Figure 3-4, is following a trend of similar temperatures.

The average temperature of the mixture chamber in Figure 3-4 from 0-150 minutes was constantly rising. It was 23.4°C at t = 0 minutes, 35.2°C at t = 30 minutes, 44.75°C at t = 40 minutes, 52.1°C at t = 100 minutes, 54. °C at t = 120 minutes and 58.6°C at t = 150 minutes. The concentration of MB dye is decreasing in the setup during and after this time period till 360 minutes without catalyst. It cannot be concluded whether the results of 28.8% decomposition of MB dye without catalyst is also influenced by temperature effects. However, the temperatures effects on the decomposition of this dye are not conducted in the present study. The kinetics involved is not the scope of this research. If temperatures are effecting the decomposition of dye then the data in Figure 3-4, using the lowest dosage of catalyst is inclusive of their effects.

A 1.2 ppm of initial concentration of MB dye was utilized according to the limited amount of TiO<sub>2</sub> P90 available for the experiments. The maximum dosage of 127.4 mg•L<sup>-1</sup> of catalyst was available in these experiments. From this limitation, positive cleaning results from this system had to be acquired. Hence 1.2 ppm was the lowest amount of concentration of dye that could address cleaning using low dosages of TiO<sub>2</sub> P90 available. The results from the experiments have shown that photosensitization is occurring and they also demonstrate that photocatalysis is surely prominent. 12.7 mg•L<sup>-1</sup>, 25.7 mg•L<sup>-1</sup>, 50.9 mg•L<sup>-1</sup>, 76.9 mg•L<sup>-1</sup> and 127.4 mg•L<sup>-1</sup> of TiO<sub>2</sub> P90 were used in the study were attained from 250, 500, 1000, 1500 and 2500 mg of catalyst dispersed in the system. Approximately 28, 40.4, 47.36, 56 and 80% of 1.2 ppm MB dye was decomposed with respect to this amount of catalyst. These are the limitations of this device using this low amount of MB dye. Over all the results are not conclusive of the full capability of this device, since higher concentrations of MB dye are needed.

### 3.5 Data analysis

Heat transfer analysis is done using the temperature data and correlations in previous work to attain the thermal efficiency of the collector. A 2-D heat transfer model is used (shown in Figure 3-5). No transverse variation in temperature on this collector (x-direction) was witnessed and the 2-D analysis was performed in the y and z plane (of cross section A-A in Figure 3-1). The heat transfer model in Figure 3-5 provides guidance of data reduction to attain the thermal efficiency of the collector and the mass flow rates of the mixture.

It is assumed in this analysis that the heat transfer in the glass from the air chamber to the mixture chamber does not have significant value since the temperatures of the glass between these two chambers is not very deviant. It is assumed that the heat absorbed by the solar absorber sheet, the Miotherm® sheet, at the air chamber is not completely transferred to the mixture chamber. Some amount of it is lost via natural convection heat transfer and radiation heat transfer to the glass surface above it. Thus, correlations need to be utilized to attain these heat losses.

In the air chamber, the value of heat loss from natural convection,  $q''_{\text{conv}}$  and radiation  $q''_{\text{rad}}$  (refer to figure 3-5) by the absorber to the glass above it is deducted from the heat absorbed by the absorber sheet from halogen light,  $q''_{\text{abs}}$ , which yields the heat transfer to the mixture chamber in this device. Adding this value to the transmitted light in the mixture,  $q''_{\text{in}}$ , yields the total thermal heat gain of the mixture. The subtraction of the heat loss by the glass over the mixture from natural convection and radiation to the environment, from this mixture heat gain, equals the heat contained by the mixture in this device and transported to the cold reservoir,  $q''_{\text{out}}$ .

The ratio of this heat out of the collector by the irradiance,  $G$ , is the thermal efficiency. The heat transfer model assumes that the sides of the collector were adiabatic since they were at room temperature. It also assumes that the control volume of the present study is comprised of the collector's air and mixture chamber, the absorber connection, and the air above these chambers shown in Figure 3-5.



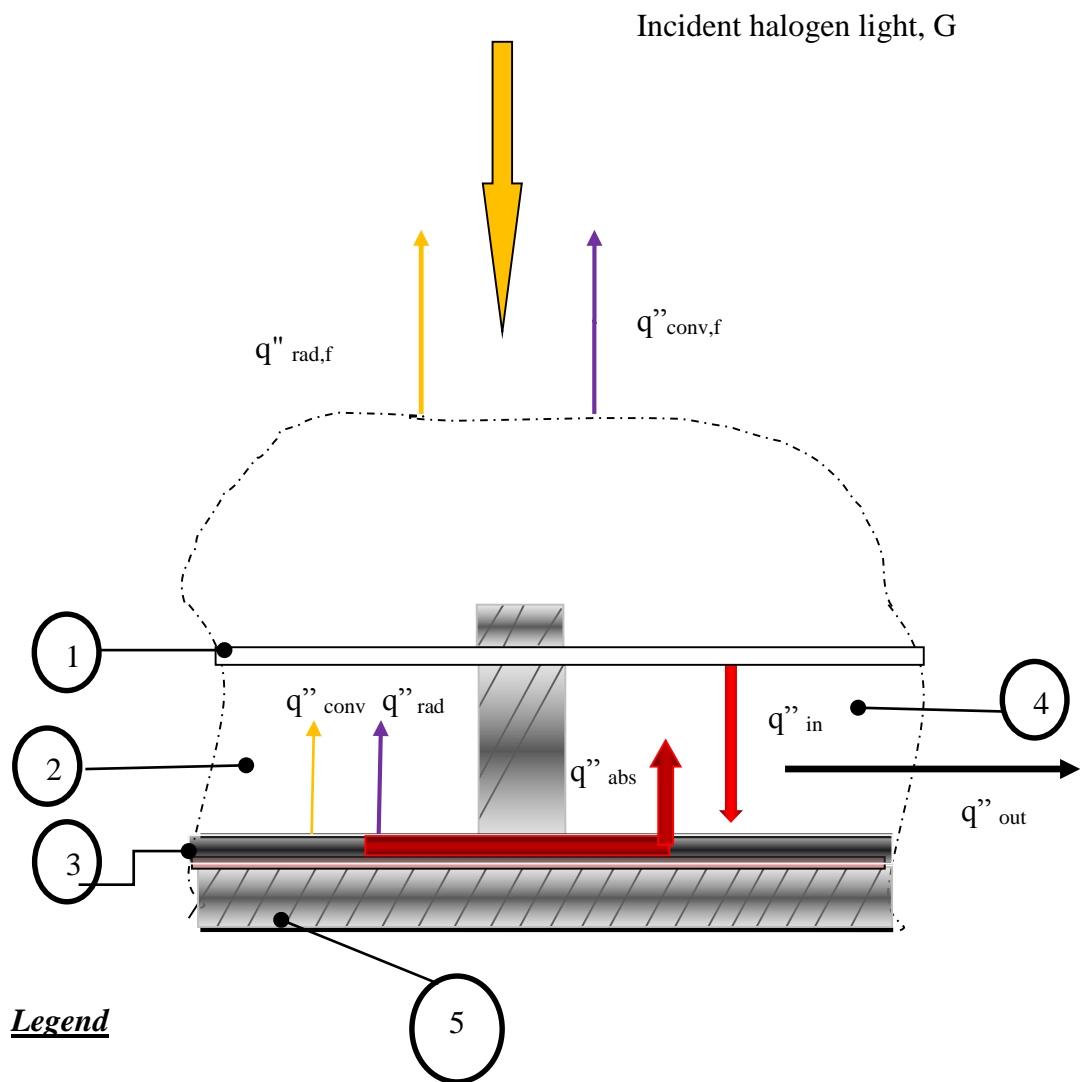


**Figure 3-5: The heat transfer model of the collector**

Natural convection heat transfer from the absorber to the glass in the air chamber is attained from heat transfer Nusselt number relation of Ruth *et al.*[27], derived from the relations of horizontal differentially heated cavities. Natural convection occurs when  $Nu > 1$  in this cavity. The Nusselt number,  $Nu$  is the ratio of heat transfer by convection to that by condition. Nusselt number from natural convection is a function of Rayleigh number, fluid Pradtl number and the characteristic length of heat transfer. The Rayleigh number for a fluid is a dimensionless number associated with buoyancy driven flow/natural convection.  $Ra$  is calculated from the expression:

$$Ra_{(x)} = \frac{g\beta(T_{abs}-T_g)L^3}{\nu^2} Pr \quad (3-2)$$

Here  $g$  is the acceleration due to gravity equal to  $9.8 \text{ ms}^{-2}$ ,  $\beta$  is the volumetric expansion coefficient of fluid attained to be  $2.83 \times 10^3 \text{ k}^{-1}$  (for air),  $\nu$  is the kinematic viscosity of value  $2.11 \times 10^{-5} \text{ m}^2 \cdot \text{s}^{-1}$  and  $Pr$  is the Pradtl number equal to 0.706, both values are for air as the working fluid.  $L$  is the thickness of the air chamber equal to 0.025 m. The thermal properties are attained from the average temperatures of the air. Experimental determination of heat transfer in inclined air layers (heated from below), from previous work, has explicitly stated that the Rayleigh number,  $Ra$ , must exceed its critical value equalling  $1708/\cos\theta$  for inclined cavity to achieve natural convection. For  $\theta = 30^\circ$ , this value is  $Ra = 1972.3$ . The Rayleigh number  $Ra = 9.69 \times 10^3$  is present in the air chamber, which surpasses the critical Rayleigh number to onset natural convection. Thus natural convection heat loss,  $q''_{\text{conv}}$  is present. Its value is attained by a simple process. Catton *et al.* [28] experimentally determined a correlation of the Nusselt number to attain the heat transfer Nusselt number in inclined cavities, as that of this air chamber, and the relation is applicable from the formula:

$$Nu_{(x)\theta=30^\circ} = Nu_{(x)\theta=0^\circ} \left[ \frac{Nu_{(x)\theta=90^\circ}}{Nu_{(x)\theta=0^\circ}} \right]^{\frac{\theta}{\theta_{cr}}} \times (\sin\theta_{cr})^{\frac{\theta}{4\theta_{cr}}} \quad (3-3)$$

Here  $Nu_{(x)}$  is the local Nusselt number on the thermal absorber,  $\theta_{cr}$  is the critical tilt angle,  $\theta = 0^\circ$  is for the cavity when horizontal and  $\theta = 90^\circ$  is when it is vertical. Nusselt number

symbolized as  $Nu_{\theta=0^\circ}$  is the heat transfer term when the air chamber of the present study is horizontal oriented. It is attained by the expression [29]:

$$Nu_{(x)\theta=0^\circ} = 0.195 Ra^{\frac{1}{4}} \quad (3-4)$$

This equation is valid for  $0.5 \leq Pr \leq 2$  and  $10^4 \leq Ra \leq 4 \times 10^5$ . The above provides  $Nu_{\theta=0^\circ} \approx 1.87$ . This is a low value.  $Nu_{\theta=90^\circ}$  is the Nusselt number when the cavity/chamber of the present study is vertical and is attained from the expression of Berkovsky & Polevikov [30]:

$$Nu_{(x)\theta=90^\circ} = 0.22 \left( \frac{Pr}{0.2+Pr} Ra \right)^{0.28} \left( \frac{H}{L} \right)^{-\frac{1}{4}} \quad (3-5)$$

This equation is applicable for  $2 \leq H/L \leq 10$ ,  $Pr \leq 10^5$  and  $10^3 \leq Ra \leq 10^5$  leading to  $Nu_{\theta=90^\circ} = 1.45$ . This is also a low value. The critical tilt angle for  $H/L = 10.6$  of the present study is not available in previous work. Previous work states that for  $H/L = 6$  and  $12$  the critical tilt angle is  $\theta_{cr} = 60$  and  $67^\circ$ . Using  $H/L = 6$  and  $H/L = 12$  in Eq (3-5) and the Nusselt numbers from Eq (3-3) for  $\theta = 30^\circ$  yield the Nusselt number in the air chamber to be between  $Nu_{\theta=30^\circ} = 1.69-1.73$ . Thus it is assumed that  $Nu_{\theta=30^\circ}$  for a cavity of  $H/L = 10.6$  would be between this Nusselt number range of  $1.69-1.73$ . To be very conservative, and account for maximum heat loss from the absorber to the glass,  $Nu = 1.73$  is chosen. This provides the maximum amount of heat transfer from the absorber to the glass in the air chamber via natural convection. The heat flux from the absorber to the glass from natural convection at different locations is attained from the formula of Newton's law of cooling:

$$q''_{conv}(x) = \frac{Nu(x)K}{L} (T_{abs} - T_g) \quad (3-6)$$

This yields an integrated value over  $x = 0-0.248$  m (height of air chamber) of  $q''_{conv} = 30.5 \pm 0.45$  W•m<sup>-2</sup>. The second mode of heat loss is from radiation heat transfer. The radiation heat transfer from the absorber to the glass at different locations in the air chamber is attained by using the radiation heat transfer equation [31]:

$$q''_{rad}(x) = F \frac{\sigma(T_{abs}^4 - T_g^4)}{\frac{1}{\epsilon_{abs}} + \frac{1}{\epsilon_g} - 1} \quad (3-7)$$

Here  $\sigma$  is the Stefan–Boltzmann constant equal to  $5.67 \times 10^{-8}$  W•m<sup>-2</sup>•K<sup>4</sup>,  $\epsilon_{abs} = 0.03$  and  $\epsilon_g = 0.92$  as per the vendor specifications and that in previous work for mid-to-high aluminum

substrate thermal absorbers, the same type used in the present study [32]. The view factor,  $F$ , is unity since the angle between the normal of the absorber and the normal of the glass is  $0^\circ$ . The data reduction provides an integrated radiation heat transfer flux of  $q''_{rad} = 9.70 \text{ W}\cdot\text{m}^{-2}$ , from the absorber to the glass in the air chamber. Thus radiation heat transfer is very small. The total heat transferred by the absorber sheet to the mixture chamber is:

$$q''_{abs} = \alpha_{abs} (\tau_g G - (q''_{rad} + q''_{conv})) \quad (3-8)$$

This is equal to  $586.4 \pm 2.34 \text{ W}\cdot\text{m}^{-2}$ . This value confirms the utilization of the selective absorber sheet in this research and the two chamber design is successful. This value is added to the heat gain by the mixture from the irradiance from halogen lights is, which is determined from:

$$q''_{in} = (\tau_g G) \quad (3-9)$$

This states that the heat input into the mixture is the transmitted irradiance by the glass. This value is  $673.14 \pm 2.5 \text{ W}\cdot\text{m}^{-2}$ . Transmission of the glass is  $\tau_g = 0.71$ , which was acquired by experimental work in this study in section 3.3.1. Commercially available grades of window and green-house glass have normal incidence transmittances of about 0.87 and 0.85 according to previous work [23]. Instead of assuming these values, the transmission was determined in the present study and provides a lower transmission of light. The total heat gain by the mixture is the sum of the direct and indirect heat transfer attained from Eq (3-8) and Eq (3-9). However, this is not realistic since some of this heat is lost by the glass covering.

This cover was considerably hot, and it is assumed that it is losing heat to the surrounding air via natural convection and radiation to the surroundings. Natural convection heat loss from the front surface is signified by the Nusselt number and Rayleigh numbers. It is assumed that at thermal steady state, the glass is not absorbing any more heat. It is assumed that a velocity and thermal boundary layer develops on the surface of the glass over the mixture due to natural convection.

The thickness of this boundary layers is dependent on the thermal properties of the fluid on the glass, properties of  $\nu$ , which is the kinematic viscosity,  $\alpha$  thermal diffusivity and  $\beta$ , the thermal expansion coefficient [33]. Outside this natural convection boundary layer, the fluid is assumed to be immobile at ambient laboratory temperature,  $T_a$ . The expression of the dimensionless heat transfer parameter  $Nu_{(x)}$  by the relation of Fuji & Imura [34], is applicable to attain the Nusselt number from [35]:

$$Nu_{(x)} = 0.14 \times \left( (Ra)^{\frac{1}{3}} - (Gr_{cr}Pr)^{\frac{1}{3}} \right) + 0.56 (Gr_{cr}Pr \times \cos(\theta))^{\frac{1}{4}} \quad (3-10)$$

This expression is valid for  $10^7 < Ra_{(x)} \cos\theta < 10^{11}$  and  $15^\circ < \theta < 75^\circ$ ,  $0 < Pr < \infty$ . The critical Grashof number,  $Gr_{cr}$ , is when the Nusselt number starts deviating from laminar behavior. For  $\theta = 15^\circ, 30^\circ, 60^\circ$  and  $70^\circ$ ,  $Gr_{cr}$  is given as  $5 \times 10^9, 2 \times 10^9, 10^8$ , and  $10^6$ . Using the characteristic length as the height of the mixture chamber, 0.247 m, the Rayleigh number is  $Ra = 7.89 \times 10^7$ . This signifies laminar natural convection.

The heat transfer Nusselt number is  $Nu = 9.05 \pm 0.23$ . The convective heat loss from Equation (3-10) is  $q''_{conv,f} = 39.07 \text{ W}\cdot\text{m}^{-2}$ . Although this is small, the radiation heat loss from this front surface is immense and achieved from the expression [35]:

$$q''_{rad,f} = F\sigma (T_g^2 - T_a^2)_{air} + F\sigma (T_g^2 - T_a^2)_{ground} \quad (3-11)$$

F is the view factor of the glass surface to the ground and to the ambient air of the laboratory. These view factors are the same as those used in Eq (2-11) of this thesis. The calculation conveys that  $308.07 \pm 2.5 \text{ W}\cdot\text{m}^{-2}$  of radiation is being emitted by the glass. The thermal efficiency of the collector is then attained by the heat output from this chamber:

$$q''_{out} = q''_{abs} + q''_{in} - q''_{conv,f} + q''_{rad,f} \quad (3-12)$$

This value is divided by the total irradiance from halogen lamps which yields the thermal efficiency:

$$\eta_{th} = \frac{q''_{out}}{G} \quad (3-13)$$

The collector has a thermal efficiency of  $\eta_{th} = 0.67$  at the reduced temperature of  $0 \text{ }^\circ\text{C}\cdot\text{m}^{-2}\cdot\text{W}^{-1}$ . Thus forth this collector extracts 67.0% of the irradiance of under zero wind conditions. The mass flow rate of this mixture is attained from:

$$\dot{m} = \frac{q''_{out}}{(T_{in} - T_{out}) C_w} \quad (3-14)$$

Here  $C_w = 4182 \text{ kJ}\cdot\text{kg}^{-1}\cdot\text{K}^{-1}$  is the heat capacity of water. This yields a low mass flow rate of  $\dot{m} = 3.56 \times 10^{-3} \text{ kg}\cdot\text{s}^{-1}$ . This concludes the analysis segment and its findings are discussed.

### 3.6 Discussion

Firstly the limitations of the present study with regard to decomposition of MB dye are discussed. The material limitation of  $\text{TiO}_2$  P90 yielded the low initial concentration of MB dye in the system to be experimented with. Different dosages of the catalyst were trialed and even a reference graph of the effect of no catalyst was provided. With this reference it was evident that surely photosensitization was present due to the large availability of VIS light. With the limited catalyst, it was demonstrated that photocatalysis is occurring. These are the most comprehensive results that can be acquired from the materials available for water cleaning. However, with more catalyst material, a higher concentration of MB dye should have been trialed for decomposition in this collector. These results are not claimed to be limited to a 1.2 ppm initial concentration of MB dye without any future work. Also, high UV light is required by photocatalysis, as commonly known. Previous in-door laboratory work by Houas *et al.*[9] and Lacheb *et al.* [8] have utilized 125 W UV lamps in an indoor photo-reactor which decompose 60 ppm of MB dye while the present study utilizes  $7 \text{ W}\cdot\text{m}^{-2}$  of UV light on an indoor collector with 1.2 ppm initial concentration. These previous indoor works include hydrogen peroxide and oxygen bubble in their setups to aid the reduction-oxidation of MB dye while the present study does not. These indoor works have conducted experiments on mixture with room temperature while the present study has experimented with changing temperatures. The present study cannot compete with the results of these indoor studies.

The thermal decomposition of MB dye is assumed to be negligible between temperatures of 0-47°C, with the presence of hydrogen peroxide as seen in previous work [36]. However, there are no claims that are being made, whether or not thermal decolouration with MB dye was occurring in the present study without exploration on this matter in the future.

The results of the present study for water cleaning can be compared with those of novel devices emerging for power generation and solar water cleaning. The drawbacks of the two combined PV-photocatalytic devices were discussed. The present study does involve PV panels to power a water pump in-order to circulate the mixture in the system. It relies on the thermosyphon effect to do so. Thermosyphoning is a common flow but not utilized in previous work in such devices, as reviewed. However, these devices have demonstrated more decomposition of MB dye with their selected dosages of catalyst.

Arias *et al.* [15] reported the photocatalytic de-colorization of 10 ppm MB dye in a CPC and tubular collector within 315 minutes. These best results were attained including hydrogen peroxide and oxygen bubbles as the supporting reducing and oxidizing agents. Outcomes showed 5 ppm of initial concentration of MB degrading to 70.8% using the CPC (0.44 g•L<sup>-1</sup> of TiO<sub>2</sub> P25), in contrast to tubular collectors; 63.46% degradation (0.38 g•L<sup>-1</sup> of TiO<sub>2</sub> P25). The present study uses lower concentrations of MB dye and limited material of TiO<sub>2</sub> P90. The results of the present study cannot be compared to this particular work using solar collectors under UV light.

The device in the present study utilizes non-concentrating collectors with lower mass flow rates compared to those present in the DSSR and TFFBR. DSSR was not utilized for MB dye decomposition that the present author is aware of. However, The TFFBR has decomposed a higher concentration of MB using TiO<sub>2</sub> P25 in their setup. Furthermore the current device, in comparison to these water cleaners, is of a smaller scale and does not utilize water pumps, which is an advantage. It also provides reasonable thermal efficiencies, a quality missing or unreported in previous non-concentrating solar photocatalytic collectors.

The present study provides the ability to collect hot water efficiency like solar collectors designed for water heating. However, there are limitations to the thermal efficiency and mass flow rates of the device of the present study. The thermal efficiency can be increased by decreasing the immense heat losses from its front surface. The front surface of the glass covering the mixture has a Rayleigh number of  $Ra = 7.89 \times 10^7$ , and shows that natural convection is not large but radiation heat transfer is immense. Without future experimental work on this matter, no suggestions can be made on how to decrease the radiation heat losses.

A lot of experimental investigation is needed on evaluation of the heat transfer from the air chamber to the mixture chamber via the absorber sheet. Embedded thermocouples are needed in the absorber, if possible and a conduction heat transfer equation needs to be utilized to attain the heat transfer within this absorber.

The thermal efficiency of the current device translated 67% conversion of incident halogen light. It is near to that of previous solar collectors used for water heating, but not competitive. There are no claims about how this thermal efficiency would be affected once the collector would operate outdoors under solar light. It is feared that the heat transfer from the front surface would increase when winds are present. This is understood from the heat low transfer coefficient of  $2.8 \text{ W}\cdot\text{m}^{-2}\cdot\text{K}^{-1}$  with natural convection, attained in the present study. This value would drastically increase with the presence of winds when operating this collector outdoors. Also, the current device has been tested at a fixed reduced temperature and this needs to be varied to attain a comprehensive thermal efficiency. All previous water heaters reviewed in the present study have demonstrated thermal efficiencies above or equal to 0.7, under varying solar irradiance and they need not be mentioned in this discussion. Over all the present study has its limitations, but its outcome of the integration of the functions of water cleaning and heating has not been performed in previous work.

### **3.7 Conclusion**

Integrated water cleaning and water heating functions are possible in a two chamber device, provided that the heat gain by the mixture is much greater than 70% of the incident light.



Its thermal efficiency is 67% ( $\eta_{th} = 0.67$ ). Heat losses from these device must be minimized and the heat gain of the mixture should be increased. Furthermore, low mass flow rates from thermosyphoning are to be measured in the future rather than analytically determined.

Halogen light sources are deficient in UV light for indoor experimental work but provide a steady simulator to test this device indoors. It is sufficient for thermal efficiency evaluation and to acquire decomposition of MB dye. The decomposition of low concentrations of MB dye, 1.2 ppm, against  $127.4 \text{ mg.L}^{-1}$  of  $\text{TiO}_2$  P90 can be performed in this device. The decomposition is highly dependent on the dosages of this catalyst used. Adsorption of MB dye is not significant, nor is decomposition by photosensitization. The results are mostly contributed from photocatalysis of MB dye. Work to improve an integrated device as such is recommended with detailed experimental results to assess its function further.

### 3.8 References

- [1] Hoffmann, W., 2006, "PV solar electricity industry: Market growth and perspective," *Solar energy materials and solar cells*, 90(18), pp. 3285-3311.
- [2] Ahmadi, P., Dincer, I., and Rosen, M. A., 2014, "Transient thermal performance assessment of a hybrid solar-fuel cell system in Toronto, Canada," *International Journal of Hydrogen Energy*.
- [3] He, W., Chow, T.-T., Ji, J., Lu, J., Pei, G., and Chan, L.-s., 2006, "Hybrid photovoltaic and thermal solar-collector designed for natural circulation of water," *Applied energy*, 83(3), pp. 199-210.
- [4] Fernández, P., Blanco, J., Sichel, C., and Malato, S., 2005, "Water disinfection by solar photocatalysis using compound parabolic collectors," *Catalysis Today*, 101(3), pp. 345-352.
- [5] Sandnes, B., and Rekstad, J., 2002, "A photovoltaic/thermal (PV/T) collector with a polymer absorber plate. Experimental study and analytical model," *Solar Energy*, 72(1), pp. 63-73.

- [6] Malato, S., Blanco, J., Vidal, A., Alarcón, D., Maldonado, M. I., Cáceres, J., and Gernjak, W., 2003, "Applied studies in solar photocatalytic detoxification: an overview," *Solar Energy*, 75(4), pp. 329-336.
- [7] Hashimoto, K., Irie, H., and Fujishima, A., 2005, "TiO<sub>2</sub> photocatalysis: a historical overview and future prospects," *Japanese journal of applied physics*, 44(12R), p. 8269.
- [8] Lachheb, H., Puzenat, E., Houas, A., Ksibi, M., Elaloui, E., Guillard, C., and Herrmann, J.-M., 2002, "Photocatalytic degradation of various types of dyes (Alizarin S, Crocein Orange G, Methyl Red, Congo Red, Methylene Blue) in water by UV-irradiated titania," *Applied Catalysis B: Environmental*, 39(1), pp. 75-90.
- [9] Houas, A., Lachheb, H., Ksibi, M., Elaloui, E., Guillard, C., and Herrmann, J.-M., 2001, "Photocatalytic degradation pathway of methylene blue in water," *Applied Catalysis B: Environmental*, 31(2), pp. 145-157.
- [10] Wang, Z., Wang, Y., Vivar, M., Fuentes, M., Zhu, L., and Qin, L., 2014, "Photovoltaic and photocatalytic performance study of SOLWAT system for the degradation of Methylene Blue, Acid Red 26 and 4-Chlorophenol," *Applied Energy*, 120, pp. 1-10.
- [11] Sarria, V., Kenfack, S., Malato, S., Blanco, J., and Pulgarin, C., 2005, "New helio-photocatalytic–photovoltaic hybrid system for simultaneous water decontamination and solar energy conversion," *Solar Energy*, 79(4), pp. 353-359.
- [12] Fuentes, M., Vivar, M., Scott, J., Srithar, K., and Skryabin, I., 2012, "Results from a first autonomous optically adapted photocatalytic–photovoltaic module for water purification," *Solar Energy Materials and Solar Cells*, 100, pp. 216-225.
- [13] van Well, M., Dillert, R. H., Bahnemann, D. W., Benz, V. W., and Mueller, M., 1997, "A novel nonconcentrating reactor for solar water detoxification," *Journal of Solar Energy Engineering*, 119(2), pp. 114-119.
- [14] Zayani, G., Bousselmi, L., Mhenni, F., and Ghrabi, A., 2009, "Solar photocatalytic degradation of commercial textile azo dyes: Performance of pilot plant scale thin film fixed-bed reactor," *Desalination*, 246(1), pp. 344-352.

- [15] Arias, F., Ortiz, E., López-Vásquez, A., Colina-Márquez, J., and Machuca, F., 2008, "Photocatalytic decolorization of methylene blue with two photoreactors," *Journal of Advanced Oxidation Technologies*, 11(1), pp. 33-41.
- [16] Romero, M., Blanco, J., Sanchez, B., Vidal, A., Malato, S., Cardona, A. I., and Garcia, E., 1999, "Solar photocatalytic degradation of water and air pollutants: challenges and perspectives," *Solar Energy*, 66(2), pp. 169-182.
- [17] Ajona, J., and Vidal, A., 2000, "The use of CPC collectors for detoxification of contaminated water: Design, construction and preliminary results," *Solar Energy*, 68(1), pp. 109-120.
- [18] Bakos, G., Ioannidis, I., Tsagas, N., and Seftelis, I., 2001, "Design, optimisation and conversion-efficiency determination of a line-focus parabolic-trough solar-collector (PTC)," *Applied energy*, 68(1), pp. 43-50.
- [19] Hua, M., Zhang, L., Fan, L., Lv, Y., Lu, H., Yu, Z., and Cen, K., 2015, "Experimental investigation of effect of heat load on thermal performance of natural circulation steam generation system as applied to PTC-based solar system," *Energy Conversion and Management*, 91, pp. 101-109.
- [20] Kim, Y., Han, G., and Seo, T., 2008, "An evaluation on thermal performance of CPC solar collector," *International Communications in Heat and Mass Transfer*, 35(4), pp. 446-457.
- [21] Okoronkwo, C. A., Ogueke, N. V., and Nwaigwe, K. N. A., E.E 2008, "Evaluation of the thermal performance of thermosyphon water heating systems using compound parabolic solar collector " *International Journal of Engineering and Innovative Technology* 4(3), pp. 1-5.
- [22] Taherian, H., Rezaei, A., Sadeghi, S., and Ganji, D., 2011, "Experimental validation of dynamic simulation of the flat plate collector in a closed thermosyphon solar water heater," *Energy Conversion and Management*, 52(1), pp. 301-307.
- [23] Kalogirou, S. A., 2004, "Solar thermal collectors and applications," *Progress in Energy and Combustion Science*, 30(3), pp. 231-295.
- [24] Doudrick, K., Monzón, O., Mangonon, A., Hristovski, K., and Westerhoff, P., 2011, "Nitrate reduction in water using commercial titanium dioxide photocatalysts (P25,

- P90, and Hombikat UV100)," *Journal of Environmental Engineering*, 138(8), pp. 852-861.
- [25] Deguchi, S., Kariya, B., Isu, N., Shimasaki, S., Banno, H., Miwa, S., Sawada, K., Tsuge, J., Imaizumi, S., and Kato, H., 2014, "Enhancement of Photocatalytic Water Splitting Rate via Rayleigh Convection," *Green and Sustainable Chemistry*, 2014.
- [26] Santamouris, M., 2014, "Spectral selective material for efficient visible, solar and thermal radiation control " *Solar thermal technologies for buildings: the state of the art*, M. Santamouris, ed., Routledge, pp. 39-41.
- [27] Ruth, D. W., Hollands, K., and Raithby, G., 1980, "On free convection experiments in inclined air layers heated from below," *Journal of Fluid Mechanics*, 96(03), pp. 461-479.
- [28] Catton, I., Ayyaswamy, P., and Clever, R., 1974, "Natural convection flow in a finite, rectangular slot arbitrarily oriented with respect to the gravity vector," *International Journal of Heat and Mass Transfer*, 17(2), pp. 173-184.
- [29] Jorge, K., Muneer, T., and Thomas, G., 2003, "Natural convection," *Heat Transfer: A Problem Solving Approach*, Routledge, Taylor & Francis pp. 260-261.
- [30] Berkovsky, B., and Polevikov, V., 1977, "Numerical study of problems on high-intensive free convection," *Heat Transfer and Turbulent Natural Convection*, Hemisphere Publishing Corporation, Washington DC, pp. 443-455.
- [31] Bergman, T. L., Incropera, F. P., and Lavine, A. S., 2011, "one-dimensional steady-state heat conduction " *Fundamentals of Heat and Mass Transfer*, John Wiley & Sons, pp. 164-171.
- [32] Selvakumar, N., and Barshilia, H. C., 2012, "Review of physical vapor deposited (PVD) spectrally selective coatings for mid-and high-temperature solar thermal applications," *Solar Energy Materials and Solar Cells*, 98, pp. 1-23.
- [33] Martynenko, O. G., and Khramtsov, P. P., 2005, "Free convection on a plane," *Free-Convective Heat Transfer: With Many Photographs of Flows and Heat Exchange*, Springer Science & Business Media, New York, pp. 88-89.
- [34] Fujii, T., and Imura, H., 1972, "Natural-convection heat transfer from a plate with arbitrary inclination," *International Journal of Heat and Mass Transfer*, 15(4), pp. 755-767.

- [35] Armstrong, S., and Hurley, W., 2010, "A thermal model for photovoltaic panels under varying atmospheric conditions," *Applied Thermal Engineering*, 30(11), pp. 1488-1495.
- [36] Benetoli, L. O. d. B., Cadorin, B. M., Postiglione, C. d. S., Souza, I. G. d., and Debacher, N. A., 2011, "Effect of temperature on methylene blue decolorization in aqueous medium in electrical discharge plasma reactor," *Journal of the Brazilian Chemical Society*, 22(9), pp. 1669-1678.

## CHAPTER 4

### Conclusion

#### 4.1 Research summary

The objectives of the present study were to experimentally investigate various cooling configurations at the rear of a commercial PV panel and secondly to experimentally investigate the feasibility of an integrated device for simultaneous water treatment and heating using sunlight. The approach for the investigations was via conducting the experiments in a controlled laboratory setting so that the wind is stagnant and the irradiance on the devices are controlled and steady.

An open rack pc-Si PV panel under controlled laboratory setting of high irradiance (normal light on its surface) and no wind cooling was compared to three configurations at its rear. A novel two chamber-integrated photocatalytic collector in a closed looped system for water heating and cleaning was fabricated and experimentally studied.

The approach of the first study was an experimental study on a commercial KYOCERA 20 Watt pc-Si solar panel under simulated halogen light, no winds and constant ambient temperature. The panel was placed on an open rack mount support frame and inclined at 30° from the ground. Its front and rear were exposed to the ambient air to allow for natural convection and radiation heat loss from its surfaces. This panel was placed under an artificial solar simulator, created from halogen lights. To attain high temperatures of the panel a high intensity of halogen light was used. The spectrum of the halogen light and the halogen irradiance on the panel were studied carefully. It was understood that there was uniformity in UV light, while most non-uniformity was in VIS light, and NIR radiation was uniform over the panel. The UV light from the halogen light of the present study is less as compared to solar light, solar light of type AM 1.5 spectrum and global irradiance. The VIS light is high and NIR radiation is lower. Because of the low UV light, the factory rated power output of this panel was not acquired. The power output was less from the halogen light source.

The simulator provided the main function of raising the front surface and rear surface temperatures of the panel. Front surface temperatures were at 84 °C and rear at 89.4 °C. Three configurations were installed at the rear of this panel under the same laboratory conditions and irradiance intensity, in order to study their effect of cooling.

The first configuration was the attachment of a heat sink at the rear of this hot panel. The heat sink is 197 aluminum cylindrical clear coated pin fins arranged in a staggered form on a base plate. The geometry of pins are  $d = 4.35 \times 10^{-3}$  m,  $l = 6.67 \times 10^{-3}$  m and they are spaced in a staggered form with spacing  $S = 9.01 \times 10^{-3}$  m between each other. The heat sink density is  $1.12 \text{ fins} \cdot \text{cm}^{-2}$ . The heat sink only occupied a small area at the rear of the panel and the remaining surfaces, at the front and rear, were insulated. The array design enhanced the area of the rear, compared to the bare panel, by 12 times.

The second configuration was a water cavity of longitudinal aspect ratio  $(H/W) \beta^* = 12.08$ , attached to the entire rear of the hot panel. The thickness of this cavity is  $L = 0.025$  m. A cavity of larger thickness/ smaller aspect ratio broke the panel. The third configuration was a channel of horizontal aspect ratio  $(W/L) \alpha^* = 0.08$  at the rear of the panel. This device was similar to a traditional PV/T collector. The thickness of the single channel was  $L = 0.025$  m. Water is used as the working fluid. It flowed freely from the channel to and from the cold reservoir via the thermosyphon effect.

Temperatures and power outputs of the bare panel and the three configurations were measured. It was noticed that the front and rear panel temperatures dropped using all three configurations. The channel provided the lowest temperatures followed by the heat sink, while the cavity did not reach steady conditions.

The power output of the bare panel, the cavity and the channel were measured. The panel with heat sink was not read for its power output because most of the panel was shaded. Power outputs demonstrated that the cavity and channel provided a higher power output than the bare panel, as judged from their lower temperatures. Hence forth, it was assumed that cooling was being achieved at the rear of the panel using all the configurations and the next step was an analysis of the convective heat transfer coefficient at the rear of the panels. The analysis provided a clearer picture of the viability of the cooling methods. This

coefficient was evaluated for Nusselt numbers greater than 1, hence this analysis demonstrated cooling from natural convection only.

The convective heat transfer coefficient at the rear of the panel,  $h_{\text{conv,r}}$ , is  $4.4 \text{ W}\cdot\text{m}^{-2}\cdot\text{K}^{-1}$  while it lowers to  $1.3 \text{ W}\cdot\text{m}^{-2}\cdot\text{K}^{-1}$  using the heat sink at steady state (steady reached at 140 minutes). Using the cavity, the heat transfer coefficient decreases from  $105.6 \text{ W}\cdot\text{m}^{-2}\cdot\text{K}^{-1}$  decays to  $25.6 \text{ W}\cdot\text{m}^{-2}\cdot\text{K}^{-1}$  at  $t = 140$  minutes. A heat transfer coefficient of  $25.6 \text{ W}\cdot\text{m}^{-2}\cdot\text{K}^{-1}$  signifies  $\text{Nu} < 1$  when using water. The heat transfer coefficient at the rear is  $h_{\text{conv,r}} = 357.0 \text{ W}\cdot\text{m}^{-2}\cdot\text{K}^{-1}$  at  $t = 28$  minutes which decays to  $141.5 \text{ W}\cdot\text{m}^{-2}\cdot\text{K}^{-1}$  at  $t = 140$  minutes. Thus the channel is the best method of cooling.

It was hypothesized that with Rayleigh numbers evaluated at the heat sink base, the relevant Nusselt number would be greater than 80 on this surface. It was also hypothesized that with the current modified Rayleigh number  $\text{Ra}^*$ , of value of 661, the Nusselt number would be 9.2. The heat sink has a Nusselt number of 3.04 only, attained from the analysis. The heat sink is enhancing the heat transfer at the rear of the panel by 1.53 times the amount at the rear of the bare panel. Hence, cooling is achieved by the heat sink via laminar natural convection and strong radiation heat transfer. The water cavity was evaluated for its Rayleigh numbers in the analysis and although the Rayleigh number is above the theoretical limits for attaining laminar natural convection in the water, it is not greater than those of previous studies. Hence no natural convection is occurring in this cavity.

The strength of the flow in the channel was hypothesized to be stronger than attained in the experimental work. It was hypothesized that thermally developed flow would be attained. This provides  $\text{Nu} = 8.44$  near the entrance and  $\text{Nu} = 5.35$  near the exit. In the present study, a Nusselt number of  $\text{Nu} = 5.94$  near the entrance and  $\text{Nu} = 5.13$  near the exit are acquired. These are integrated over the channel height to be equal to an average of  $\text{Nu} = 5.67$ . However, previous PV/T collectors with channels below the panel assume their Nusselt number values and state thermally developed flow. The present study provides a comparison of previous work Nusselt numbers and those of the hypothetical and the analytically determined Nusselt numbers of the present study. The comparison demonstrates the benefits of having thermally developed flow in channels attached to the panel for future considerations.



Previous PV/T collectors have utilized different irradiances and have not reported wind speeds or the heat losses. They have not experimentally determined what the Nusselt number is in their channels, nor have they reported any cell temperatures. In comparison, the present study provides a thermal efficiency of  $\eta_{th} = 0.51$  at  $\approx 0 \text{ C}\cdot\text{m}^2\cdot\text{W}^{-1}$  reduced temperature and cell temperatures are analytically assessed to drop from  $T_{cell} = 87.5 \pm 1.2^\circ\text{C}$  to  $63.8 \pm 1.2^\circ\text{C}$ . The thermal efficiency is lower in the present study as compared to previous PV/T collectors.

Since the problems with low power output of pc-Si panels in combined PV- photocatalytic devices were discussed in the review, it was sought to create a novel collector that provides clean water without PV panels, with free circulation of the mixture, and provides an added function of efficiency hot water production. The latter function is of solar thermal collectors, a separate technology from solar photocatalytic collectors and combined devices. The objective of this particular study in this thesis, was to experimentally investigate the feasibility of an integrated device of such types, for simultaneous water treatment and heating using sunlight.

A two chamber collector for these purposes was created and it operated successfully. This collector shows water cleaning and useful thermal output (reasonable thermal efficiency). It utilized the thermosyphon effect to circulate the mixture of catalyst and waste water freely in the system to which it was connected in. Such methods of free circulation are present in collection setups of solar thermal-collectors in previous studies. It was aimed to decompose a model pollutant via photocatalysis in this novel collector while attaining a thermal efficiency goal of  $\eta_{th} > 0.7$ .

The light sources powering this mechanism were four halogen lamps. Its intensity was  $1000 \text{ W}\cdot\text{m}^{-2}$ . The simulator was carefully analyzed and it had the same properties as that of the simulator used to test the PV panel configurations. The collector lay under this light source, oriented at  $30^\circ$  from the floor and the wind conditions were calms. Ambient temperatures were constant as well.

The dye's initial concentration and final concentrations were read using a spectrophotometer, as done in previous studies and results show that there are minimal

effects of photosensitization of the dye and the decomposition of this harmful substance is being performed by photocatalysis. Photocatalysis was studied using various catalyst dosages in the system. This mixture flowed freely, to and from the cold reservoir during the experimental time period. No particle sedimentation was observed.

However, low UV light is available from halogen lights in these experiments which are predicted to yield lower decomposition of MB dye. The results of photocatalysis have been demonstrated in this thesis by using a low concentration of MB dye (1.2ppm) and low dosages of TiO<sub>2</sub> P90 catalyst. These concentrations provide comprehensive results within the limitations of these material amounts which are; i) adsorption of dye on catalyst, (ii) photosensitization of dye without catalyst and (iii), decomposition from photocatalysis. However, the devices limitations to clean water and or/it's maximum capacity of water cleaning requires more material amounts.

Previous indoor work has established a significant decomposition of MB dye using TiO<sub>2</sub> P25, such as the indoor Pyrex reactors which use 125 W of indoor UV lamps. Outdoor works are commonly done utilizing CPCs and TCs with MB dye as the model pollutant. Low amounts of UV light are available for photocatalysis outdoors but it is well known that MB dye responds to VIS light as well and these works have shown significant results. Such results were not achieved in the device in the present study. Combined PV- photocatalytic devices provide higher decomposition of dye because they are using high dosages of catalyst and more UV light available from the sun. The present device needs to utilize more catalyst and needs to be experimented outdoors. CPCs and TCs that decompose MB dye under UV lamps indoors also have utilized higher dosages of catalyst. The present device thus, needs to be experimented outdoors along with more materials for water cleaning tests to compare to these photocatalytic collectors in previous works.

However, none of these previous works for solar water cleaning have provided the integration of water treatment and water heating, delivered by the device in the present study. Water heating abilities were assessed via heat transfer analysis.

It was found that 58.6 % the irradiance from halogen light is transferred to the mixture by the air chamber. 67 % of the irradiance is absorbed by the mixture from the halogen lights.

Approximately 33 % is lost via laminar natural convection and radiation heat transfer to the environment from this device. The total thermal efficiency of the collector is  $\eta_{th} = 0.67$ , in the experimental conditions utilized.

To attain higher thermal efficiency, the transmittance of the glass has to be increased or a different glass should be used. This is only a suggestion and it is not known what the effects of replacing the current tempered borosilicate glass would be in the future.

Current design contains a glass transmitting approximately 70 % of the irradiance from a halogen light source and this might not be the same value under solar light. Secondly it is vital that the heat losses from the collector's front surface be minimized. The front surface of the glass over the mixture demonstrates that convection heat losses are weak but radiation heat losses are significant.

Furthermore, the mass flow rate of the mixture circulating in the system needs to be measured since it is very low. Analysis can only predict the mass flow rate but low-flow meters are needed to validate low thermosyphon flows.

The aim of the thermal efficiency of the present work arose from the reviewed thermal efficiencies of PTCs, CPCs and flat plate collectors that are solely for water heating. These collectors of previous studies have been evaluated under various weather conditions and operating conditions and they have demonstrated large thermal efficiencies (most have  $\eta_{th} > 0.7$ ). However, the present study is yet to be experimented outdoors to provide a comparison. It is not known if the thermal efficiency of the device created in the present study would be higher or lower under solar light. The photocatalytic collector for water cleaning and efficient water heating delivers its predicted functions under the experimental conditions of the present study only.

## **4.2 Significance of the findings**

The following significances of these studies are reported:

- i. Cylindrical pin fin arrays can enhance the heat transfer at the rear of the panel via natural convection and radiation. However, natural convection heat transfer

coefficient is lower than that of a bare panel. Hence using a large surface area at the rear of the panel to enhance the heat transfer is a good option for cooling.

- ii. The panel is best cooled using a water channel below it, as those of the methods of traditional PV/T collectors present in previous studies. It has a higher convection heat transfer coefficient than that of the heat sink.
- iii. A two-chamber photocatalytic collector is functional under halogen lamps to deliver photocatalytic water cleaning and water heating. Dosages of TiO<sub>2</sub> P90 limit the amount of MB dye decomposition in this type of device while the surface heat losses of the collector lower its thermal efficiency.

### **4.3 Future recommendations**

The following recommendations are given:

- i. Experiment with different levels of irradiance on the PV panel configurations and assess the heat transfer coefficient at the rear.
- ii. Optimize the geometry of the heat sink used for PV cooling to attain possibility of higher natural convection heat transfer.
- iii. Negate any use of a water cavity to naturally cool the panel for any future work.
- iv. Install more temperature sensors in the channel at the rear of the panel to acquire more local Nusselt number values.
- v. Install thermocouples inside the PV panel to attain exact values of cell temperatures at various locations for all the devices in the present study.
- vi. Measure the flow rates in the photocatalytic collector using ultrasound flow meters.
- vii. Vary the concentration of MB dye and increase dosages TiO<sub>2</sub> P90. of
- viii. Conduct the experimental work in the present study in outdoor conditions and repeat the data acquisition and reduction for more realistic results.

# Curriculum Vitae

**Usman Rajput, M.E.Sc, B.A.Sc, EIT**

**Birth place:** Morden, MB

## **EDUCATION and RESEARCH WORK**

**WESTERN UNIVERSITY**

**Masters in Engineering Sciences, Mechanical Engineering,**

**UNIVERSITY OF WINDSOR**

**Bachelor of Applied Sciences, Mechanical Engineering (Honors), 2009**

## **EMPLOYMENT EXPERIENCE**

**WESTERN UNIVERSITY, London, ON**

**Graduate research assistant & Teaching assistant, 2016**

**THINK PATH ENGINEERING SERVICES, Toronto, ON**

Contracted at: **Siemens Power Generation, Hamilton, ON**

**Turbine blade Designer, 2010**

**NEMAK, Essex, ON, 2008**

**Intern Process Engineer**

**CENTERLINE LTD (R&D DIVISION), Windsor, ON, 2007**

**Intern product development engineer**